

## N O T I C E

THIS DOCUMENT HAS BEEN REPRODUCED FROM  
MICROFICHE. ALTHOUGH IT IS RECOGNIZED THAT  
CERTAIN PORTIONS ARE ILLEGIBLE, IT IS BEING RELEASED  
IN THE INTEREST OF MAKING AVAILABLE AS MUCH  
INFORMATION AS POSSIBLE

# Composite

## Structural Program

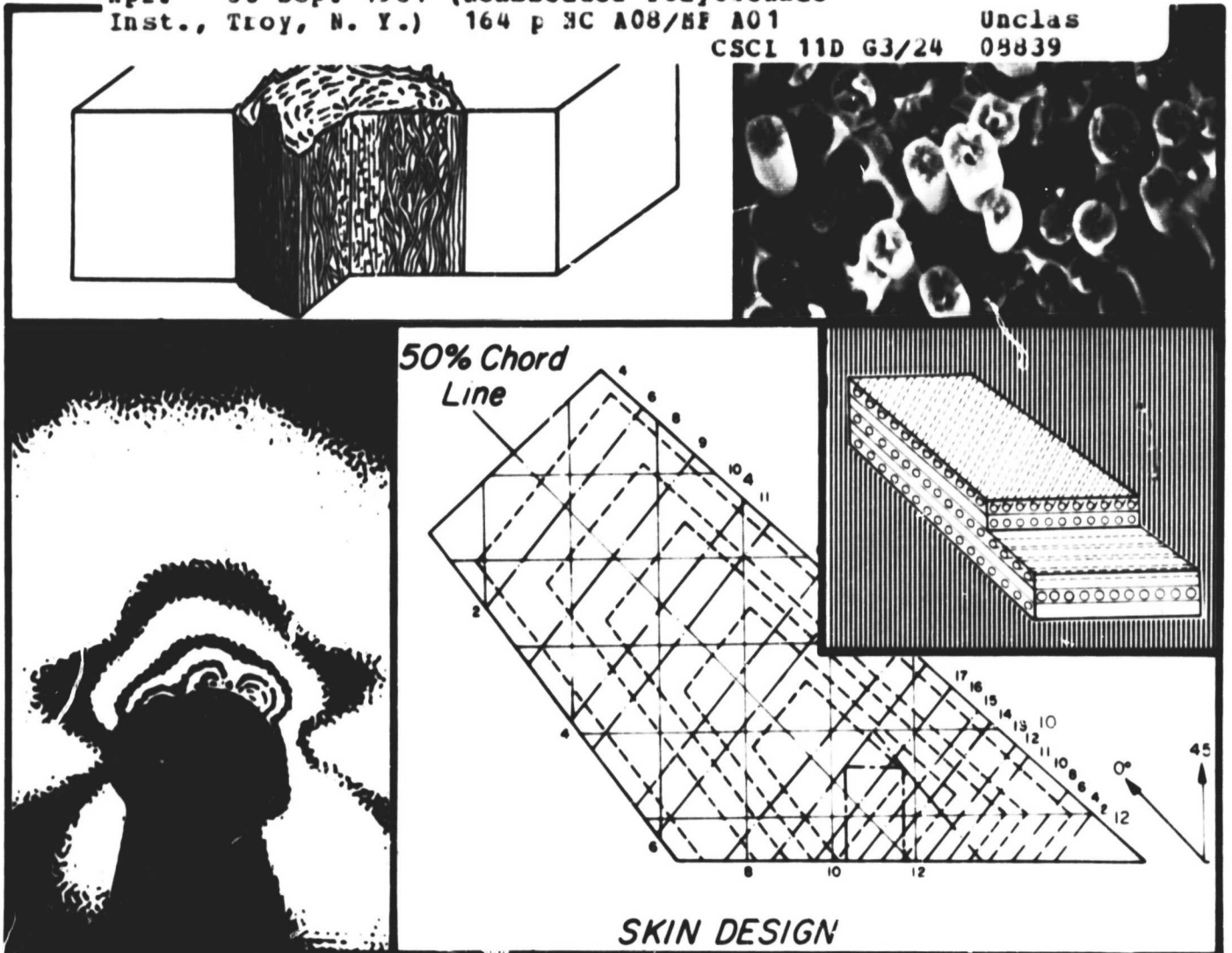
Rensselaer Polytechnic Institute  
Troy, N.Y. 12181

(NASA-CR-165121) COMPOSITE STRUCTURAL  
MATERIALS Semiannual Progress Report, 30  
Apr. - 30 Sep. 1981 (Rensselaer Polytechnic  
Inst., Troy, N. Y.) 164 p HC A08/BF A01

N82-16182

Unclas

CSCI 11D G3/24 09839



Sponsored by  
**NASA/AFOSR**

Semi-Annual Progress Report  
April 30, 1981 through September 30, 1981

COMPOSITE STRUCTURAL MATERIALS

Air Force Office of Scientific Research  
and  
National Aeronautics and Space Administration  
Grant No. NGL 33-018-003

Co-Principal Investigators:

George S. Ansell  
Dean, School of Engineering

Robert G. Loewy  
Institute Professor

and

Stephen E. Wiberley  
Professor of Chemistry

Rensselaer Polytechnic Institute  
Troy, New York 12181

NASA Technical Officer  
Michael A. Greenfield  
Materials and Structures Division  
NASA Headquarters

## CONTENTS

	<u>Page</u>
PART I. INTRODUCTION .....	1
1. General .....	3
2. The RPI Program .....	4
3. Technical Interchange .....	9
4. Summary .. ..	18
PART II. CONSTITUENT MATERIALS .....	19
II-A A STEP IN DETERMINING TRANSVERSE FIBER PROPERTIES: CHARACTERIZATION OF HOMOGENEITY IN COMPOSITE MATERIALS (R. J. Diefendorf) .....	21
1. Introduction .....	21
2. Status .....	22
3. Progress During Report Period .....	23
4. Plans for Upcoming Period .....	33
PART III. COMPOSITE MATERIALS .....	34
III-A ADVANCED ANALYSIS METHODS (E. J. Brunelle) ...	36
1. Introduction .....	36
2. Status .....	36
3. Progress During Report Period .....	37
4. Plans for Upcoming Period .....	45
5. Current Publications or Presentations by Professor Brunelle on this Subject .....	46
III-B FATIGUE IN COMPOSITE MATERIALS (E. Krempl) ...	47
1. Introduction .....	47
2. Status .....	47
3. Progress During Report Period .....	47
4. Plans for Upcoming Period .....	48
5. Current Publications or Presentations by Professor Krempl on this Subject .....	48
III-C MOISTURE AND TEMPERATURE EFFECTS ON THE MECHANICAL PROPERTIES OF LAMINATES (S. Sternstein) .....	49
1. Introduction .....	49
2. Status .....	49

	<u>Page</u>
3. Progress During Report Period .....	50
4. Plans for Upcoming Period .....	54
5. Current Publications or Presentations by Professor Sternstein on this Subject .....	57
III-D NUMERICAL INVESTIGATION OF MOISTURE EFFECTS (M. Shephard) .....	58
1. Introduction .....	58
2. Status .....	58
3. Progress During Report Period .....	58
4. Plans for Upcoming Period .....	62
III-E NUMERICAL INVESTIGATION OF THE MICROMECHANICS OF COMPOSITE FRACTURE (M. Shephard) .....	64
1. Introduction .....	64
2. Status .....	64
3. Progress During Report Period .....	65
4. Plans for Upcoming Period .....	67
5. References .....	67
PART IV. GENERIC STRUCTURAL ELEMENTS .....	69
INTRODUCTION TO PART IV .....	71
IV-A 727 ELEVATOR ATTACHMENT RIB (D. Goetschel, R. Loewy and H. Scarton) .....	73
1. Construction Details of the Final 727 Elevator Rib .....	74
2. Test Procedure and Results for the Final 727 Elevator Rib .....	78
IV-B LOCKHEED L-1011 ENGINE DRAG STRUT (CAPCOMP II) (D. Goetschel) .....	105
1. Introduction .....	105
2. Status .....	105
3. Progress During Report Period .....	109
4. Plans for Upcoming Period .....	111
IV-C MECHANICAL JOINTS IN COMPOSITES (D. Goetschel and R. Loewy) .....	115
1. Analysis of Heavily Loaded Mechanical Joints ..	115
a. Introduction .....	115
b. Review of Previous Work .....	116

	<u>Page</u>
c. Progress During Report Period .....	118
d. Plans for Upcoming Period .....	121
e. Current Publications or Presentations on this Subject by Professor Hoff and Dr. Muser .....	121
2. Pin-Loaded Holes in Uniform Composite Plates .	121
a. Introduction .....	121
b. Status .....	122
c. Progress During Report Period .....	123
d. Plans for Upcoming Period .....	136
IV-D COMPUTER SOFTWARE DEVELOPMENTS (M. S. Shephard)	137
1. Introduction and Status .....	137
2. Progress During Report Period .....	137
3. Plans for Upcoming Period .....	143
4. Current Publications or Presentations by Pro- fessor Shephard on this Subject .....	143
PART V. PROCESSING SCIENCE AND TECHNOLOGY .....	147
V-A INITIAL SAILPLANE PROJECT: THE RP-1 (F. Bundy, R. J. Diefendorf and H. Hagerup) .....	149
V-B SECOND SAILPLANE PROJECT: THE RP-2 (F. Bundy, R. J. Diefendorf and H. Hagerup) .....	152
PART VI. PERSONNEL, AUTHOR INDEX .....	155
PERSONNEL .....	157
AUTHOR INDEX .....	161

## LIST OF TABLES

		<u>Page</u>
TABLE I-1	CALENDAR OF COMPOSITES-RELATED MEETINGS .	10
TABLE I-2	COMPOSITES-RELATED TECHNICAL MEETINGS ATTENDED OFF-CAMPUS .....	11
TABLE I-3	COMPOSITES-RELATED MEETINGS/TALKS HELD AT RPI .....	13
TABLE I-4	COMPOSITES-RELATED VISITS TO RELEVANT ORGANIZATIONS .....	14
TABLE II-A-1	SPECIFIC GRAVITY AND VOLUME FRACTIONS USING NITRIC ACID DIGESTION .....	23
TABLE II-A-2	COMPARISON OF VOLUME FRACTION DETERMINA- TIONS USING GRID AND IMAGE ANALYSIS TECH- NIQUES .....	25
TABLE II-A-3	VOLUME FRACTION RESULTS FROM PHOTOMICRO- GRAPH GRID ANALYSIS .....	28
TABLE II-A-4	VOLUME FRACTION DATA FROM SUBFIELD ANALY- SIS .....	29
TABLE IV-A-2	ACOUSTIC EMISSION SENSOR CHARACTERISTICS	82
TABLE IV-C-2-a	STRENGTH AS INFLUENCED BY D/t FACTOR, [+45°/0°] <sub>ns</sub> .....	127

## LIST OF FIGURES

<u>Figure No.</u>		<u>Page</u>
II-A-1.	Schematic Diagram of the Variation of Volume Fraction Within a Fabricated Part ..	23
II-A-2.	Bausch & Lomb FAS/II - Image Analysis System .....	27
II-A-3.	Variance versus (Area) <sup>-1</sup> .....	30
II-A-4.	Volume Fraction of Fibers versus Area (Number of Fields) .....	32
III-C-1.	Storage Modulus vs Temperature with Various Wetnesses .....	51
III-C-2.	Loss Modulus vs Temperature with Various Wetnesses .....	52
III-C-3.	Glass Transition Temperature as a Function of % Weight Gain .....	53
III-C-4.	Storage and Loss Moduli as a Function of Temperature: Dry .....	55
III-C-5.	Storage and Loss Moduli as a Function of Temperature: Wet .....	56
III-D-1.	Finite Element Mesh Used in Single Fiber Analysis .....	61
III-D-2.	Displaced Shape for the Free Swelling Case	61
III-D-3.	Displaced Shape for 80% Humidity .....	63
III-D-4.	Maximum Principal Stress Contours for 80% Humidity .....	63
IV-A-1-a.	727 Elevator Actuator Attachment Rib (8/6/81) .....	76
IV-A-1-b.	Failed Section and Strain Gage .....	77
IV-A-2-a.	Rib Test Fixture .....	79
IV-A-2-b.	Elevator Actuator Attachment Rib Test Fixture in Instron/333 (without personnel protection barrier) .....	80
IV-A-2-c.	Elevator Actuator Rib Test Fixture and Instrumentation (with personnel protection barrier) .....	83
IV-A-2-d.	Variable Thickness Homogeneous Finite Element Specimen .....	84
IV-A-2-e.	Finite Element Maximum Principal Stress Distribution .....	85

<u>Figure No.</u>		<u>Page</u>
IV-A-2-f.	Close-up of Finite Element Maximum Principal Stress Region of Highest Stress .....	86
IV-A-2-g.	Finite Element Simulation of Final Strained Shape .....	87
IV-A-2-h.	Strain Gage and Acoustic Emission Sensor Locations .....	88
IV-A-2-i.	Specimen Load Versus Stroke Curve .....	90
IV-A-2-j.	Amplitude Distribution at 43 kN (9700 pounds) During Run 1 .....	91
IV-A-2-k.	Cumulative Counts Versus Time Run Number 2	92
IV-A-2-l.	Final Amplitude Distribution at Failure ...	94
IV-A-2-m.	Strain Values in Y Direction at E & EP ....	96
IV-A-2-n.	Strains, Principal Strains and Principal Stresses at the Instant of Failure .....	97
IV-A-2-o(1).	Failed Actuator: (a) Overall View, Side 1	99
IV-A-2-o(2).	Failed Actuator (b), Failure Site at Point E, View 1 .....	100
IV-A-2-o(3).	Failed Actuator (c), Failure Site at Point E, View 2 .....	101
IV-A-2-o(4).	Failed Actuator (d), Failed Site at Point E, View 3 .....	102
IV-A-2-o(5).	Failed Actuator (e). Top View .....	103
IV-A-2-o(6).	Failed Actuator (f), Pin Rotation at Point E, Side 2 .....	104
IV-E-1.	Lockheed L-1011 Engine Drag Strut (Schematic) .....	106
IV-B-2.	Lockheed L-1011 Wing Pylon Structure Assembly .....	107
IV-B-3.	Design Forces for Strut .....	108
IV-B-4.	Lug Experiment: 1/4-Scale L-1011 Drag Strut	113
IV-C-1-a.	Geometry of the Cylindrically Orthotropic Plate with Unloaded Hole .....	117
IV-C-1-b.	Geometry of the Cylindrically Orthotropic Plate with Loaded Hole .....	120
IV-C-2-a.	Problem Idealization .....	124
IV-C-2-b.	Photoelastic Specimen .....	130
IV-C-2-c.	Isochromatic Fringes .....	131

<u>Figure No.</u>		<u>Page</u>
IV-C-2-d.	Maximum Shear Strain Distribution .....	133
IV-C-2-e.	Enlarged Picture of Figure IV-C-2-d .....	134
IV-C-2-f.	Applied Load Versus Contact Angle .....	135
IV-D-1.	Control Page for Edge Load Segment of At- tribute Editor .....	139
IV-D-2.	Use of ECHO Function to Check Edge Load ...	139
IV-D-3.	Control Page for Surface Load Segment of the Attribute Editor .....	140
IV-D-4.	Application of Linearly Varying Surface Load Matching Neighboring Constant Surface Load .....	140
IV-D-5.	Completed Set of Surface Loads .....	142
IV-D-6.	Use of ECHO Function to Check Surface Loads	142
IV-D-7.	Definition of Three-Dimensional Boundary Curves .....	144
IV-D-8.	Surface Mesh Generated Using Boundary Curves .....	144
IV-D-9.	Surface Mesh Example .....	145
IV-D-10.	Rotated View of Surface Mesh Example .....	145
V-A-1.	RP-1 Glide Polar - Preliminary Data .....	150

PART I  
INTRODUCTION



As technology of composite materials and structures moves toward fuller adoption into aerospace structures, some of the problems of an earlier era are being solved, others which seemed important are being put into perspective as relatively minor, and still others unanticipated or put aside are emerging as of high priority. The purpose of the RPI program as funded by NASA and AFOSR has been to develop critical advanced technology in the areas of physical properties, structural concepts and analysis, manufacturing, reliability and life prediction.

## 2. The RPI Program

Our approach to accomplishing these goals is through an interdisciplinary program, unusual in at least two important aspects for a university. First, the nature of the research is comprehensive - from fiber and matrix constituent properties research, through the integration of constituents into composite materials and their characterization, the behavior of composites as they are used in generic structural components, their non-destructive and proof testing to the logical conclusion of such activities; namely research into the composite structure's long term integrity under conditions pertinent to service use. Inherent in the RPI program is the motivation which basic research into the structural aspects provides for research at the materials level, and vice versa.

Second, interactions among faculty contributing to program objectives - which is a group wider than that supported under

the project - is on a day to day basis, regardless of organizational lines. Program management is largely at the working level, and administrative, scientific and technical decisions are made, for the most part, independent of considerations normally associated with academic departments. Involvement of this kind includes - depending on the flow of the research - faculty, staff and students from chemistry, chemical engineering, civil engineering, materials engineering, and the department of mechanical engineering, aeronautical engineering and mechanics.

Both of these characteristics of the NASA/AFOSR program of research in composite materials and structures foster the kinds of fundamental advances which are triggered by insights into aspects beyond the narrow confines of an individual discipline. This is a program characteristic often sought in many fields at a university, but seldom achieved.

The program objective of advancing fundamental knowledge in the areas of physical properties, structural concepts and analysis, manufacturing, reliability and life prediction, continues as our program evolves, but changes in direction will be instituted in the next six months recognizing the evolution of the use of composites in the industry and among certain government agencies such as FAA, DOD and NASA itself.

Research on new structural design concepts at RPI will move away from redesign of actual aircraft components, such as the 727 elevator actuator attachment rib and the L-1011 engine drag strut (formerly known under the acronym CAPCOMP

for Composite Aircraft Program Component), toward those specific subjects which these efforts have revealed as areas of critical technological need.

Currently, such specific subjects include the following:

(a) attempts to quantify St. Venants' principle for typical composite materials and member cross sections. This is needed to determine how far from points of concentrated load introduction (such as occur in mechanical joints) structural cross sections must vary before constant cross sections can be efficiently used.

(b) research into scaling laws for composite structures. Here at least two aspects introduce uncertainty; first, the effect of constituent material property differences with size as related to cure processing exothermic reactions, and second, the effect of the ratio of fiber diameter to the smallest dimension in the scaled part. The importance of advancing understanding in this area is in the usefulness and efficiency of experiments in the development of large, complex structures such as are the stock-in-trade of the aerospace industry. Developments using scaled test specimens would reduce material costs; ease handling, manufacturing equipment and test equipment requirements; and generally shorten development schedules.

(c) lug design using composites. In this area, the favorable strength to weight ratio of composite materials tends to be offset by their less than favorable strength to volume ratio. The complex load-paths, furthermore, tend to frustrate attempts to use the unidirectional advantages of

"tailored materials". Considerable promise remains, however, in the possibility of spacially "tailoring" material properties both azimuthally and radially from the points of load introduction. Much remains to be done of a fundamental nature in this area both theoretically and experimentally.

Overall program emphasis, in future months - on all aspects - will move from specific applications to more basic, long-term research in the following categories: (a) constituent materials, (b) composite materials, (c) generic structural elements, (d) processing science technology and (e) maintaining long-term structural integrity. Those computer software developments will be pursued which both support Rensselaer projects in composite materials and structures research in the areas listed above and which also represent research with the potential of widely useful results in their own right.

The sailplane project (called CAPGLIDE for Composite Aircraft Program Glider) involving design, fabrication and testing of an advanced, full-scale, flight-worthy, all-composite aircraft will be continued as a highly productive way to conduct research on processing science and technology for low-cost aerospace structures. The list of innovative designs and processes resulting from that research to date includes:

- a) A simplified fabrication process without molds for accurate, smooth surface airfoils in wings and tail surfaces up to roughly twenty feet semi-span,
- b) Single sided, composite-foam "sandwich" structures which can be successfully joined to

sub-structures to form ultra-light weight surfaces capable of carrying useful distributed loads,

- c) Composite hinge configurations that are integrally bonded into airfoil contours to minimize peel-strength problems,
- d) Proper mixtures of hardeners and experimental, especially low viscosity resins to achieve both minimum-depth bond and surfaces for ultra-light weight and acceptable strength, and
- e) A technique for fabricating smooth-surfaced graphite/epoxy tubes of relatively small diameter, without the use of release agents or external molds, through the use of teflon rods as mandrels.

The impetus toward innovation in processing science will be preserved as the project evolves, by undertaking continually more challenging structural functions in sailplane design. Further, research on problems within the disciplined context of actual manned flight testing can be expected to contribute to fundamental knowledge as regards monitoring and maintaining structural integrity of functioning, low-cost aerospace structures.

The changes in program direction discussed above will not begin to take effect until the six-month period immediately ahead. This report, however, presents progress achieved in all elements of the program under a format better suited to the new program orientation, as reflective of converting to operation in the new mode.

Accordingly, program element headings in the following pages will be

Constituent Materials,  
Composite Materials,  
Generic Structural Elements,  
Processing Science and Technology and  
Maintaining Structural Integrity.

### 3. Technical Interchange

Technical meetings, on- and off-campus, provide important opportunities for interchange of technical information. Because of the large number of composites meetings, a central catalog with all upcoming meetings is being maintained and distributed periodically. In this way we help assure that a Rensselaer faculty/staff member can participate in important meetings. The calendar for this reporting period is shown in Table I-1. Meetings attended by RPI composites program faculty/staff/students during the reporting period are shown in Table I-2. Some meetings particularly relevant to composites, held on-campus with special speakers, are listed in Table I-3. A list of composite-related visits to relevant organizations by RPI faculty/staff/students, with the purpose of each visit outlined, is presented in Table I-4.

Two continuing education special courses, outgrowths of the composite materials and structures program, were presented for graduate engineers in industry and government during the month of July. They were "Composite Materials and Structures" and "The Finite Element Approach in Structural

TABLE I-1CALENDAR OF COMPOSITES-RELATED MEETINGS

(April 30, 1981 through September 30, 1981)

- 5/12-13 6th ASTM Conference on Composite Materials: Testing and Design, Phoenix, AZ. "Sponsored by ASTM Committee D-30."
- 5/12-14 50th Anniversary Meeting and Technical Display, Long Beach, California. "Sponsored by AIAA."
- 5/17-20 37th Annual Forum and Technical Display, New Orleans, LA. "Sponsored by AHS."
- 5/18-21 International Materials Policy and Technical Considerations for Future Automotive Design, Dearborn, MI.
- 5/18-21 International Symposium on Mechanical Behavior of Structural Media, Ottawa, Canada.
- 6/2-4 Colloquium on Advanced Mechanics of Reinforced Concrete, Delft, Netherlands. "Sponsored by ASCE."
- 6/5-7 Spring Meeting (Electro Dynamics in Solid Mechanics, Nonlinear Dynamics), Alexandria, VA. "Sponsored by SIAM."
- 6/15-17 3rd Symposium on Dynamics and Control of Large Flexible Spacecraft, Blacksburg, VA. "Sponsored by VPI and SU/AIAA."
- 6/15-19 U.S.A.-Italy Joint Symposium on Composite Materials - The Role of Polymeric Matrix in Their Processing and Structural Properties, Capri, Italy.
- 6/21-26 Pressure Vessels and Piping Conference, Denver, CO. "Sponsored by ASME."
- 6/22 ASEE National Meeting, Los Angeles, CA.
- 6/22-24 Joint ASME/ASCE Mechanics Conference, Boulder, CO.
- 6/22-26 15th Biennial Conference on Carbon, Philadelphia, PA.
- 8/17-21 6th International Conference on Structural Mechanics in Reactor Technology, Paris, France.
- 8/26-27 National American Chemical Society Meeting, N.Y.C., NY.
- 9/8-9 7th European Rotorcraft and Powered Lift Aircraft Forum, Garmisch, Germany.
- 9/16-18 International Conference on Composite Structures, Paisley, Scotland.
- 9/20-23 4th Failure Prevention and Reliability Conference (Joint ASME Vibrations, Design Automation, F-P, R Conference), Hartford, CT.
- 9/22-25 Euromech 147, Symposium on Damage Mechanics, Cachan, France.

TABLE 1-2

COMPOSITES-RELATED TECHNICAL MEETINGS ATTENDED OFF-CAMPUS

(April 30, 1981 through September 30, 1981)

- 5/12-13 6th ASTM Conference on Composite Materials: Testing and Design (Prof. Krempl), Phoenix, AZ
- ASTM E9.01 Committee Meeting: Professor Krempl presented the paper, "Time Dependent Effects During Cyclic Loading of Structural Steels at Room Temperature".
- ASTM E9.08 Committee Meeting: Professor Krempl presented the paper, "Preliminary Experience with the Instron Biaxial Extensometer".
- 5/13-16 50th Anniversary AIAA Meeting and Technical Display (Prof. Loewy), Long Beach, CA
- 6/15-19 U.S.A.-Italy Joint Symposium on Composite Materials - The Role of the Polymeric Matrix in Their Processing and Structural Properties (S. Sternstein), Capri, Italy
- Professor Sternstein, Invited Lecturer, presented the paper, "Properties of in situ Epoxy Matrices".
- 6/22 ASEE National Meeting: Education & Industry - A Joint Endeavor (Prof. Shephard), Los Angeles, CA
- Professor Shephard presented the paper, "The University's Role in Meeting Industry's Role in CAD/CAM Needs".
- 6/22-24 Joint ASME/ASCE Mechanics Conference (Profs. Hoff and Krempl and student C. Muser), Boulder, CO
- Professor Hoff presented the paper, "Stress Concentrations in Cylindrically Orthotropic Composite Plates with a Circular Hole".
- Professor Krempl presented the paper, "The Rate(Time)-Dependent Behavior of Ti-7Al-2Cu-1Ta Titanium Alloy at Room Temperature under Quasi-static Monotonic and Cyclic Loading".
- 6/22-26 15th Biennial Conference on Carbon (Prof. Diefendorf), Philadelphia, PA
- Professor Diefendorf presented the paper, "The Chemical Vapor Deposition of Carbon Matrices".

TABLE I-2 (continued)

- 8/17-21 6th International Conference on Structural Mechanics in Reactor Technology (Prof. Krempl), Paris, France
- 8/26-27 National American Chemical Society Meeting (Profs. Diefendorf and Sternstein), N.Y.C., NY  
Professor Diefendorf presented the paper, "Consequences of Residual Stress on Carbon Fiber Performance".  
Professor Sternstein presented the paper, "Viscoelastic Characterization of Neat Resins and Composites".
- 9/20-23 4th Failure Prevention and Reliability Conference (Joint ASME Vibrations, Design Automation, F-P, R Conference) (Prof. Brunelle and L. W. Chen and L. Y. Chen), Hartford, CT  
Professor Brunelle presented the paper, "Thermal Buckling of Initially Stressed Thick Plates".
- 9/22-25 Euromech 147, Symposium on Damage Mechanics (Prof. Krempl), Cachan, France  
Professor Krempl presented the paper, "Life Prediction for Creep-Fatigue".

TABLE I-3  
COMPOSITES-RELATED MEETINGS/TALKS HELD AT RPI  
 (April 30, 1981 through September 30, 1981)

<u>Topic</u>	<u>Date</u>	<u>Speaker(s)</u>
The Use of Affine Transformations in the Analysis of Stability and Vibrations of Orthotropic Plates	5/17/81	Gabriel A. Oyibo Doctoral thesis dissertation Department of Mechanical Engineering, Aeronautical Engineering and Mechanics Rensselaer Polytechnic Institute
Dornier and Composite Applications	7/17/81	H. Gunter Helwig Design Specialist for Composites Materials and Structures Testing Dornier System GmbH
Cylindrically Orthotropic Circular Plates with a Concentric Hole and with Properties Varying Radially	7/22/81	Christoph Muser Doctoral thesis dissertation Department of Mechanical Engineering, Aeronautical Engineering and Mechanics Rensselaer Polytechnic Institute
Nonlinear Thermoelastic Effects in Surface Mechanics	8/6/81	Joseph M. Pitkin Doctoral thesis dissertation Department of Mechanical Engineering, Aeronautical Engineering and Mechanics Rensselaer Polytechnic Institute
Loaded Hole Analysis in Composite Materials	8/13/81	Kenneth Bubeck Grumman Aerospace Corp.
Finite Strain Transient Response of Thin Structures	9/10/81	Jose J. A. Rodal Kaman Avi-Dyne

TABLE I-4COMPOSITES-RELATED VISITS TO RELEVANT ORGANIZATIONS

by RPI Faculty/Staff/Students

(April 30, 1981 through September 30, 1981)

<u>Visited</u>	<u>Date</u>	<u>By</u>	<u>Purpose</u>
Naval Research Laboratory, Washington, DC	5/4-5	Prof. H. Scarton	Lectured on acoustic emission techniques and demonstrated Sig- nal Processing of Acoustic Emissions from Composite Mate- rials
Sterling-Winthrop, Rensselaer, NY	5/12	Prof. R. J. Diefendorf	Gave lecture: "Anal- ysis of Experimental Data"
Krautkramer- Branson, Inc., Stratford, CT	7/19-24	Prof. H. Scarton	To discuss acoustic emission and ultra- sonic and NDE tech- niques and instruments
IBM Research Laboratory, San Jose, CA	8/4	Prof. S. S. Sternstein	Gave lecture: "Visco- elastic Properties of Composites"
Department of Energy, Washington, DC	8/23-25	Prof. H. Scarton	Took part in Review Panel activities on composite fly wheel program
Battelle Columbus Laboratories, Columbus, OH	9/14	Prof. M. S. Shephard	Presented talk: "Fi- nite Element Model Generation"

Analysis". This is the second year they were offered. Each course lasted a week, and they were run serially so that a participant might come for both on the same trip. The level of the material was planned to be particularly useful to managers of engineering structures activities who are involved in technical work but who may not have taken courses for several years. Because of the wide variety of special courses available throughout the United States dealing with this subject matter, only rather unique aspects justify additional offerings in these areas. Our programs were planned to be unusual in the respect that "hands-on" experiences were inherent and required for completion of each course. Use of hand-held programmable calculators, application of optimization programs using computer graphics, lay-up and cure of a simple part in graphite epoxy and testing tensile, shear and compression coupons to failure were all part of the first course. As part of the second course, workshop sessions were held in RPI's Computer Graphics Center. In these sessions the enrolled engineers and managers defined, "constructed" and analyzed their own finite element models on refresh graphics terminals.

Faculty-staff and attendees for the courses were as follows:

Composite Materials and Structures

Program Director:

R. G. Loewy  
Institute Professor  
Rensselaer Polytechnic Institute

## Faculty:

R. Judd Diefendorf  
Professor, Materials Eng.  
Rensselaer Polytechnic Inst.

H. Gunther Helwig  
Design Specialist, Compos-  
ites Group  
Dornier System GmbH

S. Leigh Phoenix  
Associate Professor, Me-  
chanical and Aeronautical  
Engineering  
Cornell University

Stephen W. Tsai  
Chief, Mechanics and Sur-  
face Interactions Branch  
Air Force Materials Lab.  
Wright-Patterson AFB

Dick J. Wilkins  
Sr. Engineering Specialist  
General Dynamics, Fort  
Worth

## Students:

William Appleman  
Mechanical Engineer  
David Taylor Naval Ship  
R & D Center

John T. Blaha  
Deputy Director of Flight  
Testing  
Edwards Air Force Base

Huey D. Carden  
Aerospace Technologist  
NASA Langley Research Ctr.

Dan Christmore  
Engineer  
Gates Lear Jet

James P. Cycon  
Rotor Systems Design Analyst  
Skikorsky Aircraft

John Emerson  
Structural Engineer Sales  
Manager  
Information Systems Design

Philip J. Granum  
Mechanical Engineer  
David Taylor Naval Ship  
R & D Center

Thomas F. Grapes  
Senior Engineer  
Westinghouse Electric Corp.

David Hazelton  
Development Engineer  
Oak-Fothergill, Inc.

George J. Hewitt  
Structures Supervisor  
Heath Tecna Precision  
Structures, Inc.

Alan Kemp  
Engineer Specialist  
Information Systems Design

Patrick E. Kunc  
Engineer  
Baltimore Division  
Martin Marietta Corporation

Vladimir Roth  
Research Assistant Professor  
Rensselaer Polytechnic Inst.

Charles R. Swats  
Aerospace Engineer  
Applied Technology Lab.  
United States Army Research  
and Technology Laboratories

James Y. A. Wang  
Baltimore Division  
Martin Marietta Corporation

The Finite Element Approach in Structural Analysis

Program Director:

Mark S. Shephard  
Assistant Professor  
Civil Engineering  
Rensselaer Polytechnic Inst.

Faculty:

Richard H. Gallagher  
Dean, College of Engineering  
University of Arizona

Mark S. Shephard  
Assistant Professor  
Civil Engineering  
Rensselaer Polytechnic Inst.

Students:

Gaston Beaulieu  
Structural Scientist  
Hydro-Quebec  
Varenes, Canada

James Finkel  
Development Engineer  
General Tire and Rubber Co.

Samuel M. Goldfarb  
Mechanical Engineer  
IBM, Poughkeepsie

Aaron D. Gupta  
Mechanical Engineer  
United States Army Ballistic  
Research Laboratory  
Aberdeen Proving Ground

Matt Harris  
Engineer  
Eastman Kodak Company

Zbigniew Karaszewski  
Mechanical Engineer  
Military Sealift Command,  
Atlantic

Timothy Peters  
Project Engineer  
R & D Division  
Chamberlain Manufacturing  
Corporation

Sanjay Shinde  
Senior Research Engineer  
Esso Research of Canada  
Calgary, Canada

Tommy N. White  
Aerospace Engineer  
Naval Air Rework Facility

Reaction to these offerings on the part of the participants was again highly favorable, and we plan to make these offerings again in 1982.

#### 4. Summary

In short, the NASA/AFOSR Composites Aircraft Program is a multi-faceted program planned and managed so that scientists and engineers in a number of pertinent disciplines will interact to achieve its goals. Research in the basic composition, characteristics and processing science of composite materials and their constituents is balanced against the mechanics, conceptual design, fabrication and testing of generic structural elements typical of aerospace vehicles so as to encourage the discovery of unusual solutions to present and future problems. In the following sections, more detailed descriptions of the progress achieved in the various component parts of this comprehensive program are presented.

PART II  
CONSTITUENT MATERIALS

II-A A STEP IN DETERMINING TRANSVERSE FIBER PROPERTIES:  
CHARACTERIZATION OF HOMOGENEITY IN COMPOSITE MATERIALS

PRECEDING PAGE BLANK NOT FILMED

II-A A STEP IN DETERMINING TRANSVERSE FIBER PROPERTIES:  
CHARACTERIZATION OF HOMOGENEITY IN COMPOSITE MATERIALS

Senior Investigator: R. J. Diefendorf

1. Introduction

Transverse properties are important characteristics of fibers to be used as constituent materials in structural composites. The small diameters of fibers ( $\sim 8\mu$ ), however, makes it difficult to evaluate transverse fiber properties. This is especially true for the transverse thermal expansion of a single fiber which requires accuracy of the order of several angstroms. An alternate approach is to evaluate various composite laminates with differing volume fractions and plot the property versus fiber volume percent and extrapolate to 100% fiber volume percent. The implicit assumption is that it is far easier to measure volume fraction and dimensional change on a larger object and to accomplish the task with a greater certainty than for a single fiber. Therefore, the task transforms into producing a reliable estimate for volume fraction and a theory for transverse properties with anisotropic constituents. As is well-known, the transverse properties of a fibrous composite, unlike longitudinal properties, depend upon the fiber packing geometry. A subtle concept that has, as of yet, not been fully explored\*, is the effect of localized packing geometries on the properties. For example, a composite

---

\*Holliday, Leslie (Ed), Composite Materials, p. 11, Elsevier Publishing Co., Amsterdam (1966) presents the only mention of this phenomenon known to exist.

that has an overall volume fraction of 65% may have an area with localized highs and lows of 72% and 50% respectively, while a second area (also with an overall volume fraction of 65%) could have relative high and low volume fractions of 67% and 60% (Figure II-A-1). The issue presented is to what degree, if any, does this inhomogeneity affect composite properties and performance. An extension of this concept is how can this index of homogeneity be quantified for use as a comparative measure and, if possible, to relate the index to the somewhat abstract (and often inadequately defined) concepts of poor and acceptable laminates.

## 2. Status

In order to obtain an estimate for the overall volume fraction of the fabricated laminates, the method of nitric digestion was employed. The samples were weighed, both in air and submerged in water, to determine specific gravity. Samples were then boiled in 100 ml of  $\text{HNO}_3$  (nitric acid) at a temperature of  $177^\circ\text{C}$  for 90 minutes and then drained and filtered through a porous ceramic crucible with acetone and water. The residual fibers were heated at  $120^\circ\text{C}$  for two hours and then cooled in a desiccator. Fibers were then weighed and Boeing method MS 8-212A was used to calculate the volume fraction. The measurements are presented in Table II-A-1 for several of the many specimens tested.

### 3. Progress During Report Period

It has already been established that the accurate determination of volume fraction is critical to the work. It becomes apparent that standard techniques alone, in this case nitric digestion, are not sufficient for the required accuracy. It is for this reason that two other methodologies are being evaluated to crosscheck the volume fraction, namely ASTM's photomicrograph grid technique and image analysis. To insure that only minimal discrepancies arise between the various techniques, the latter two approaches utilize the same photomicrograph.

A specimen, Number 18, was chosen from those listed in Table II-A-1 for further study. The sample was mounted in epoxy, polished and photomicrographs taken. In order to determine the volume fraction from the pictures via ASTM's grid technique, a grid network consisting of lines spaced a quarter of an inch apart in both the horizontal and vertical directions on transparent mylar film was constructed. The grid area was

TABLE II-A-1  
SPECIFIC GRAVITY AND VOLUME FRACTIONS  
USING NITRIC ACID DIGESTION

<u>Plate Number</u>	<u>Specific Gravity</u>	<u>Fiber Volume Fraction *</u>	<u>Resin Fraction *</u>	<u>Voids *</u>
18	1.6482	68.3	30.6	1.1
20	1.5403	68.1	28.9	3.0
30	1.4320	49.7	46.7	3.6
31	1.5313	69.4	26.2	4.4

\*All values are percentages.

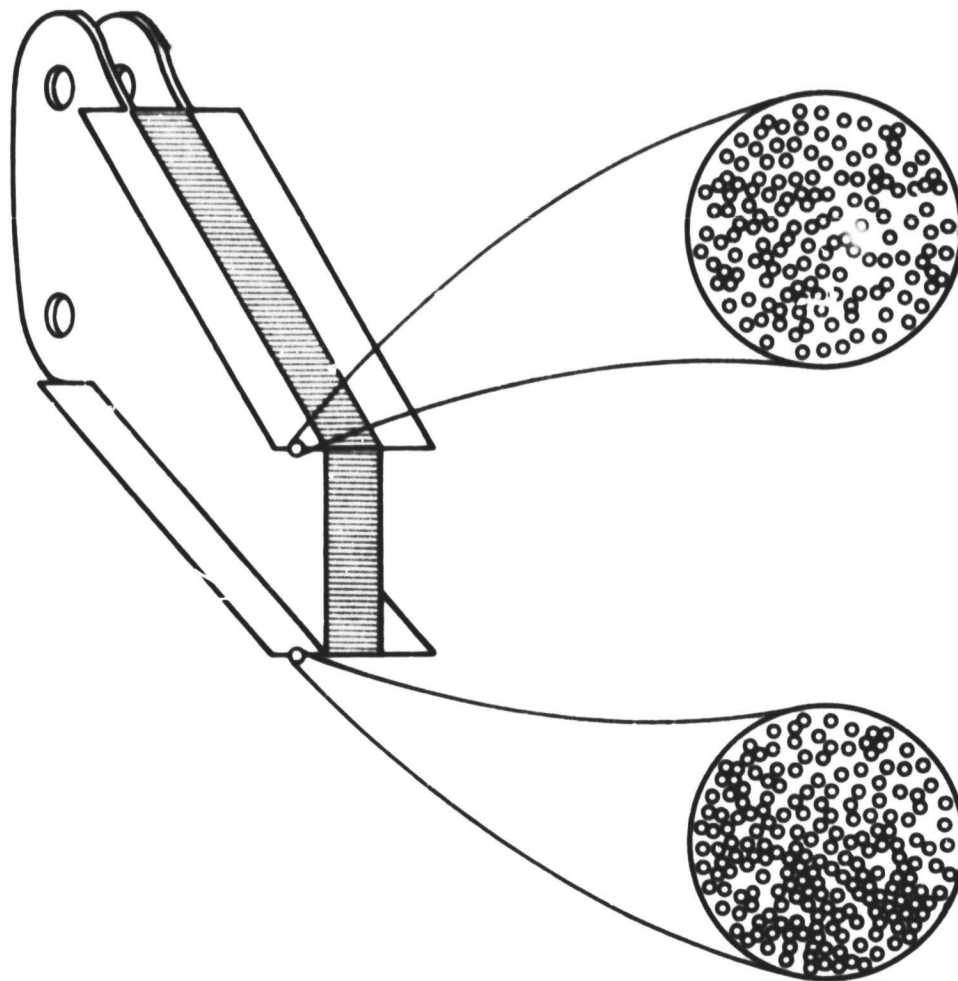


Figure II-A-1.  
Schematic Diagram of the Variation of Volume Fraction Within a Fabricated Part

constructed so as to contain ten intersections on a side (10 x 10) or 100 to the sheet. The grid was then laid at random on the photomicrograph and the number of intersections that fell on top of a fiber were counted, thus the total yields a sample value for volume fraction. This procedure was repeated ten times for each picture with the results averaged for an overall measure of volume fraction. A listing of the data is given in Table II-A-2. It is conceivable that the grid size

TABLE II-A-2  
COMPARISON OF VOLUME FRACTION DETERMINATIONS USING  
GRID AND IMAGE ANALYSIS TECHNIQUES

	Picture Number							
	<u>18-1</u>	<u>18-2</u>	<u>18-3</u>	<u>18-4</u>	<u>18-5</u>	<u>18-6</u>	<u>18-7</u>	<u>18-8</u>
Image Analysis	66.1	70.0	66.0	63.9	67.1	67.2	76.1	71.7
10 x 10 Grid	68.9	70.3	65.9	65.9	65.5	66.1	72.5	70.6
5 x 4 Grid	68.5	66.3	62.3	67.5	67.0	63.5	70.8	69.3

OVERALL STATISTICS

	<u>Image Analysis</u>	<u>10 x 10 Grid</u>	<u>5 x 4 Grid</u>
Number	24	80	80
Mean	68.4	68.2	66.9
Standard Deviation	3.69	4.39	8.46
Variance	13.03	19.06	70.70

could affect the results of the analysis significantly. A 5 x 4 grid was constructed and the analysis reperformed with the results being not too different from the original case.

Image analysis was performed on a Bausch and Lomb FAS/II image analysis system that utilizes a Data General microprocessor (Figure II-A-2). Each of the eight pictures was resolved for volume fraction with the results listed in Table II-A-3. It is important to point out that the values listed for each picture used in image analysis are the averages of three values, while for the case of the grids the values presented are the averages of ten readings. An average overall reading is also presented in the table as is data for standard deviation and variance. The variance is of particular interest since it may be helpful in formulating a homogeneity index. The next phase was the subdivision of the main field into fields of equal area. The subfields were progressively divided into halves down to one-thirty-second of the original area. Volume fraction data was collected for each of the full, half, quarter, eighth, sixteenth and one-thirty-second fields. Averaged data for groups of ten measurements is presented in Table II-A-4 and Figure II-A-3.

Each of the values of volume fraction in Table II-A-4 is an average of ten values. The values presented for standard deviation and variance result from the statistical analysis of these sets of ten measurements. The values of variance can be subdivided as follows, assuming that the contributing errors

ORIGINAL PAGE  
BLACK AND WHITE PHOTOGRAPH



Figure II-A-2.  
Bausch & Lomb FAS/II - Image Analysis System

TABLE II-A-3  
 VOLUME FRACTION RESULTS FROM PHOTOMICROGRAPH GFIL ANALYSIS

Trial #	Picture # 18-1	Picture # 18-2	Picture # 18-3	Picture # 18-4	Picture # 18-5	Picture # 18-6	Picture # 18-7	Picture # 18-8
1	76.0	75.0	69.5	61.5	62.5	70.0	75.0	68.0
2	66.0	66.0	73.0	62.5	62.0	67.0	68.0	70.5
3	64.0	74.5	74.5	73.0	64.0	64.0	76.5	71.0
4	69.0	72.0	59.0	68.5	57.5	62.5	72.5	72.0
5	64.0	69.0	61.5	67.0	69.0	66.0	65.5	75.0
6	67.0	70.5	63.5	62.0	67.0	63.5	75.0	67.0
7	71.0	71.5	65.0	64.5	69.0	62.5	72.0	74.0
8	72.5	64.5	63.0	66.5	68.5	66.5	75.5	70.0
9	68.0	68.5	60.5	63.0	66.0	67.0	74.0	68.0
10	71.0	71.0	69.5	69.5	69.0	72.0	70.5	70.5
<hr/>								
AVERAGE	68.9	70.3	65.9	65.9	65.5	66.1	72.5	70.6
<hr/>								
Standard Deviation	3.84	3.36	5.39	3.67	3.88	3.14	3.55	2.58
Variance	13.30	10.16	26.14	12.14	13.57	8.89	11.32	5.99
<hr/>								

STATISTICS FOR ALL 80 READINGS

Mean..... 68.20  
 Standard Deviation. 4.39  
 Variance..... 19.06

\* All values are percent fiber volume.

TABLE II-A-4  
VOLUME FRACTION DATA FROM SUBFIELD ANALYSIS

	<u>32<sup>nds</sup></u>	<u>16<sup>ths</sup></u>	<u>8<sup>ths</sup></u>	<u>4<sup>ths</sup></u>	<u>Halves</u>	<u>Full</u>
	62.8	52.7	62.7	63.5	67.4	68.6
	58.5	58.1	67.7	65.4	64.9	-----
	71.1	66.9	74.2	63.0	64.8	-----
	66.0	63.1	63.0	64.9	68.3	
	63.5	69.3	60.9	62.9	-----	
	64.6	65.5	62.6	66.4		
	70.6	65.4	60.8	60.8		
	70.2	71.2	67.8	65.6		
	69.2	76.5	58.7	-----		
	53.2	66.6	60.1			
	50.3	70.1	62.8			
	64.2	63.5	65.4			
	59.9	60.1	59.0			
	70.6	63.7	64.5			
	68.5	50.5	57.6			
	66.2	62.5	74.3			
-----						
Mean	64.2	63.9	64.1	66.4	66.8	66.0
Standard Deviation	6.325	5.003	1.842	1.771	2.616	-----
Variance	38.754	23.465	2.970	2.353	3.423	-----

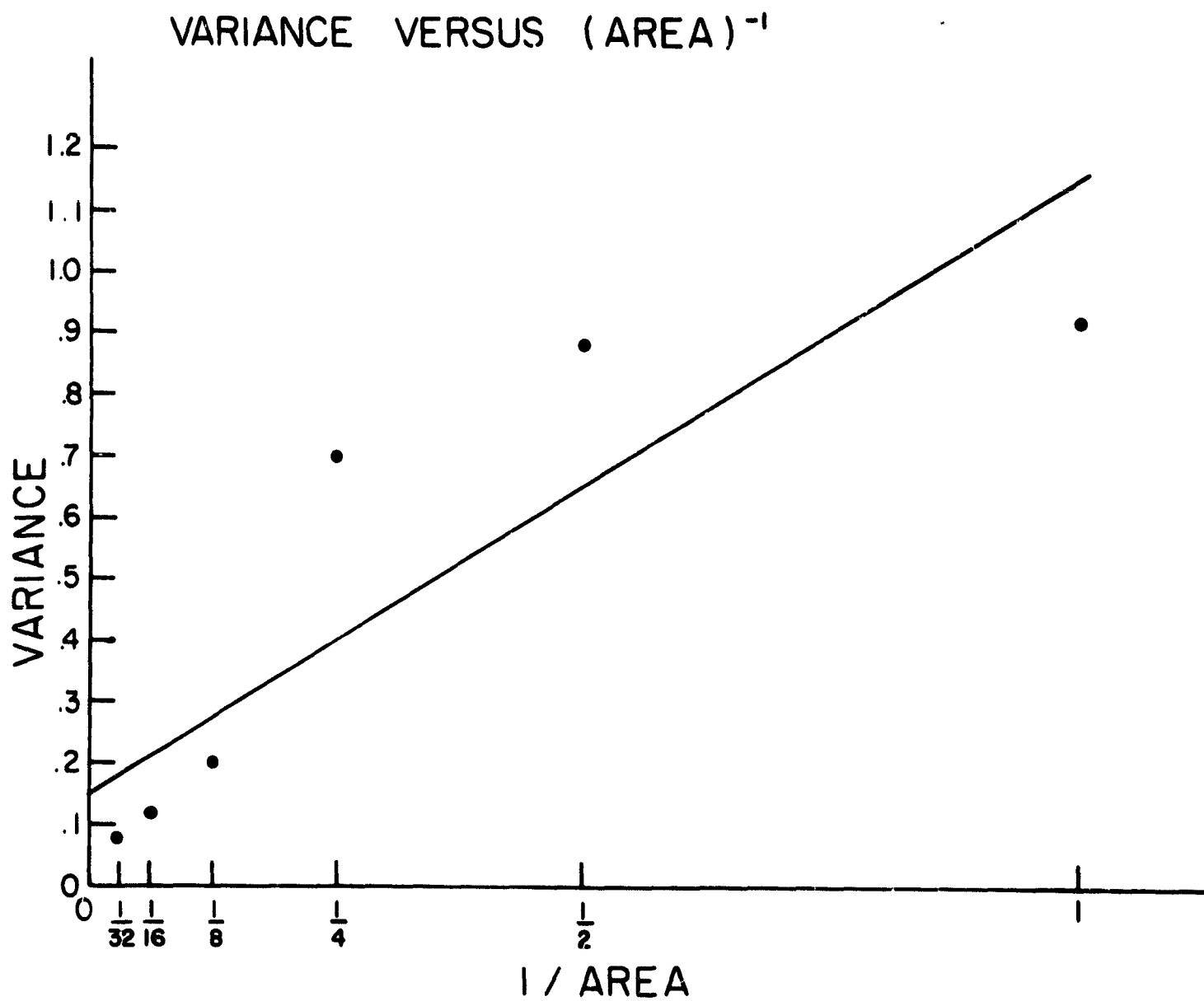


Figure (I-A-3).

are independent.

$$\sigma_m^2 = \sigma_o^2 + \sigma_{p/n}^2 \quad (1)$$

Where:

$\sigma_m^2$  is the sum of variances due to measurement,

$\sigma_o^2$  is the variance due to random events,

$\sigma_{p/n}^2$  is the variance due to the pixel count of the image analysis system divided by the number of fields.

Due to the  $\sigma_{p/n}^2$  term,  $\sigma_m^2$  is a function of the area of measurement and increases as the number of subfields increase. The data is plotted in Figure II-A-3 along with the "theoretical" curve determined by a manual, least squares fit assuming a slope of unity (the pixel errors are directly proportional to pixel count). The intercept of 0.15 implies that if a field of infinite dimensions were analyzed an infinite number of times, a variance of 0.15 would result. This variance is the  $\sigma_o^2$  term and is free from field size effects. Since  $\sigma_o^2$  and  $\sigma_{p/n}^2$  are known,  $\sigma_m^2$  can be determined. The importance of determining  $\sigma_m^2$  becomes apparent when a plot of volume fraction versus number of fields is constructed as in Figure II-A-4. In order to estimate the true sample-to-sample variance, it is necessary to correct for the contribution due to measurement error. This can be accomplished by means of the following equation which, once again, assumes that the errors are independent.

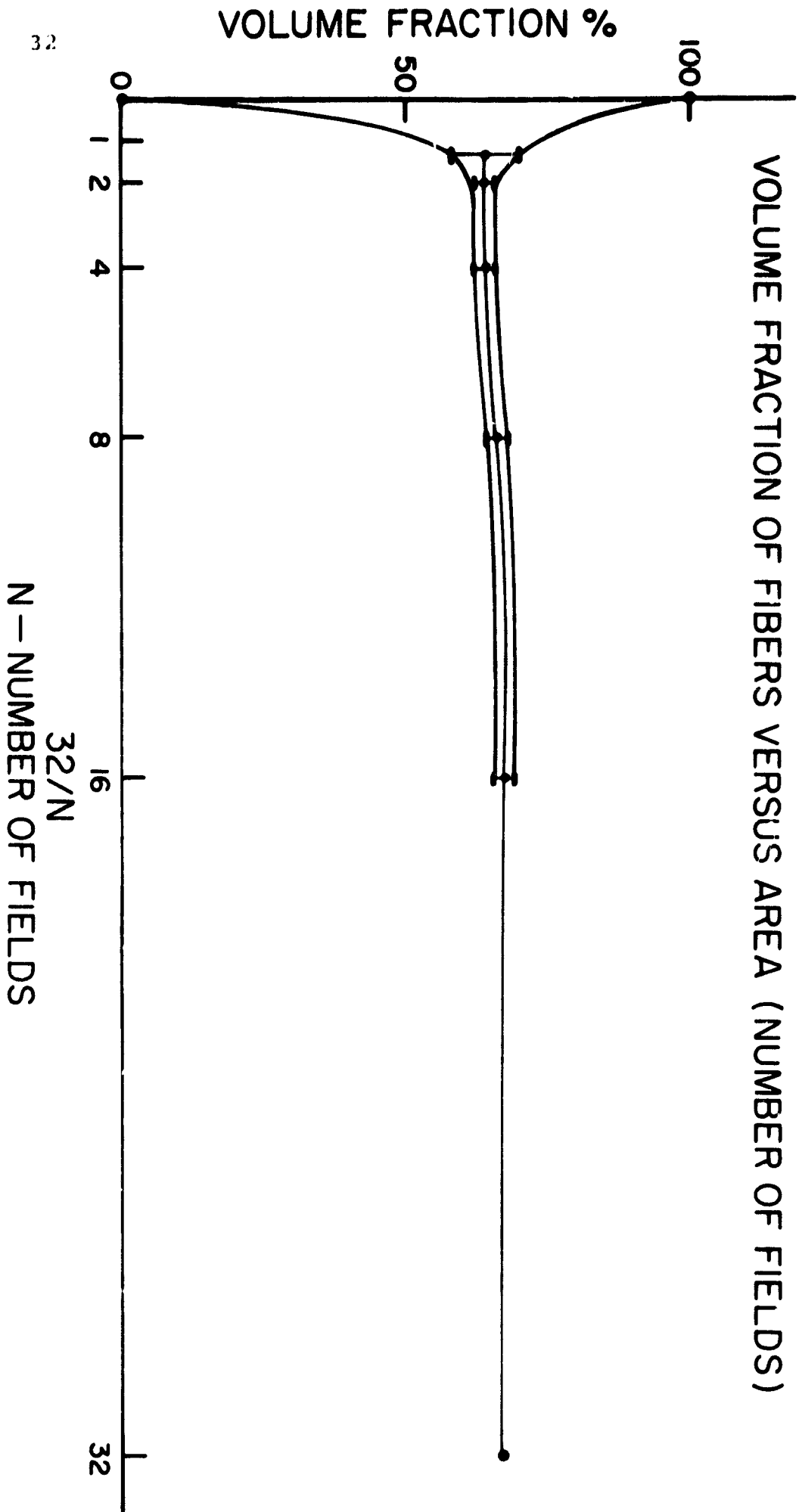


Figure II-A-4.

$$\sigma^2 = \sigma_s^2 + \sigma_m^2 \quad (2)$$

Where:

$\sigma^2$  is the overall variance for every measurement performed for a given subfield (i.e., for all 320 measurements in the case of 32nds, 160 for 16ths, etc.),

$\sigma_s^2$  is the variance due to the samples (unknown, to be solved for) and

$\sigma_m^2$  is the measurement variance as defined in Equation (1).

After  $\sigma_s^2$  has been solved for, the standard deviation is calculated by taking the square root. The "error" bars around the volume fraction data in Figure II-A-4 are one standard deviation above and below the mean value. The increase in standard deviation for small sample areas indicates an increase in the non-homogeneity of composite samples as the sample area is decreased. Comparison of this change in standard deviation with that obtained from the theoretical value associated with a uniform hexagonal or square array composite can be used as an index of homogeneity.

#### 4. Plans for Upcoming Period

Future work will evaluate the importance of considering an index of homogeneity in composite materials. Studies will continue on transverse properties in composites. Comparison of properties with the index of homogeneity will be made. Finally, transverse properties of anisotropic fibers such as carbons and aramids will be derived from composite data.

**PRECEDING PAGE BLANK NOT FILMED**

**PART III  
COMPOSITE MATERIALS**

- III-A ADVANCED ANALYSIS METHODS
- III-B FATIGUE IN COMPOSITE MATERIALS
- III-C MOISTURE AND TEMPERATURE EFFECTS ON THE MECHANICAL PROPERTIES OF LAMINATES
- III-D NUMERICAL INVESTIGATION OF MOISTURE EFFECTS
- III-E NUMERICAL INVESTIGATION OF THE MICROMECHANICS OF COMPOSITE FRACTURE

DATE 34 INTERCOMPARISON

### III-A ADVANCED ANALYSIS METHODS

Senior Investigator: E. J. Brunelle

#### 1. Introduction

Because many parameters exist in a given composite (or orthotropic) plate problem, the established methods of analysis are of little help in trying to answer the basic question "What are the general solution trends when I increment these variables and hold those variables constant?". A much clearer picture of how an individual orthotropic lamina (a plate) behaves has been made possible by previous work under joint NASA/AFOSR sponsorship. This work has continued during the current reporting period by enlarging the scope of some previous results and by introducing some new ideas.

#### 2. Status

The principal results of the last period were the following derivations, and some solutions, to a wide range of problems associated with specially (and generally) orthotropic plates.

- a) The simplest micromechanics description of  $D^* = D^*(\dot{V}_f, E_f/E_m, \nu_f, \nu_m)$  was formulated with the main intent of showing  $0 \leq D^* \leq 1$ ; this indeed was the case and additionally, light was shed on low fiber volume behavior.
- b) The generally orthotropic plate problem (and hence the generalized plane stress problem)

was transformed into rotated (thru an angle  $\theta$ ) and affinely stretched coordinates such that only three coefficients remain in the formulation ( $\bar{L}$ ,  $\bar{D}$ ,  $\bar{R}$ ) and each of these coefficients is only a function of  $D^*$ ,  $D_{11}/D_{22}$  and the rotation angle  $\theta$ .

- c) The von Kármán-Rostovstev nonlinear plate equations were reduced to equations with only two parameters,  $D^*$  and  $H^*$ , where it was possible to show additionally that  $H^* = H^*(D^*, \epsilon)$ .
- d) Similarity laws were presented for a class of buckling problems which demand only that given number pairs must be invariants when proceeding from solution 1 to solution 2.

### 3. Progress During Report Period

Effort in a number of diverse areas has produced the following results (a through d).

- a) Attempts to find general solutions for the homogeneous problem associated with the general orthotropic plate have had very limited success; the literature is replete with interesting but specialized results. The first major stumbling block is that the equation to be solved,

$$D_{11} \frac{\partial^4 w}{\partial x^4} + D_{16} \frac{\partial^4 w}{\partial x \partial y^3} + 2(D_{12} + 2D_{66}) \frac{\partial^4 w}{\partial x^2 \partial y^2} + D_{26} \frac{\partial^4 w}{\partial y \partial x^3} + D_{22} \frac{\partial^4 w}{\partial y^4} = 0,$$

has six elastic constants whose ranges are not well-defined\*. If  $D_{12} + 2D_{66}$  is considered<sup>d</sup> to be a single constant and if one divides them by any convenient constant (usually  $D_{11}$  or  $D_{22}$ ), then four hybrid constants\*\* still remain. An appropriate affine transformation, reported on in the last progress report, reduces the problem to

$$\frac{\partial^4 w}{\partial x_0^4} + \bar{L} \frac{\partial^4 w}{\partial x_c \partial y_0^3} + 2\bar{D} \frac{\partial^4 w}{\partial x_0^2 \partial y_0^2} + \bar{R} \frac{\partial^4 w}{\partial y_0 \partial x_0^3} + \frac{\partial^4 w}{\partial y_0^4} = 0$$

where

$\bar{L}$ ,  $\bar{D}$  and  $\bar{R}$  depend only on two parameters  $(D_{11}/D_{22})_{\theta=0}$  and  $(D^*)_{\theta=0}$  and the rotation angle  $\theta$ .

Assuming complex exponential solutions  $w = e^{\lambda x_0} e^{\omega y_0}$  one finds

$$\mu^4 + \bar{R}\mu^3 + 2\bar{D}\mu^2 + \bar{L}\mu + 1 = 0$$

where

$\mu = \frac{\lambda}{\omega}$  and where the "over-bars" will be dropped in the sequel.

Since complex roots are expected also for  $\mu$ , the factored form is left in terms of two quadratic expressions

$$(\mu^2 + a_1\mu + b_1)(\mu^2 + a_2\mu + b_2) = 0$$

where the  $a_\alpha$  and  $b_\alpha$  ( $\alpha = 1, 2$ ) are given by the well-known results

\* However, their dependence on the rotation angle  $\theta$  from principal directions is known explicitly.

\*\* They are called constants in most of the literature, but they are obviously parameters depending on the rotation angle  $\theta$  and their values at some reference  $\theta$ , usually  $\theta = 0$ .

$$\begin{aligned}
 a_1 + a_2 &= R \\
 b_1 + a_1 a_2 + b_2 &= D \\
 a_1 b_2 + b_1 a_2 &= L \\
 b_1 b_2 &= 1
 \end{aligned}$$

Dividing the quartic by  $\mu^4$  one finds

$$\frac{1}{\mu^4} + L \frac{1}{\mu^3} + 2D \frac{1}{\mu^2} + R \frac{1}{\mu} + 1 = 0$$

This is not usually of much help, but our constants L and R are related by

$$L(\theta) = R(90 - \theta)$$

$$R(\theta) = L(90 - \theta)$$

$$D(\theta) = D(90 - \theta)$$

hence the second quartic may be written as (switching L and R),

$$\frac{1}{\mu^4} + R \frac{1}{\mu^3} + 2D \frac{1}{\mu^2} + L \frac{1}{\mu} + 1 = 0$$

Therefore, if  $\mu_i$  ( $i = 1, 2, 3, 4$ ) are the roots of the first quartic, then  $\frac{1}{\mu_i}$  are the roots of the second (above) quartic. Furthermore, more information can be extracted from this process, and it is presented below as a new theorem of abstract algebra.

Given the quartic in the two equivalent forms shown

$$\mu^4 + R\mu^3 + 2D\mu^2 + L\mu + 1 = 0$$

and

$$(\mu^2 + a_1\mu + b_1)(\mu^2 + a_2\mu + b_2) = 0$$

then

$$b_1(R, D, L) = b_1(L, D, R)$$

with the corollary results

$$b_2(R, D, L) = b_2(L, D, R)$$

and

$$a_1 a_2(R, D, L) = a_1 a_2(L, D, R).$$

Since  $b_1$  and  $b_2$  will be positive for complex roots of the  $\mu$ -equation, it is seen that  $b_1$  (or  $b_2$ ) has the range 0 to 1. Thus it is very quick and easy to find the  $a_\alpha$  and  $b_\alpha$  coefficients. Furthermore, because of the  $L(\theta) = R(90 - \theta)$  etc. relations, the range of  $\theta$  to be examined is cut in half, which represents another large reduction in the operations to be carried out.

This work directly impacts on all the literature concerned with finding homogeneous solutions for plate problems and all plane-stress/plane-strain problems. It currently appears that all of the useful but very clumsy procedures for solving complete plate problems (reorthogonalization expansions, bi-orthogonal expansions of related first-order systems of equations, generalizations of the Fadle-Papkovitch techniques, etc.) can be expressed with much more clarity due to the above advances.

b) Exact lower solutions bounds for the specially orthotropic plate can be obtained by letting  $D^* = 0$ . Thus if we consider the vibration problem, the relation

$$\frac{\partial^4 w}{\partial x_0^4} + 2D^* \frac{\partial^4 w}{\partial x_0^2 \partial y_0^2} + \frac{\partial^4 w}{\partial y_0^4} + M\ddot{w} = 0 \quad (1)$$

becomes

$$\frac{\partial^4 w}{\partial x_0^4} + \frac{\partial^4 w}{\partial y_0^4} + M\ddot{w} = 0 \quad (2)$$

The first reaction is that one can hardly expect meaningful solutions for the  $D^* = 0$  case. However, this was exactly the case for the buckling solutions reported on previously; the  $D^* = 0$  solutions of  $k_0$  versus  $a_0/b_0$  produced very useful lower bounds, just as  $D^* = 1$  produced very meaningful upper bounds (the quasi-isotropic solution). Those  $D^* = 0$  solutions were obtained by the limiting solution of the first equation (1) and not by the direct solution of the second equation (2). Introducing

$$w(x_0, y_0, t) = X(x_0)Y(y_0)e^{i\omega t}$$

in Equation (2) for a direct solution, one obtains

$$X^{IV}Y + Y^{IV}X - M\omega^2 XY = 0 \quad (3)$$

It is seen immediately that this is a separable equation, hence, exact solutions can be found for arbitrary boundary conditions on all four edges. Thus, for example, an exact solution can be obtained for the plate clamped on all four edges when  $D^* = 0$ . Not only can the eigenvalue problems be solved (vibration and buckling), but the static deflection problems also can be solved by expansions in terms of the eigenfunctions (mode shapes) of the associated homogeneous solution (this is a standard technique of mathematical

physics). Furthermore, the dynamic response problems for  $D^* = 0$  can also be obtained in terms of generalized coordinate-weighted eigenfunction expansions (again a standard technique). Separating Equation (3) one has

$$X^{IV} + [k^4 - M\omega^4]X = 0 \quad \text{and} \quad Y^{IV} - k^4Y = 0$$

where the separation constant, for illustrative purposes, has been chosen as  $-k^4$ . It is noted that the separation constant can be  $+k^4$ ,  $-k^4$  or 0. The correct choice is that value which allows the boundary conditions of the problem to be satisfied.

As an example of this procedure, it can be verified that the exact solution for the non-dimensional frequency of the SS-C-SS-C plate with  $D^* = 0$  is

$$\Omega_{mn}^2 = \left( \frac{mb_0}{a_0} \right)^4 + \left( \frac{2n-1}{4} \right)^4$$

where

$$\Omega_{mn}^2 \equiv M\omega_{mn}^2 \left( \frac{b_0}{\pi} \right)^4$$

Furthermore, for small values of  $2D^* = \epsilon$  one may write

$$\frac{\partial^4 w}{\partial x_0^4} + \epsilon \frac{\partial^4 w}{\partial x_0^2 \partial y_0^2} + \frac{\partial^4 w}{\partial y_0^4} = q(x_0, y_0)$$

and using regular perturbation expansion techniques, one may assume

$$w = \sum_{n=0}^{\infty} w_n(x_0, y_0) \epsilon^n$$

so that the sequential set of equations

$$\frac{\partial^4 w_1}{\partial x_0^4} + \frac{\partial^4 w_1}{\partial y_0^4} = q(x_0, y_0)$$

$$\frac{\partial^4 w_2}{\partial x_0^4} + \frac{\partial^4 w_2}{\partial y_0^4} = -\frac{\partial^4 w_1}{\partial x_0^2 \partial y_0^2}$$

$$\frac{\partial^4 w_{k+1}}{\partial x_0^4} + \frac{\partial^4 w_{k+1}}{\partial y_0^4} = -\frac{\partial^4 w_k}{\partial x_0^2 \partial y_0^2}$$

may be solved to any given  $k$  value. Thus the stage is set for solving not only static problems (the above development) but also stability and dynamics problems for small  $\epsilon$ . It is noted that one is again able to specify arbitrary boundary conditions for all these problems.

c)  $D^*$  is the fundamental plate parameter for the specially orthotropic plate. Its behavior, via simple micromechanics, has been displayed versus the fiber volume for constant values of  $E_f/E_m$ ,  $\nu_f$  and  $\nu_m$ . From that perspective, much information about the incremental behavior of  $D^*$  can be obtained. An even simpler way of looking at the incremental behavior of  $D^*$  is to express  $dD^*$  in terms of the macroscopic definition of  $D^*$ . Thus, since

$$D^* = \frac{D_{12} + 2D_{66}}{\sqrt{D_{11}D_{22}}}$$

it can be verified that

$$\frac{dD^*}{D^*} = \epsilon \frac{dD_{12}}{D_{12}} + (1 - \epsilon) \frac{dD_{66}}{D_{66}} - \frac{1}{2} \left( \frac{dD_{11}}{D_{11}} + \frac{dD_{22}}{D_{22}} \right)$$

where the identity  $D^* = \epsilon D^* + (1 - \epsilon) D^*$  has been invoked.

It is thus seen that for a given incremental value of the plate constants, the  $\frac{dD_{66}}{D_{66}}$  term yields the largest contribution to the  $\frac{dD^*}{D^*}$  expression since its coefficient  $(1 - \epsilon)$  is larger than the  $\epsilon$  coefficient of  $\frac{dD_{12}}{D_{12}}$  or larger than the  $\frac{1}{2}$  coefficient of both  $\frac{dD_{11}}{D_{11}}$  and  $\frac{dD_{22}}{D_{22}}$ .

With this established,  $\frac{dk_o}{k_o}$  and  $\frac{d\Omega^2}{\Omega^2}$  may be found, and as an example, the results for a simply supported specially orthotropic plate are given below (where the similarity number  $z = \frac{b_o m}{a_o n}$  has been used).

$$\frac{dk_o}{k_o} = \left( \frac{D^*}{D^* + 1} \right)$$

$$\frac{d\Omega_{mn}^2}{\Omega^2} = \left[ \frac{2z^2}{z^4 + 2D^*z^2 + 1} \right] \left[ (z^2 + D^*) \frac{dz}{z} + D^* \frac{dD^*}{D^*} \right]$$

d) The similarity rules for vibration of a specially orthotropic plate have been derived and are being used in a nearly completed Masters' Thesis to compute the frequency spectrum  $\Omega_{ml}$ ;  $m = 1, 2, 3, \dots$  versus  $a_o/b_o$  for the  $D^*$  range of 0 to 1. Six sets of boundary conditions were chosen for the  $y_o = 0$  and  $b_o$  sides, the  $x_o = 0$  and  $a_o$  sides being simply supported.

The use of the affine transformation technique and the similarity rule have permitted, for the first time, enormous

amounts of frequency information (including important trends) to be presented in an extremely compact fashion. Letting

$$\phi = \frac{a_0}{mb_0} ,$$

the similarity rules can be written as:

$$(\phi_1)^2 = \left( \frac{D_2^*}{D_1^*} \right) (\phi_2)^2$$

and

$$(\Omega_{mn}^2)_1 = \left[ \frac{D_1^*}{(\phi_2)^2 D_2^*} \right]^2 \left[ 1 - \left( \frac{D_1^*}{D_2^*} \right)^2 \right] + \left( \frac{D_1^*}{D_2^*} \right)^4 \left[ \Omega_{mn}^2 \right]_2$$

when  $D^* = 0$ . When  $D^* = 0$  it can be verified that a single rule exists, which is

$$(\Omega_{mn}^2)_1 = (\phi_2)^{-4} \left[ -1 + (\Omega_{mn}^2)_2 (\phi_2)^4 \right] + (\phi_1)^{-4}$$

#### 4. Plans for Upcoming Period

Results are being compiled to furnish a general overview of the affine transformation process and the similarity laws for orthotropic structures and the frequency spectrum of specially orthotropic plates using the similarity laws for vibration. This latter work is that of graduate student Chikuang Chen.

At this time the new theories presented have not had enough supporting problems worked out to properly display their usefulness. As seems needed, specific problems will be worked to illustrate points of interest.

A recent composite box-beam wing theory due to Weisshaar\* will be re-cast in its affine plane form to provide results of greater generality and will be extended to include simple non-symmetric flight maneuvers that provide large bending-twist-extension effects which yield opposite trends on the left and right wing. A senior student (Mr. Don Argintar) will be doing a senior project next semester based on this rederivation and extension. Forward sweep, aft sweep and oblique sweep configurations will be considered.

5. Current Publications or Presentations by  
Professor Brunelle on this Subject

"Thermal Buckling of Initially Stressed Thick Plates"

Presented at the 4th Failure Prevention and Reliability Conference (Joint ASME Vibrations, Design Automation, F-P, R Conference), Hartford, Connecticut, September 20-23, 1981.

---

\*Weisshaar, Terrence A., "Aeroelastic Stability and Performance Characteristics of Aircraft with Advanced Composite Sweptforward Wing Structures", AFFDL-TR-78-116, Sept. 1978.

### III-B FATIGUE IN COMPOSITE MATERIALS

Senior Investigator: E. Krempl

#### 1. Introduction

The deformation and failure behavior of graphite-epoxy tubes under biaxial (tension, torsion) loading is investigated as part of the research of Ph.D. candidate T.-M. Niu. The aim of this research is to provide basic understanding and design information on the biaxial response of graphite/epoxy composites.

#### 2. Status

Static tests on thin-walled graphite/epoxy ( $\pm 45$ )<sub>4</sub> tubes showed that the axial tensile and compressive strength are approximately equal. However, the ultimate strength in torsion depends strongly on the direction of twist. Axial fatigue tests under completely reversed, load-controlled conditions showed a comparatively poor fatigue performance. Also, there was an influence of frequency on fatigue life.

#### 3. Progress During Report Period

The major emphasis was on preparatory work for fatigue tests under combined in-phase and out-of-phase loading. A total of ninety tubular specimens were made and machined. They are ready for testing.

During this reporting period, the project used a new 463 Data and Control Unit using a PDP 11/23 computer and a Tektronix 4025 terminal in conjunction with the MTS tension-torsion

servohydraulic system. Driver programs were written and debugged for biaxial in-phase and out-of-phase loading. Difficulties were encountered initially with the MTS software (RPI received the first 463 Data and Control Unit) which are now resolved. The programs have been tested with and without graphite/epoxy tubes. The driver programs and the data acquisition system are now fully operational.

A technical report entitled "Graphite/Epoxy ( $\pm 45$ )<sub>4</sub> Tubes: Their Static Axial and Shear Properties and Their Fatigue Behavior under Completely Reversed, Load-Controlled Loading" was written and is the first item in Section 5 below. It has been submitted for publication.

#### 4. Plans for Upcoming Period

Fatigue tests under completely reversed, load-controlled conditions will be performed for biaxial in-phase and out-of-phase cycling.

#### 5. Current Publications or Presentations by Professor Krempf on this Subject

- 1) "Graphite/Epoxy ( $\pm 45$ )<sub>s</sub> Tubes: Their Static Axial and Shear Properties and Their Fatigue Behavior under Completely Reversed Load Controlled Loading"
 

Published as RPI Report No. RPI CS81-2, September 1981, (with T.-M. Niu).
- 2) "Preliminary Experience with the Instron Biaxial Extensometer"
 

Presented at the ASTM E9.08 Committee Meeting, Phoenix, Arizona, May 13, 1981.
- 3) "Life Prediction for Creep-Fatigue"
 

Presented at the Euromech 147, Symposium on Damage Mechanics, Cachan, France, September 1981.

III-C MOISTURE AND TEMPERATURE EFFECTS ON THE MECHANICAL  
PROPERTIES OF LAMINATES

Senior Investigator: S. Sternstein

1. Introduction

This project is concerned with those properties of high performance composites which are strongly dependent on the physical properties of the matrix resin. To date, the research has involved the precise viscoelastic characterization of epoxy neat resins, interlaminar failure of composites and the inhomogeneous swelling of and the effects of moisture on composites.

2. Status

In the previous report, the dynamic mechanical properties of carbon/epoxy laminates were presented. It was shown that the dispersion characteristics of neat resin and in situ resin were equivalent and that time-temperature superposition was obeyed in the glass transition region of the epoxy. Using the centro-symmetric deformation (CSD) testing method described previously, we have investigated the effects of water on the dynamic mechanical properties, as reported here for fiberite laminates\*.

---

\*Fiberite prepreg HYE-1048AIE was used to prepare laminates.

### 3. Progress During Report Period

Repetitive dynamic mechanical tests have been performed on dry laminate samples, and it is found that the glass transition temperature increases slightly from run to run until a final, fully cured  $T_g$  of  $160^\circ\text{C}$  is obtained. If a postcured laminate sample is subjected to moisture, then it is found that the glass transition temperature varies directly with moisture content as measured by weight gain. This is shown in Figures III-C-1 and 2 which give the in-phase and out-of-phase components of the dynamic modulus at 6.5 Hz, respectively. The glass transition is shown versus weight gain (water) in Figure III-C-3. The effects shown in Figures III-C-1 and 3 are reversible, in that a sample which is dried will recover its original glass transition temperature.

Laminate samples which have not been previously post-cured display quite different effects when exposed to moisture. The initial exposure to moisture results in a decrease of glass transition temperature which is not recovered after drying. Typically the decrease in  $T_g$  is five to ten degrees, depending on the moisture treatment. Subsequent dynamic mechanical tests on wet samples indicate that moisture interacts strongly with the postcure kinetics. We are currently investigating these kinetics by performing dynamic modulus tests versus time, at constant temperature. It appears that even after the sample has dried there is still a residual

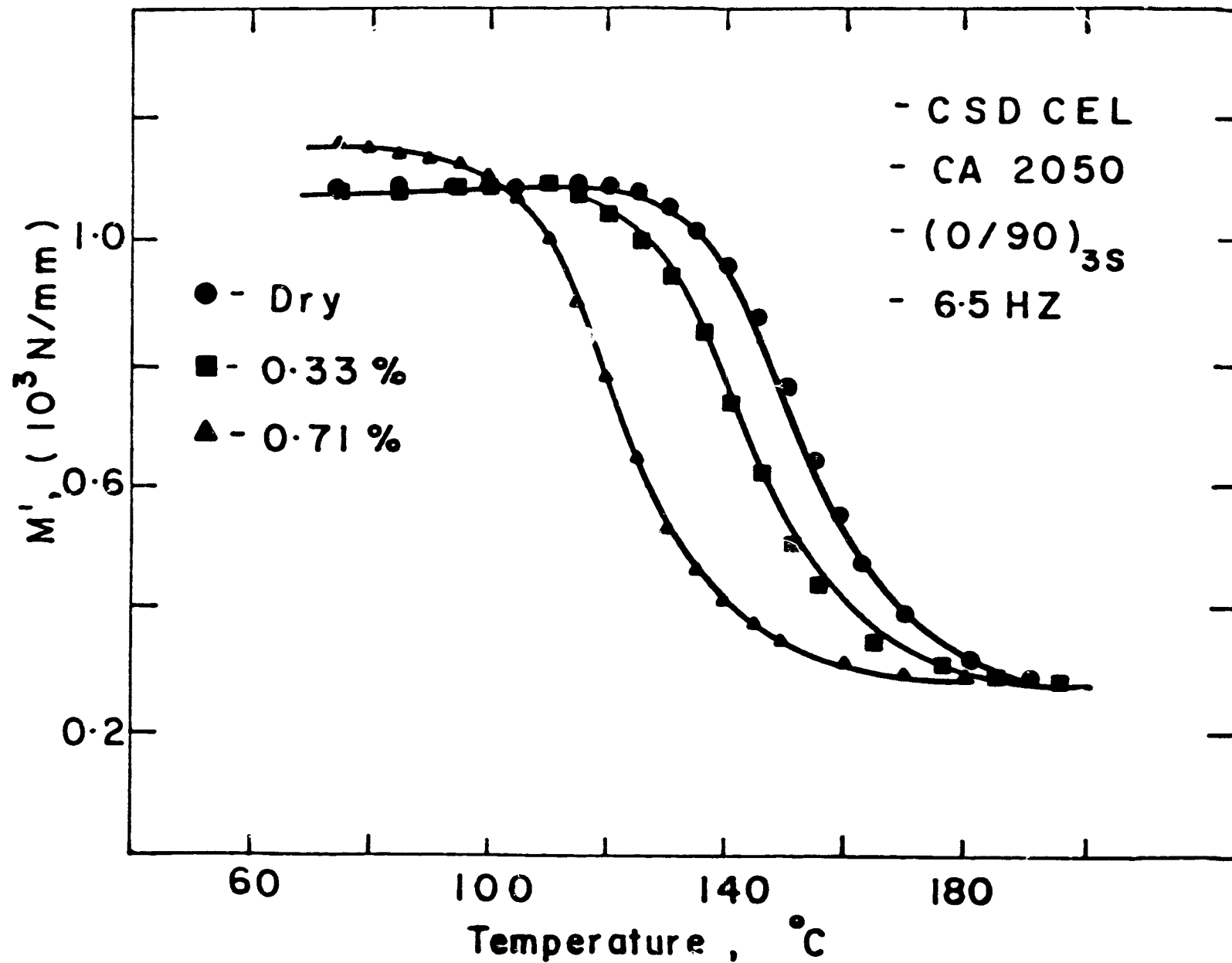


Figure III-C-1. Storage Modulus vs Temperature with Various Wetnesses

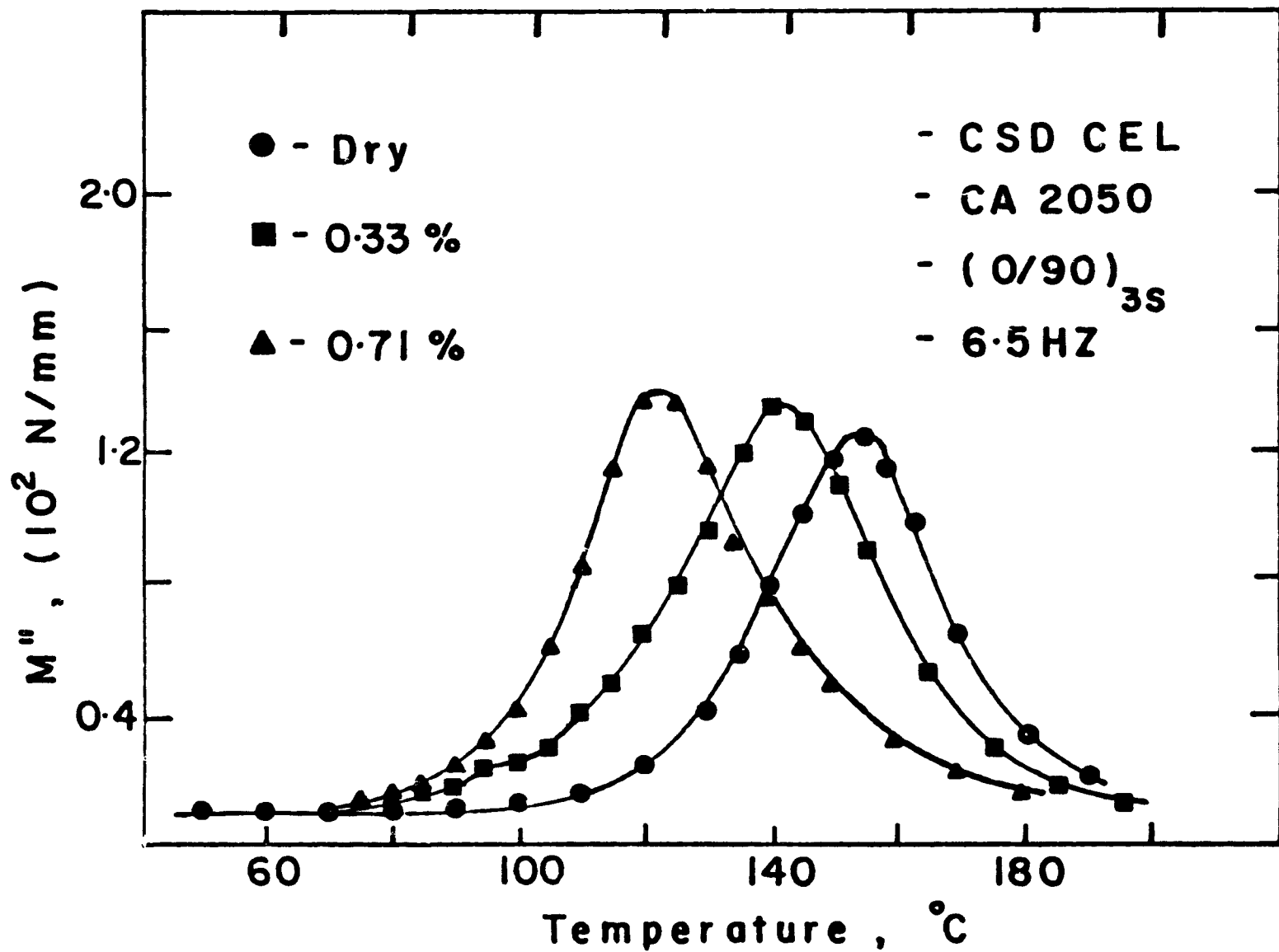


Figure III-C-2. Loss Modulus vs Temperature with Various Wetnesses

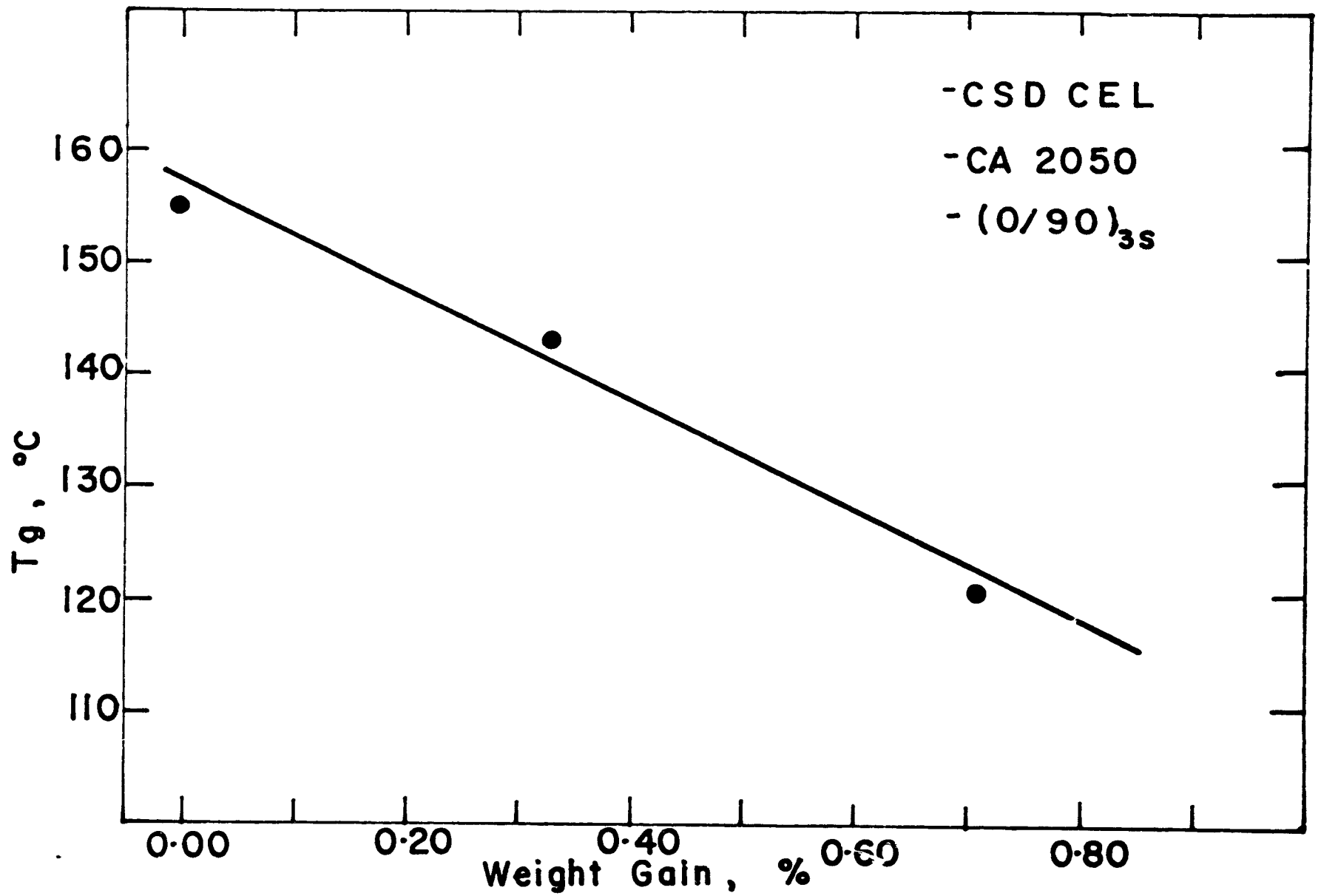


Figure III-C-3. Glass Transition Temperature as a Function of % Weight Gain

effect on postcure kinetics. These results are being prepared for publication and will be available shortly.

Finally, we have investigated the dynamic behavior of both wet and dry neat resin samples of Narmco 5208. The wet samples were conditioned at 62°C, 100% R.H. vapor for about 2 years which was the time required to reach weight gain equilibrium. The in-phase and out-of-phase moduli at 6.5 Hz are shown for the dry sample in Figure III-C-4 and the wet sample in Figure III-C-5. The broad out-of-phase modulus peak ( $M''$ ) in Figure III-C-5, extending from 160°C to 240°C, should be compared with the peak at 240°C in Figure III-C-4. This broadness of the wet glass transition peak may be direct rheological evidence for the presence of structure in the resin. Previously, other investigators have suggested that an amorphous structure exists in thermosets, based on electron microscopy of fracture surfaces. Since Figures III-C-4 and 5 represent bulk behavior, not surface behavior, these results may be of considerable utility in probing the structural features of epoxy resins.

#### 4. Plans for Upcoming Period

During the next period we plan to continue research to characterize the effect on dynamic mechanical properties of moisture interaction with neat resins and composites. Additional studies on resin cure rheology and inter-laminar creep will also be initiated.

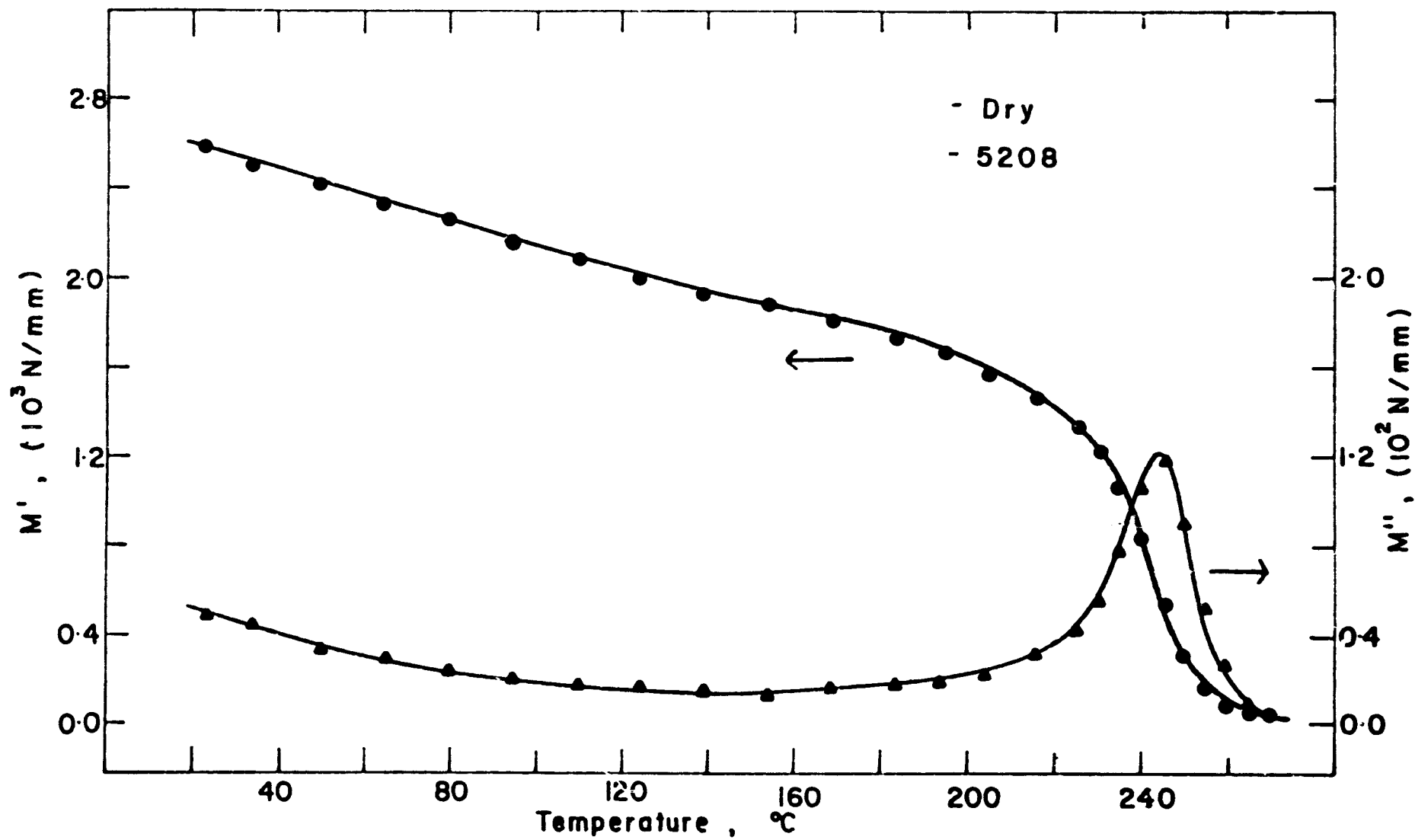


Figure III-C-4. Storage and Loss Moduli as a Function of Temperature: Dry

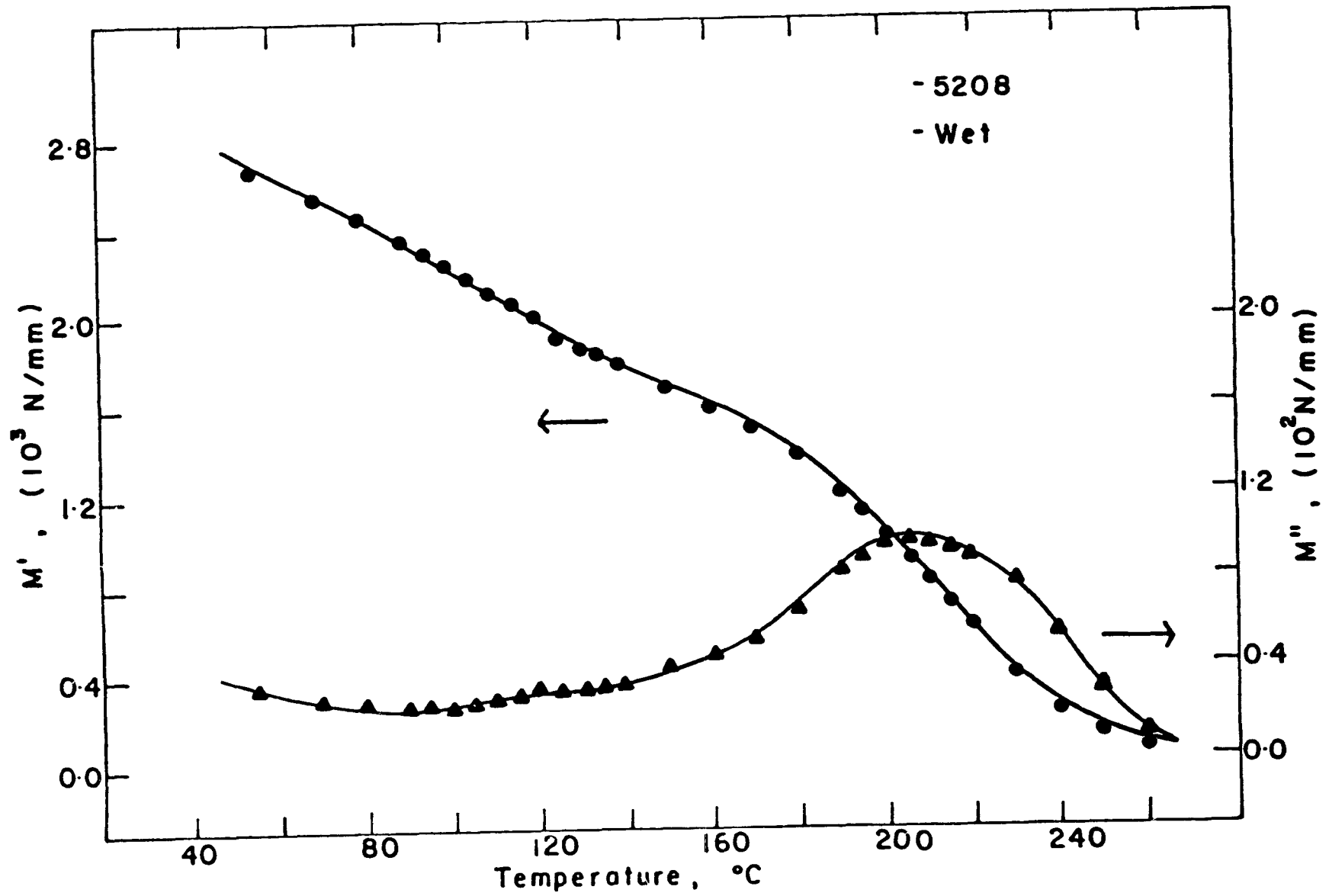


Figure III-C-5. Storage and Loss Moduli as a Function of Temperature: Wet

5. Current Publications or Presentations by  
Professor Sternstein on this Subject

1) "Properties of in situ Epoxy Matrices"

Presented Invited Lecture at the U. S. A. - Italy Joint Symposium on Composite Materials - The Role of the Polymeric Matrix in Their Processing and Structural Properties, Capri, Italy, June 15-19, 1981.

2) "Viscoelastic Properties of Composites"

Presented at the IBM Research Laboratory, San Jose, California, August 4, 1981.

3) "Viscoelastic Characterization of Neat Resins and Composites"

Presented at the National A.C.S. Meeting, New York City, New York, August 27, 1981.

### III-D NUMERICAL INVESTIGATION OF MOISTURE EFFECTS

Senior Investigator: M. Shephard

#### 1. Introduction

This analysis builds on the theoretical developments of Professor S. Sternstein (reported in progress reports dated December '79 and June '80) in which the fully-coupled, non-linear thermomechanical equations of inhomogeneous swelling of composites in the presence of moisture and temperature are analyzed. Here the one-dimensional case of a single fiber in an infinite matrix is being extended to two-dimensional, multiple fiber cases.

#### 2. Status

As discussed in the previous progress report, moisture effects have been introduced into the problem through a non-linear constitutive relation. The principle of virtual displacements is employed to develop a nonlinear matrix equation using displacement-based finite elements. These nonlinear matrix equations are then solved using quasi-Newton methods.

#### 3. Progress During Report Period

Effort has been continued during the last reporting period by graduate student Frida Lumban-Tobing in testing the program on some sample problems and establishing additional features in the program. The first problem considered was that of a single fiber embedded in an epoxy matrix. This

problem was considered because, as has been noted, it is a one-dimensional problem that has been solved under the supervision of Professor S. Sternstein\*. The constitutive equation employed in this one-dimensional analysis is written in the principal direction as

$$\sigma_i \bar{V}_i = \alpha RT + \frac{2\tau_i}{\tau_j \tau_k} \left[ V_1 + \frac{\partial \Delta V_{12}}{\partial \eta_1} \right] \left[ \frac{\partial W}{\partial I_1} + \frac{\partial W}{\partial I_2} (\tau_1 - \lambda_1^2) + \frac{\partial W}{\partial I_3} \frac{I_3}{\lambda_1^2} \right] \quad (1)$$

where:

$\sigma_i$  = principal stress

$I_1, I_2, I_3 \triangleq$  invariants of the deformation tensor

$W \triangleq W(I_1, I_2, I_3)$  = the work function

$\lambda_i^2 = 1 + 2\epsilon_i$ ;  $\epsilon_i$  = the principal strain tensor

$\bar{V}_1$  = partial molar volume of the solvent in polymer

$V_1$  = molar volume of pure solvent

$\Delta V_{12}$  = volume change as a result of mixing polymer and solvent, per unit volume of polymer

$\eta_1$  = number of moles of solvent absorbed, per unit volume of polymer

$\alpha = \ln(a_1)$ ;  $a_1$  = the activity of the solvent in the polymer

$R$  = gas constant

$T$  = absolute temperature

\* Herbert, P. F., "Moisture Induced Swelling in Graphite/Epoxy Composites", Masters Thesis submitted to the Graduate Faculty, Rensselaer Polytechnic Institute, 1981.

After rearranging, this expression can be fit into the non-linear constitutive relationship employed in the program as:

$$\alpha_{ij} = A\delta_{ij} + B\epsilon_{ij} + C\epsilon_{ik}\epsilon_{kj} \quad (2)$$

where

$$A = \frac{\alpha RT}{\bar{V}_1} + \frac{2}{\bar{V}_1} \left[ V_1 + \frac{\partial \Delta V_{12}}{\partial \eta_1} \right] \left[ \frac{1}{\sqrt{I_3}} \frac{\partial W}{\partial I_1} + \frac{(I_1 - 1)}{\sqrt{I_3}} \frac{\partial W}{\partial I_2} + \sqrt{I_3} \frac{\partial W}{\partial I_3} \right]$$

$$B = \frac{4}{\bar{V}_1 \sqrt{I_3}} \left[ V_1 + \frac{\partial \Delta V_{12}}{\partial \eta_1} \right] \left[ \frac{\partial W}{\partial I_1} + (I_1 - 2) \frac{\partial W}{\partial I_2} \right]$$

$$C = \frac{-8}{\bar{V}_1 \sqrt{I_3}} \left[ V_1 + \frac{\partial \Delta V_{12}}{\partial \eta_1} \right] \frac{\partial W}{\partial I_2}$$

The basic finite element idealization employed consists of a fiber of radius  $r$  embedded in a  $6r$  radius cylinder of matrix material as shown in Figure III-D-1. The first check analysis done was a free swelling analysis where both the outside and fiber boundaries are allowed to move. Figure III-D-2 shows the displaced mesh for this analysis. As would be expected, the stresses throughout the swollen medium were essentially zero. The second check analysis was for the case in which all the boundaries are fixed. In that case, the results were as expected, with the matrix in uniform compression.

The boundary conditions for the analysis of the reference on the preceding page are defined as fiber boundary fixed and outer boundary free. This problem was solved for various

ORIGINAL PAGE IS  
OF POOR QUALITY.

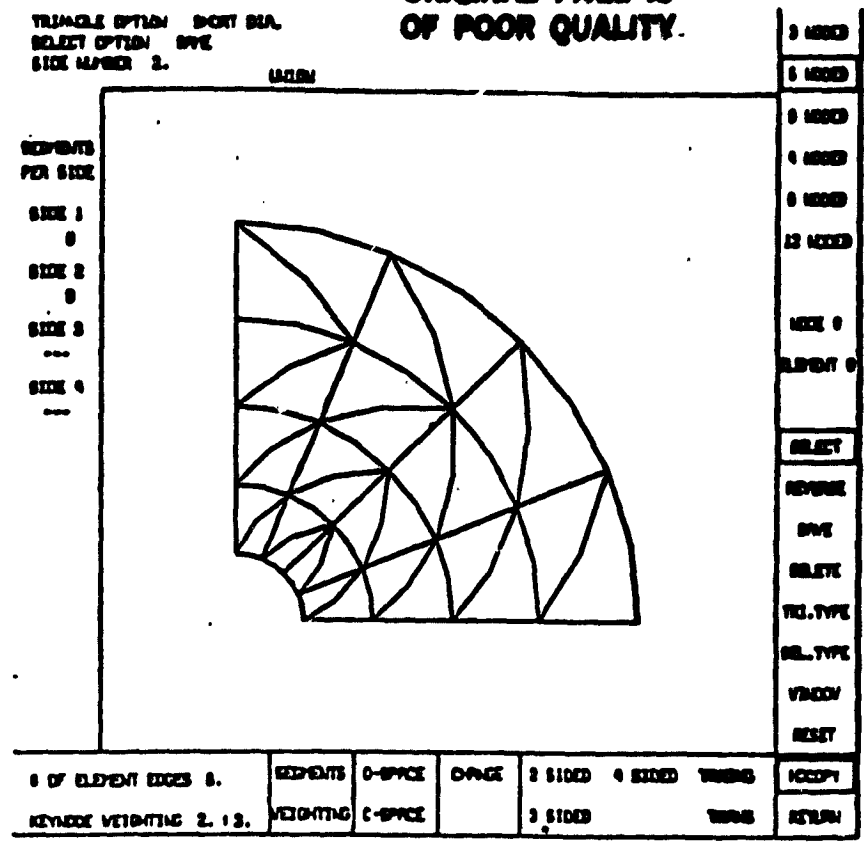


Figure III-D-1. Finite Element Mesh Used in Single Fiber Analysis

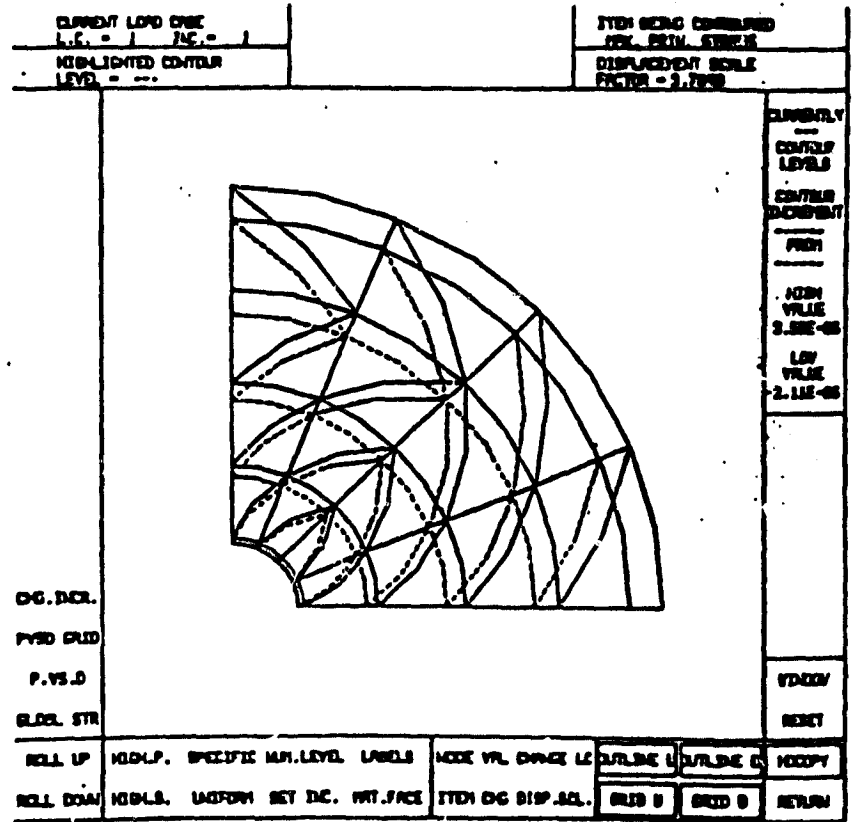


Figure III-D-2. Displaced Shape for the Free Swelling Case

moisture contents. Some numerical ill conditioning problems due to the log terms were experienced. These were alleviated, however, by adding features to the standard quasi-Newton procedures. The stability of the quasi-Newton approach was improved by adding line searches which improve the direction of the steps taken. In addition, when the size of the residual vectors exceeded a pre-set threshold, one step of standard Newton iteration was performed.

The solutions obtained compared very well with those presented in the reference on page 57. Figure III-D-3 shows the displaced shape for 80% humidity, while Figure III-D-4 shows the principal stress contours at the same humidity.

#### 4. Plans for Upcoming Period

Development of the nonlinear program for moisture effects should be completed in the next reporting procedure for the multi-fiber, two-dimensional use. A series of analysis studies will be run. These studies will consider various composite configurations and conditions including fiber spacing, epoxy properties, moisture contents and loading conditions.

ORIGINAL PAGE IS  
OF POOR QUALITY

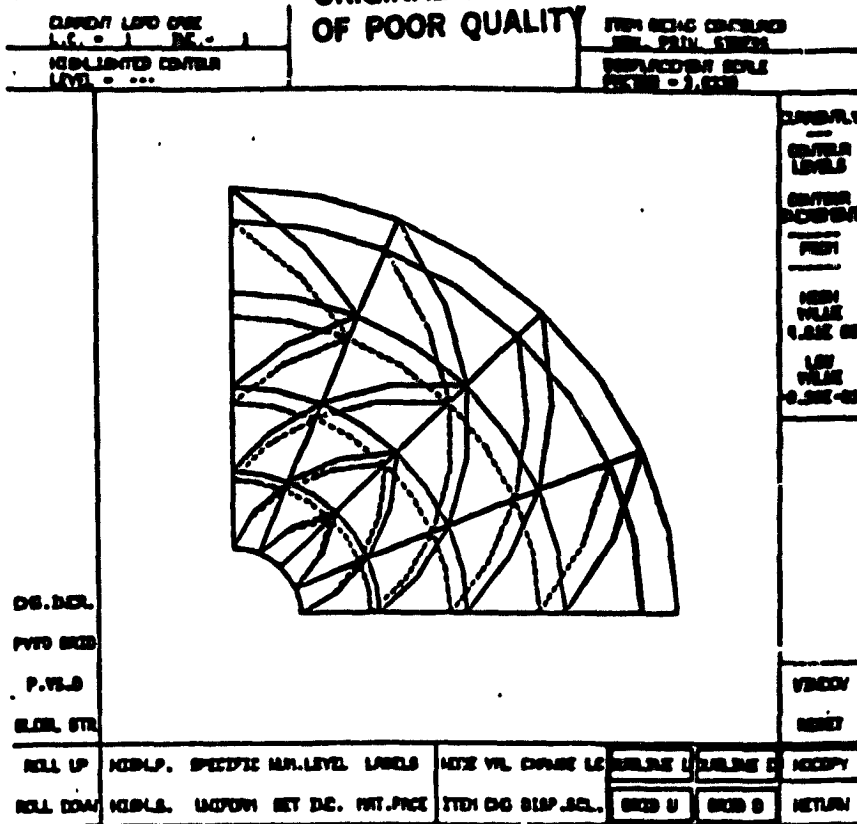


Figure III-D-3. Displaced Shape for 80% Humidity

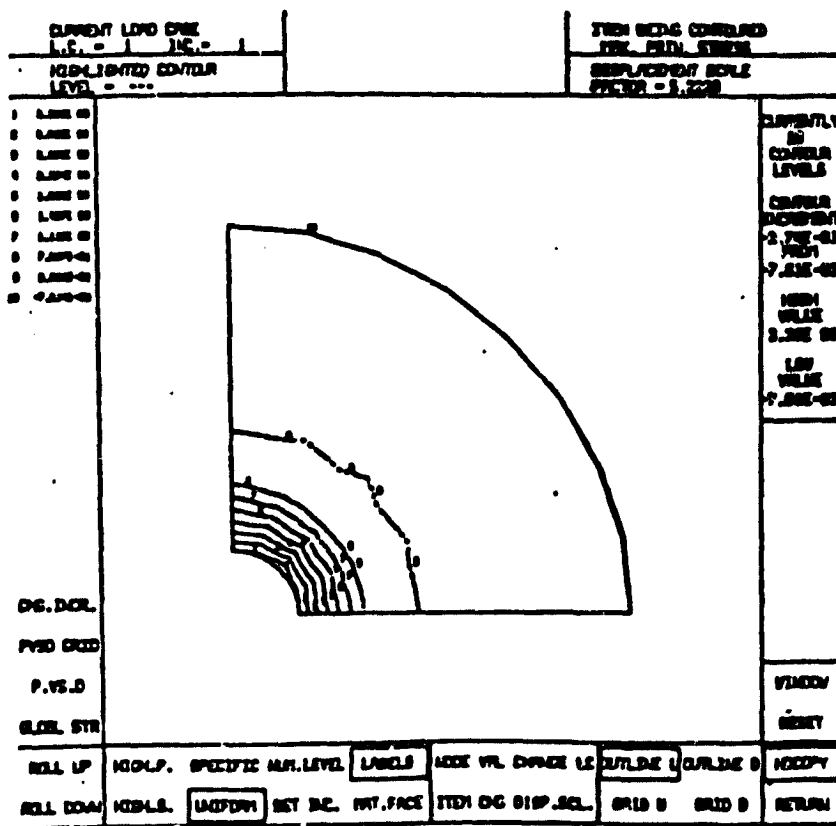


Figure III-D-4.  
Maximum Principal Stress Contours for 80% Humidity

### III-E NUMERICAL INVESTIGATION OF THE MICROMECHANICS OF COMPOSITE FRACTURE

Senior Investigator: M. Shephard

#### 1. Introduction

To understand the mechanisms of failure in composites it is necessary to develop insight into the micromechanical behavior, including interactions between matrix and fibers as the load is increased from zero to that corresponding to failure. Investigations of these phenomena, either experimental or numerical, are difficult. The purpose of this project, being carried out by graduate student Nabil Yehia, is to develop a nonlinear finite element analysis capability for performing numerical investigations of the micromechanical failure of composites.

#### 2. Status

To gain some feel for the processes involved in composite fracture at the micromechanical level, a step-by-step analysis of the failure of a simple three-fiber system was planned where one fiber is initially broken. Each step would consist of a linear analysis where the load would be increased until the next model modification would be called for. In addition to demonstrating how difficult it would be to perform a step-by-step analysis, the results were expected to indicate that one must track the formation and growth of a crack, consider material nonlinearities, and in some very localized region, consider large strains.

Based on previous published works, it was anticipated that to be able to adequately model the desired behavior we would have to develop a nonlinear finite element program with the following features:

- (a) nonlinear constitutive relations,
- (b) nonlinear strain displacement relations and
- (c) crack modeling abilities.

If only the first two forms of nonlinear behavior were required it would be possible to employ available nonlinear finite element codes. However, crack modeling ability is not available in existing programs. Thus, the design and development of a special nonlinear code was indicated.

### 3. Progress During Report Period

In addition to a survey of the applicable literature, the basic structure of the required FEM program has been designed and many of the procedures to be included selected. Coding of the first set of features has begun. The following paragraphs summarize approaches to be incorporated in the program.

The matrix material tends to be nonlinear for most values of strain, thus a constitutive relation based on a strain energy function was selected because of its ability to represent general nonlinear relationships. For the case of two-dimensional isotropic materials, for example, the relationship for the direct stress terms take the form (see, for example, Reference III-E-1):

$$\begin{aligned} \sigma_1 = & R_{111}e_1 + R_{112}e_2 + R_{1111}e_1^2 + R_{1112}e_1e_2 + R_{1122}e_2^2 + R_{11111}e_1^3 \\ & + R_{11112}e_1^2e_2 + R_{11122}e_1e_2^2 + R_{11222}e_2^3 \end{aligned}$$

and the shearing stress is of the form:

$$\sigma_6 = R_{666}e_6 + R_{6666}e_6^3$$

The inelastic portion of the behavior will initially be handled employing standard yield criteria (Ref. III-E-2).

Large strains will be handled using the standard non-linear strain-displacement relations (Reference III-C-3).

The ability to model crack initiation and growth requires several features that must be built into the program. First, one must be able to determine when a crack will initiate. Then one must determine when a crack will propagate, in which direction it will grow and how far it will go. This in turn requires the ability to change the geometry of the finite element model. The methods to be employed to attack this problem will rely heavily on fracture mechanics concepts and the use of special singular finite elements. In particular, the fracture criteria to be employed include:

- a) For cracks inside one material, the strain energy density factor S-criterion will be used (Ref. III-E-4).
- b) For cracks at a material interface, the S-criterion (Ref. III-E-4) and a maximum bond strength criterion will be used.
- c) In computing the stress intensity factors, K, the displacement method will be used (Ref. III-E-5).

- d) The crack tip region will be modeled by a layer of six-noded singular elements (Refs. III-E-6 and 7) followed by one or two layers of eight-noded transition elements (Ref. III-E-8).
- e) The mesh of the region(s) in which the crack is embedded will be regenerated after each crack preparation. The scheme for doing that has not yet been worked out.

#### 4. Plans for Upcoming Period

Efforts in the coming reporting period on the micro-mechanical failure of composites will be concentrated on implementation and initial testing of the various features being built into the analysis package. Attempts will also be made to devise a general procedure for handling mesh modifications as required by crack growth during load increases.

#### 5. References

- 1) Green, A. E. and J. E. Adkins, "Large Elastic Deformations", Clarendon Press, Oxford, 1970.
- 2) Kachanov, L. M., "Fundamentals of the Theory of Plasticity", MIR Publishers, Moscow, 1974.
- 3) Oden, J. T. and E. A. Ripperger, "Mechanics of Elastic Structures", 2nd Edition, McGraw-Hill, 1981.
- 4) Sih, G. S. and B. Macdonald, "Fracture Mechanics Applied to Engineering Problems - Strain Energy Density Fracture Criterion", Eng. Fract. Mech., Vol. 6, 1974, pp. 361-386.
- 5) Ingraffea, A. R. and C. Manu, "Stress-Intensity Factor Computation in Three Dimensions with Quarter-Point Elements", Int. J. Num. Meth. Engng., Vol. 15, 1980, pp. 1427-1445.
- 6) Barsoum, R. S., "On the Use of Isoparametric Finite Elements in Linear Fracture Mechanics", Inter. J. Num. Meth. Engng., Vol. 10, No. 1, 1976, pp. 25-37.

- 7) Freese, C. E. and D. E. Tracey, "The Natural Isoparametric Triangle Versus Collapsed Quadrilateral for Elastic Crack Analysis", *Int. J. of Fracture*, Vol. 12, 1976, pp. 767-770.
- 8) Lynn, P. P. and A. R. Ingraffea, "Transition Elements to be Used with Quarter-Point Crack-Tip Elements", *Int. J. for Num. Meth. in Engng.*, Vol. 12, 1978, pp. 1031-1036.

PART IV  
GENERIC STRUCTURAL ELEMENTS

- IV-A 727 ELEVATOR ACTUATOR ATTACHMENT RIB
- IV-B LOCKHEED L-1011 ENGINE DRAG STRUT (CAPCOMP II)
- IV-C MECHANICAL JOINTS IN COMPOSITES
- IV-D COMPUTER SOFTWARE DEVELOPMENTS

## INTRODUCTION TO PART IV

The redesign of flight-critical structural components currently in service as metal parts on existing aircraft was included as part of RPI's composite materials and structures program to assure relevance and realism to the project's direction and to contribute to the nation's pool of innovative structural design concepts. Two such components were selected in cooperation with major commercial airframe manufacturers, Boeing Commercial Airplane Co. and Lockheed California Company, and with advice from NASA. The first, the 727 airplane's elevator actuator attachment rib, has completed the cycle planned at the project's inception. That is, several alternate redesigns were attempted; one was selected, analyzed and finalized; and two specimens were fabricated and tested to ultimate load. The second, a redesign of the wing-mounted engine drag strut for the L-1011 airplane has been carried to the point where (a) the usefulness of certain basic research performed earlier at RPI under the NASA/AFOSR program was made very clear and was called on in the design process, and (b) several areas of research in which results are needed for such a redesign - but are not now available - have been identified.

As a matter of fact, a number of basic research projects motivated by the early work on the 727 elevator rib, have been reported in these project reports for some time. Some

of these have been completed, others are reported here in connection with the conceptual design research on the two specific airframe components, as discussed above, and still others are planned for the future as having the potential to contribute significantly to classes of generic Composite Aerospace Structures, as the specific aircraft structural component redesign research is phased out. Progress on projects typical of the original program and projects of generic research, as will be pursued in the redirected program, are both reported in the sections that follow.

IV-A 727 ELEVATOR ACTUATOR ATTACHMENT RIB

Senior Investigators: D. Goetschel  
R. Loewy  
H. Scarton

This program element involved a structures demonstration project using the actuator attachment lugs and rib of the 727 elevator, paralleling that of NASA and its aerospace contractor, the Boeing Commercial Airplane Company. Our design, fabrication and test effort emphasized designs using advanced composite construction for the purpose of minimizing the weight of the structure, but on a scale consistent with the university context and funding level. The staff of RPI is very grateful to the Boeing Company and its engineers for their wholehearted support of this work at RPI.

One of two different designs was reported previously (July and December, 1979) as suitable for replacing the largely metal attachment produced by Boeing. This so-called "Berg Design" makes use of quasi-isotropic, graphite/epoxy laminates and was selected for further analysis, redesign, fabrication and testing. The conventional aluminum alloy elevator of the Boeing 727, the new version of the elevator redesigned by Boeing in graphite epoxy, and Berg's design for the RPI graphite/epoxy Nomex honeycomb elevator rib are all described in earlier reports (July, 1981). In each case the attachment was designed to carry loads up to 19,000 pounds and for directions of load varying as the elevator

rotates over an angle of 28 degrees from the full-down to the full-up position.

The first specimen of the Berg-designed, composite 727 aircraft elevator actuator attachment rib was fabricated by undergraduate student Francis DeTaranto and was tested to failure on December 12, 1980. As reported in the semi-annual report dated July, 1981, this was a completely successful test in virtually all respects. The design failed at approximately 120 per cent of design ultimate load, failures occurred close to where they were expected and failures were multiple in nature. The major failure appeared to have initiated near the leading end of the tension flange (i.e., the flange connecting the rib to the elevators' upper-surface skin).

#### 1. Construction Details of the Final 727 Elevator Rib

During the current reporting period a second and final test specimen was fabricated by undergraduate student Frank DeTaranto and graduate student Shu-Ping Chen. Four adjustments were made in the detailed design of and processes used to fabricate the second part. The changes were intended to improve the part's behavior in the area where failures initiated in tests of the first rib.

First, "wrinkles" were observed to have developed in fabrication along the inner radius of some of the flange-web junctions, running parallel to it. It appeared, initially, that the cause of the "wrinkling" was the bunching-up of

fibers from shrinkage during curing or from vacuum bag dragging outer layers into overlapping as pressure was applied and the bag tightened. None of the attempted remedies, however, had a significant effect.

Photomicrography finally revealed that the real cause of the "wrinkling" was the separation of zero degree fibers in the surface ply, and their piling-up on either side of a "chasm" to cause what only appeared to be a wrinkle. Figure IV-A-1-a is a typical micrograph of the "wrinkle" with 0°/outer plies (i.e., parallel to the corner). Reordering of the stacking sequence cured the problem. In the second part, the surface ply was oriented at 90° (i.e., perpendicular to the axis of the corner). This also increased the local bending strength and stiffness of the flange.

To describe the second design change, one must call attention to the build-up of the end of the flange on the first actuator rib (Figure I-20 in the July, 1981 report, reproduced here as Figure IV-A-1-b). This build-up increased the stiffness of the flange at the flange leading edge, allowing more load to be picked up by the flange in the region of the first fastener. This is where failure occurred. Thus, on the final actuator attachment rib, this build-up was eliminated.

The third modification was spreading Hy-lock fastener locations away from the web as the chordwise position of these connectors between skin and flange moves from trailing

ORIGINAL PAGE  
BLACK AND WHITE PHOTOGRAPH

Figure IV-A-1-a. 727 Elevator Actuator Attachment Rib (8/6/81)



FILLET CREASE  
MAGNIFICATION 50X

ORIGINAL PAGE  
BLACK AND WHITE PHOTOGRAPH

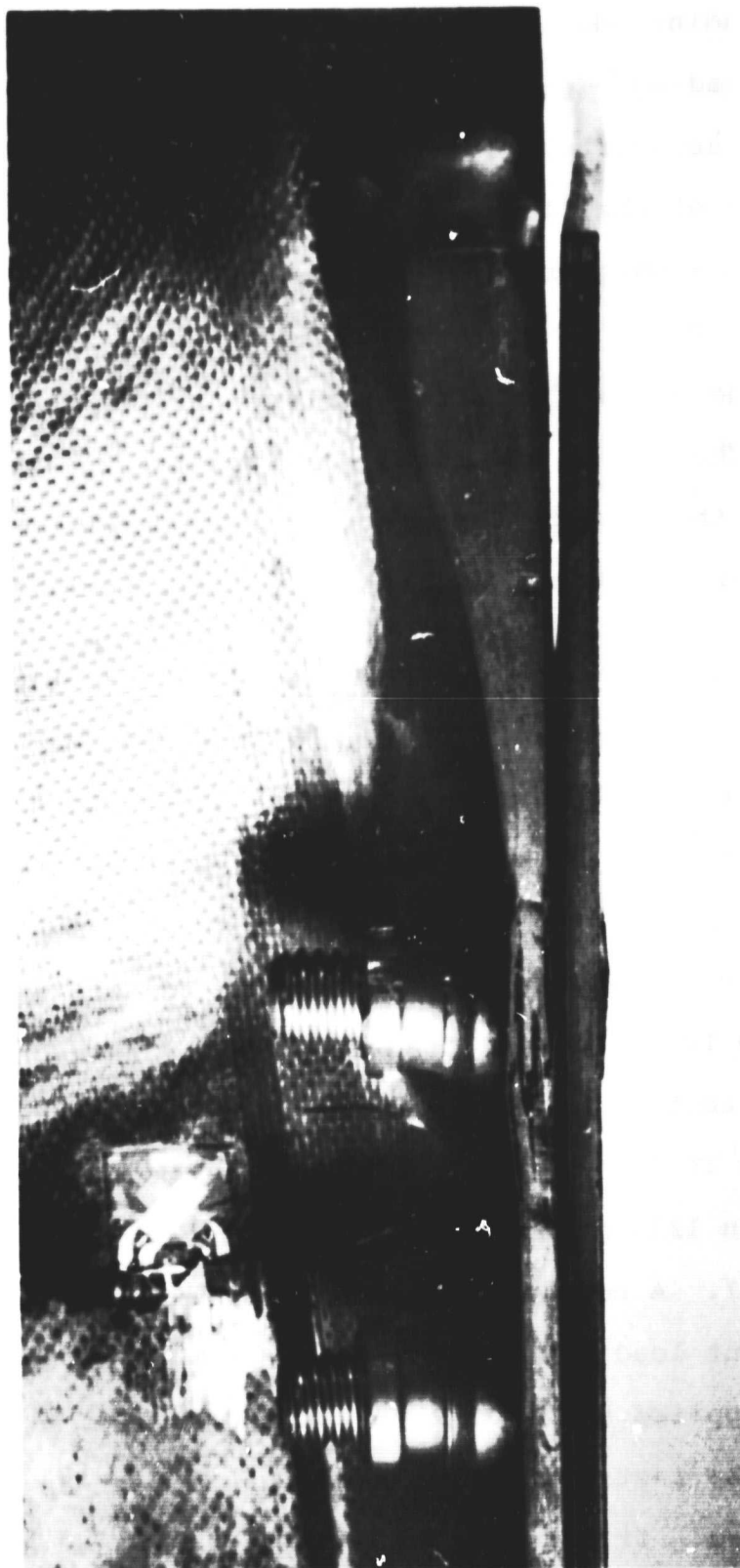


Figure IV-A-1-b.  
Failed Section and Strain Gage

to leading edge. The actuator rib web becomes thicker near the leading edge of the rib to carry the more concentrated loads associated with the actuator attachment lug. The fillet of the flange thus is thicker in those areas, resulting in a sharper taper in flange thickness from fillet to edge. This, in turn, requires a wider fastener spacing to provide a flat "seating" surface for the fasteners.

The fourth and final modification was the use of washers under the Hy-lock fasteners to improve the uniform distribution of stress between fastener and composite.

## 2. Test Procedure and Results for the Final 727 Elevator Rib

On September 11, 1981, the revised Boeing 727 elevator actuator attachment was tested. Figure IV-A-2-a shows the schematic of the test apparatus, which had been modified from that used in testing the first specimen by including spherical-ball bearings at the pin connections (points A in Figure IV-A-2-a) and load-carrying transition pieces at the lower section of the loading fixture (point B in the figure). Figure IV-A-2-b shows the elevator attachment placed in the Instron 1333 machine whose maximum capacity is 252 kN (56,500 pounds). A continuous monotonically increasing loading with constant load rate was used. In the final test run, load was supplied at 0.135 kN/s (30 pounds/sec) to the specimen.

The instrumentation used in the test is shown in Figure IV-A-2-c. It consists of an FX Data Logger Strain Monitor with four 45° strain rosettes and seven unidirectional strain

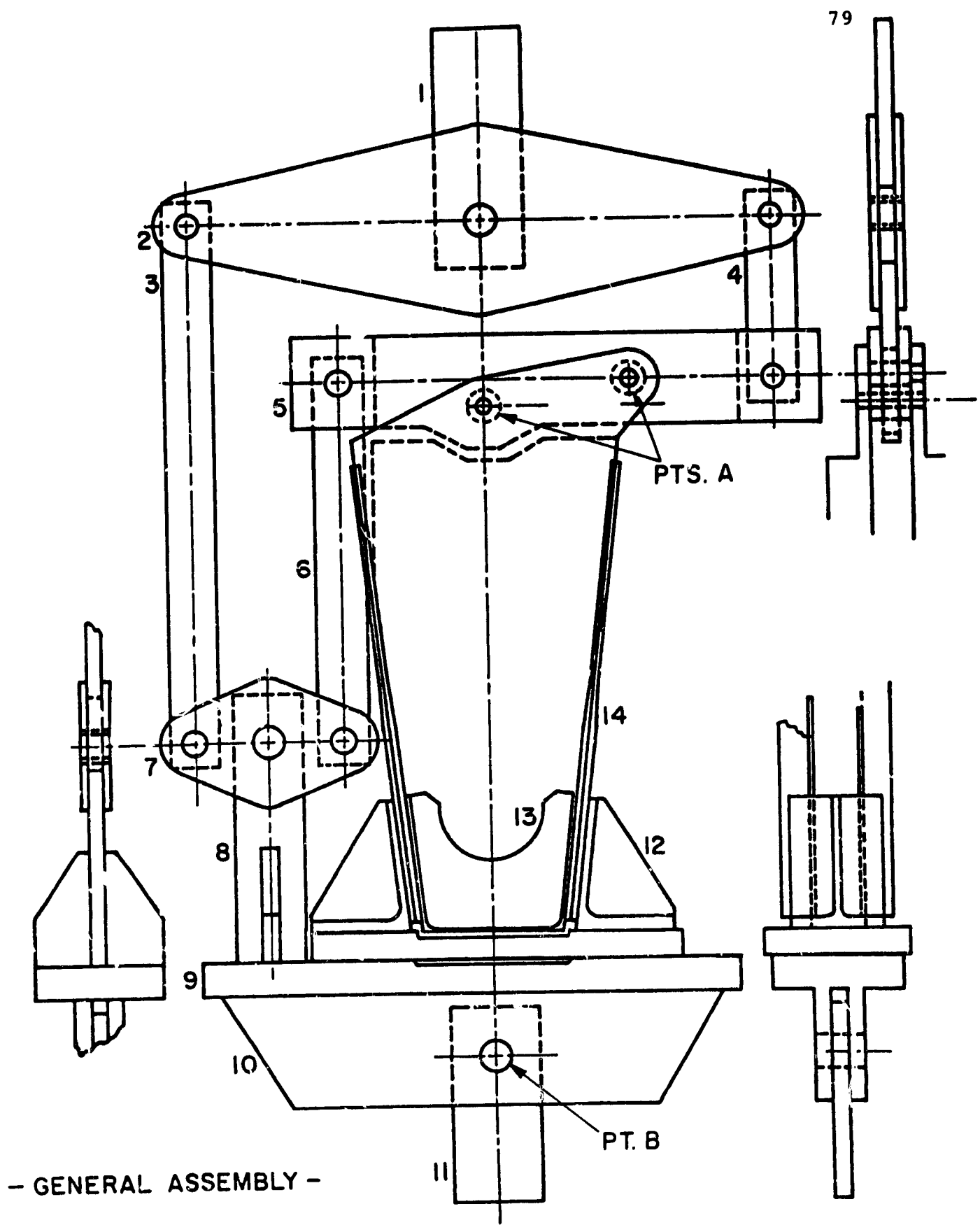


Figure IV-A-2-a. Rib Test Fixture

ORIGINAL PAGE  
BLACK AND WHITE PHOTOGRAPH

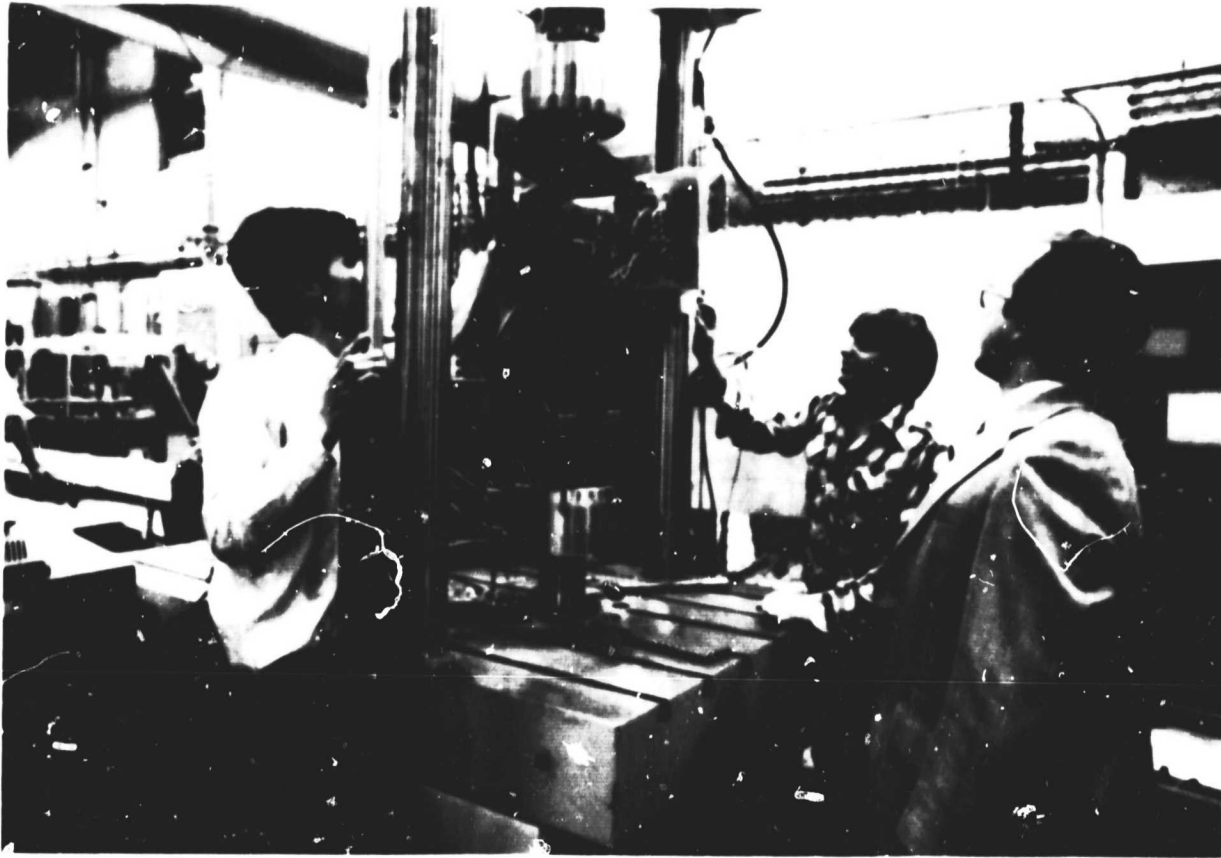


Figure IV-A-2-b.  
Elevator Actuator Attachment Rib Test Fixture in Instron/333  
(without personnel protection barrier)

gauges. A Physical Acoustics Corporation Model 3400 four-channel acoustic emission monitor supplied for the test through the courtesy of the Physical Acoustics Corporation was also used. RPI graduate student Chi-Min Chang and Mr. John Crowell from PAC supplied strain gauge and AE instrumentation support, respectively, both during and after the test. A personnel protection barrier is also shown in Figure IV-A-2-c. Table IV-A-2 lists the acoustic sensors used in the test.

In order to place strain gauges and AE sensors as close as possible to the ultimate failure location, a simplified two-dimensional finite element analysis was performed using a finite element mesh which represented thickness variations as shown in Figure IV-A-2-d. Figure IV-A-2-e presents the overall maximum principal stress contours which resulted from this analysis. The results of a pre-test study of the lug, shown in Figure IV-A-2-f for maximum principal stresses and shown in Figure IV-A-2-g for specimen distortion in the vicinity of the edge of the upper pin hole, suggested that this was likely to be the region of ultimate failure. On this basis the AE sensors and strain gauges were located as indicated in Figure IV-A-2-h. The AE sensors were calibrated using five clicks on a 0.5 mm 2 H hardness Pentel pencil and then by breaking the lead held at an angle of 45°. These impulses have consistent amplitudes of 80 dB.

The actuator was then loaded to 2,000 pounds and all

TABLE IV-A-2  
ACOUSTIC EMISSION SENSOR CHARACTERISTICS

<u>Acoustic Sensor Number</u>	<u>Type</u>	<u>Resonance (kHz)</u>	<u>Preamp Model NU</u>	<u>Gain dB</u>	<u>Preamp Bandwidth (kHz)</u>	<u>Sensors Bandwidth (3 dB down)</u>
1	R-15	150	1220 A	40 dB	20-1200 kHz	20 kHz
2	R-15	150	1220 A	40 dB	20-1200 kHz	20 kHz
3	R-15	150	1220 A	40 dB	20-1200 kHz	20 kHz
4	R-151	150	1220 A	40 dB	20-1200 kHz	20 kHz

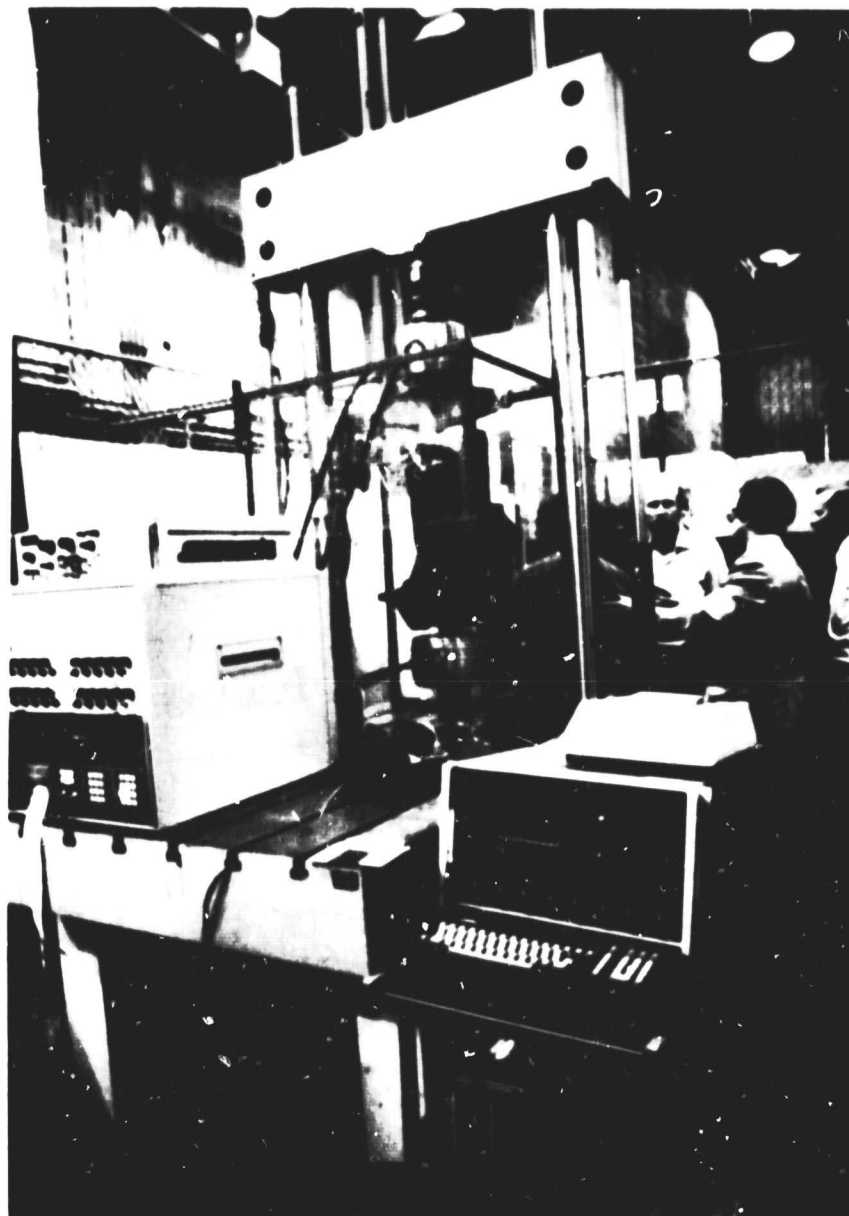


Figure IV-A-2-c.  
Elevator Actuator Rib Test Fixture and Instrumentation  
(with personnel protection barrier)

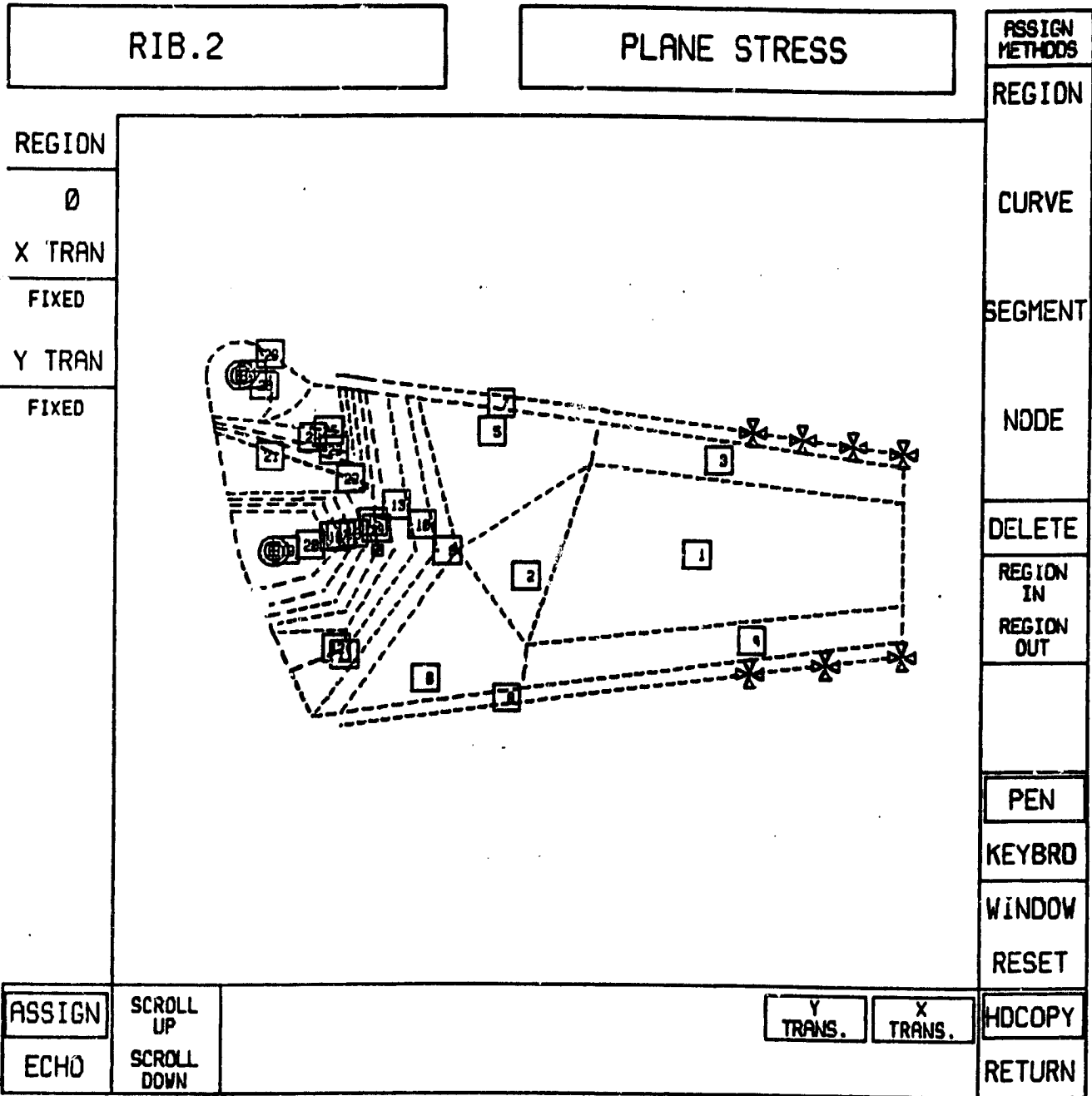


Figure IV-A-2-d.  
Variable Thickness Homogeneous Finite Element Specimen

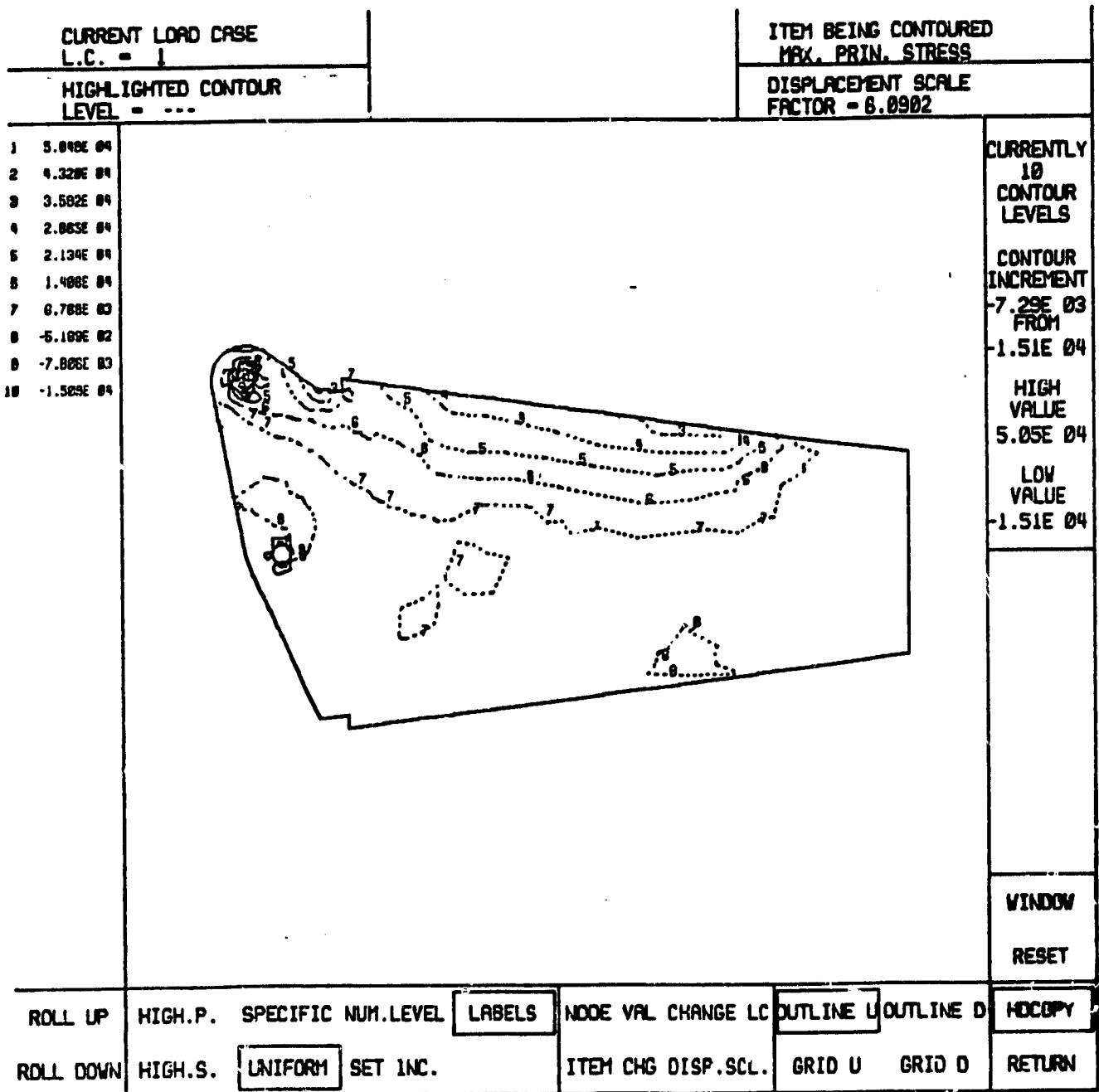


Figure IV-A-2-e.  
Finite Element Maximum Principal Stress Distribution

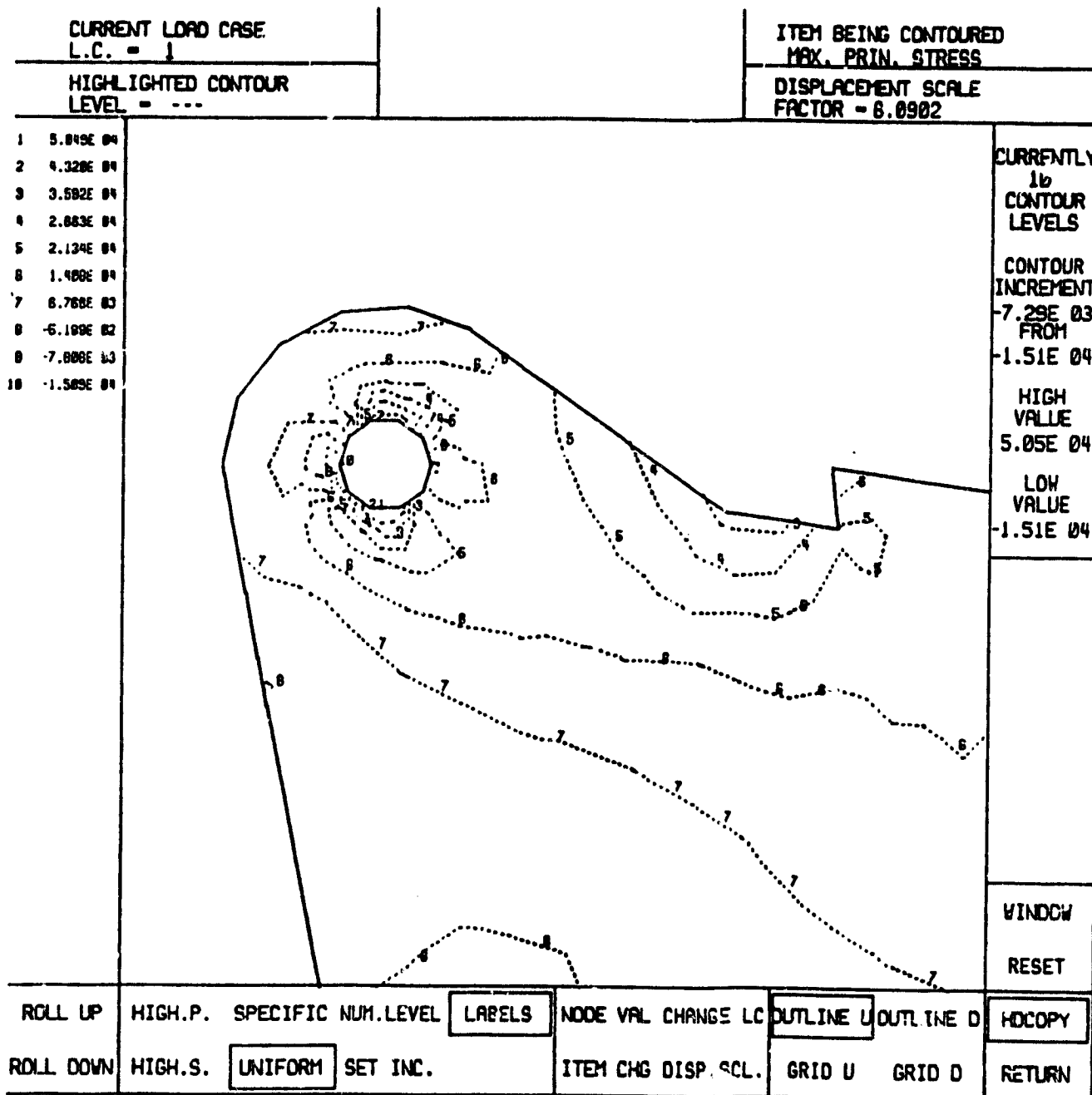


Figure IV-A-2-f.  
 Close-up of Finite Element Maximum Principal  
 Stress Region of Highest Stress

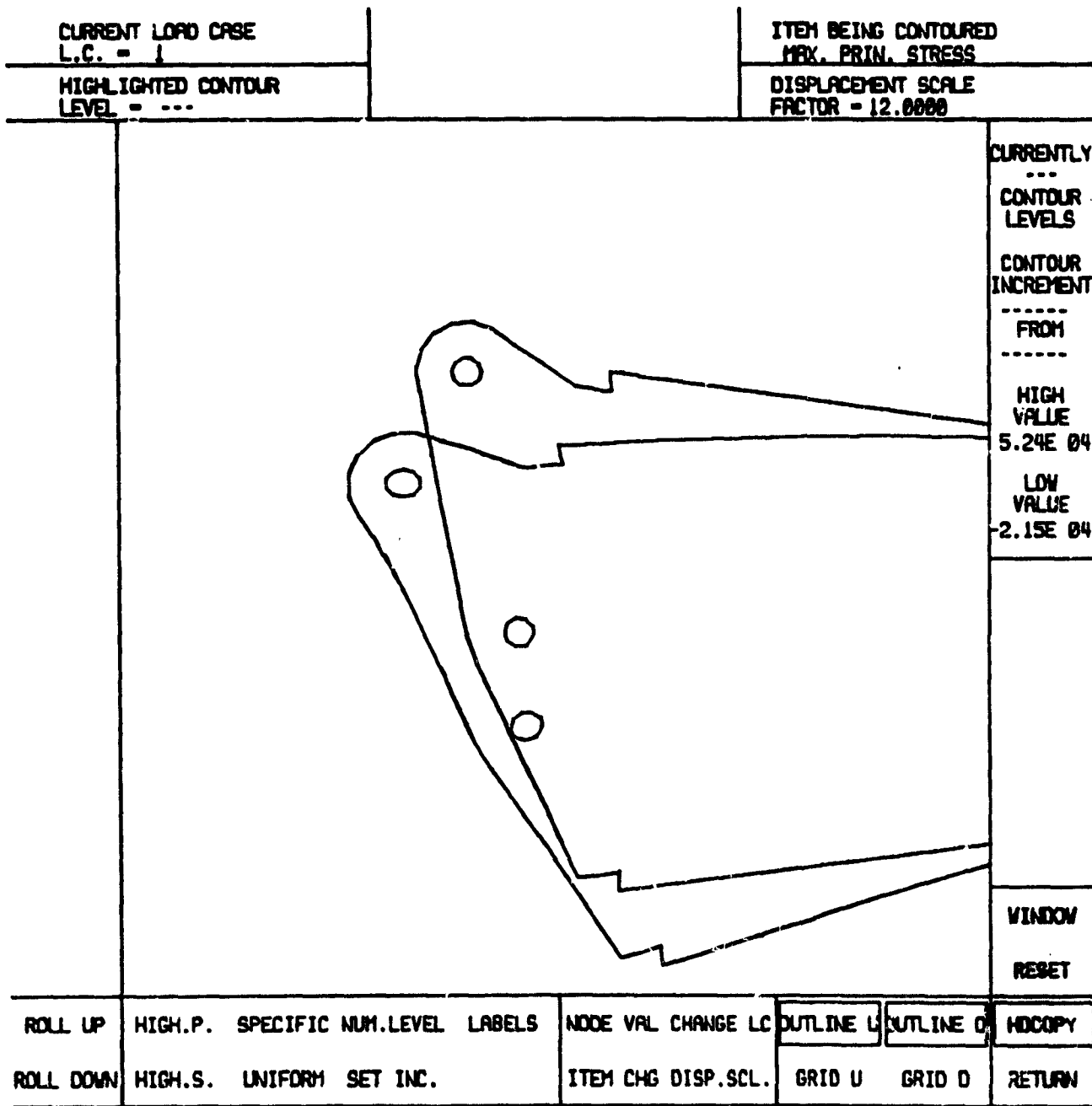


Figure IV-A-2-g.  
Finite Element Simulation of Final Strained Shape

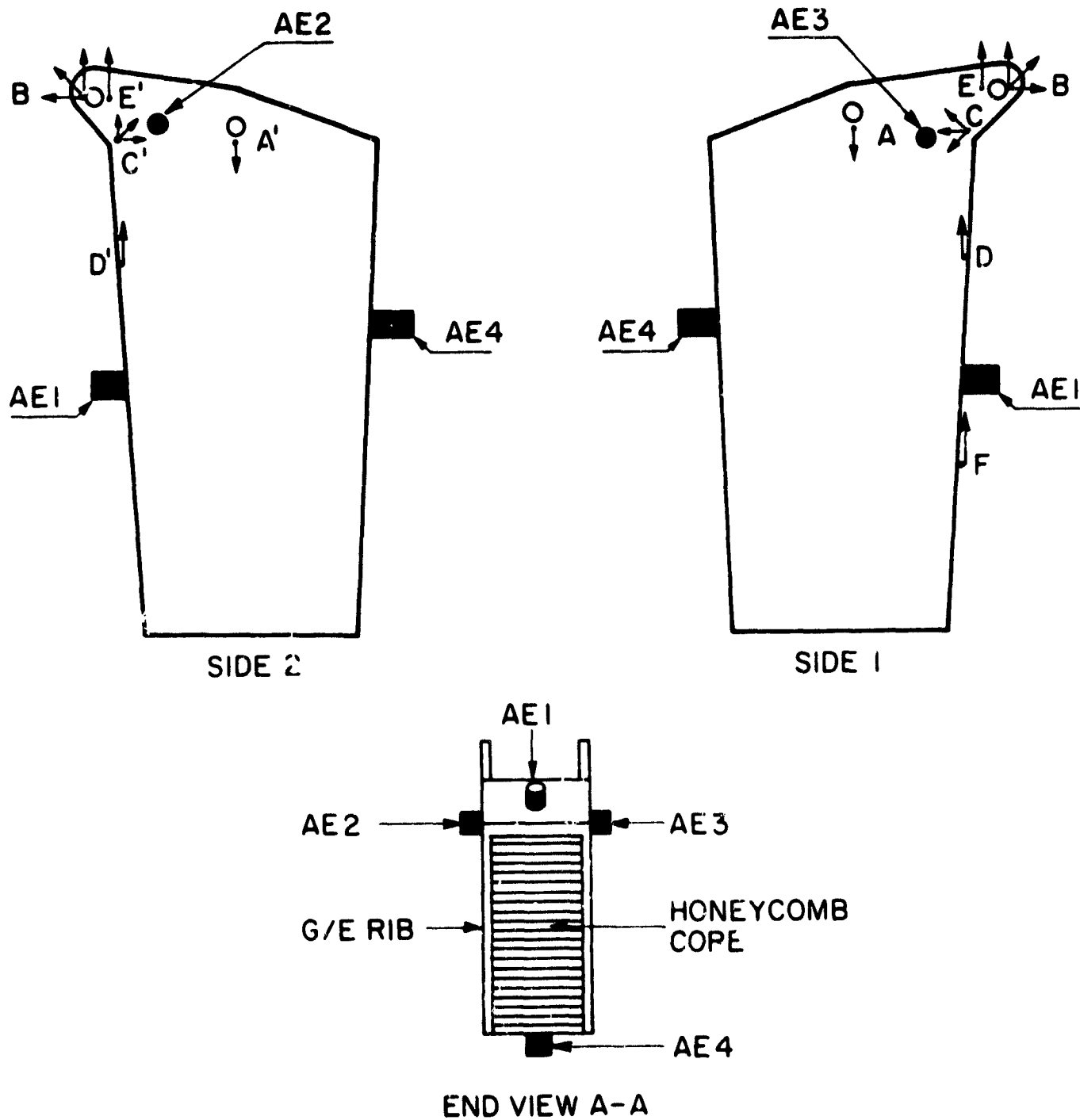


Figure IV-A-2-h.  
Strain Gage and Acoustic Emission Sensor Locations

strain gauges interrogated. Although some asymmetry in the strains was reported, a decision was made to proceed with the test.

The load was removed and the Instron was readied. An initial ramp loading of the specimen was carried out, to a load of 55.9 kN (12,600 pounds) (Figure IV-A-2-i). Because it was discovered that a lower loading rate was needed, the test was halted at this point and the load removed. It was confirmed in post-test analysis of the AE data that, during the first loading, over ten large amplitude events (exceeding 90 dB) were observed (Figure IV-A-2-j). The loading rate was reduced by a factor of 10 to 0.135 kN/s (30 pounds/sec).

The test was then restarted with all AE data channels reinitialized to zero. The test continued until ultimate failure occurred at 721 seconds, at a load of 96.2 kN (21,630 pounds) or 14% over the design load of 85.5 kN (19,000 pounds).

During the test cumulative counts versus time were monitored in real time (see Figure IV-A-2-k). A pronounced Kaiser effect can be seen in the second run, where no counts were observed until the load exceeded 53 kN (12,016 pounds, close to the maximum established during the first ramp loading. Although there are a number of possible points of critical activity wherein the slope of the curve of number of counts versus load increases precipitately, two points appear to have noteworthy critical activity; one at 66.56 kN (15,015 pounds) and another at 84 kN (18,700 pounds). Post-test

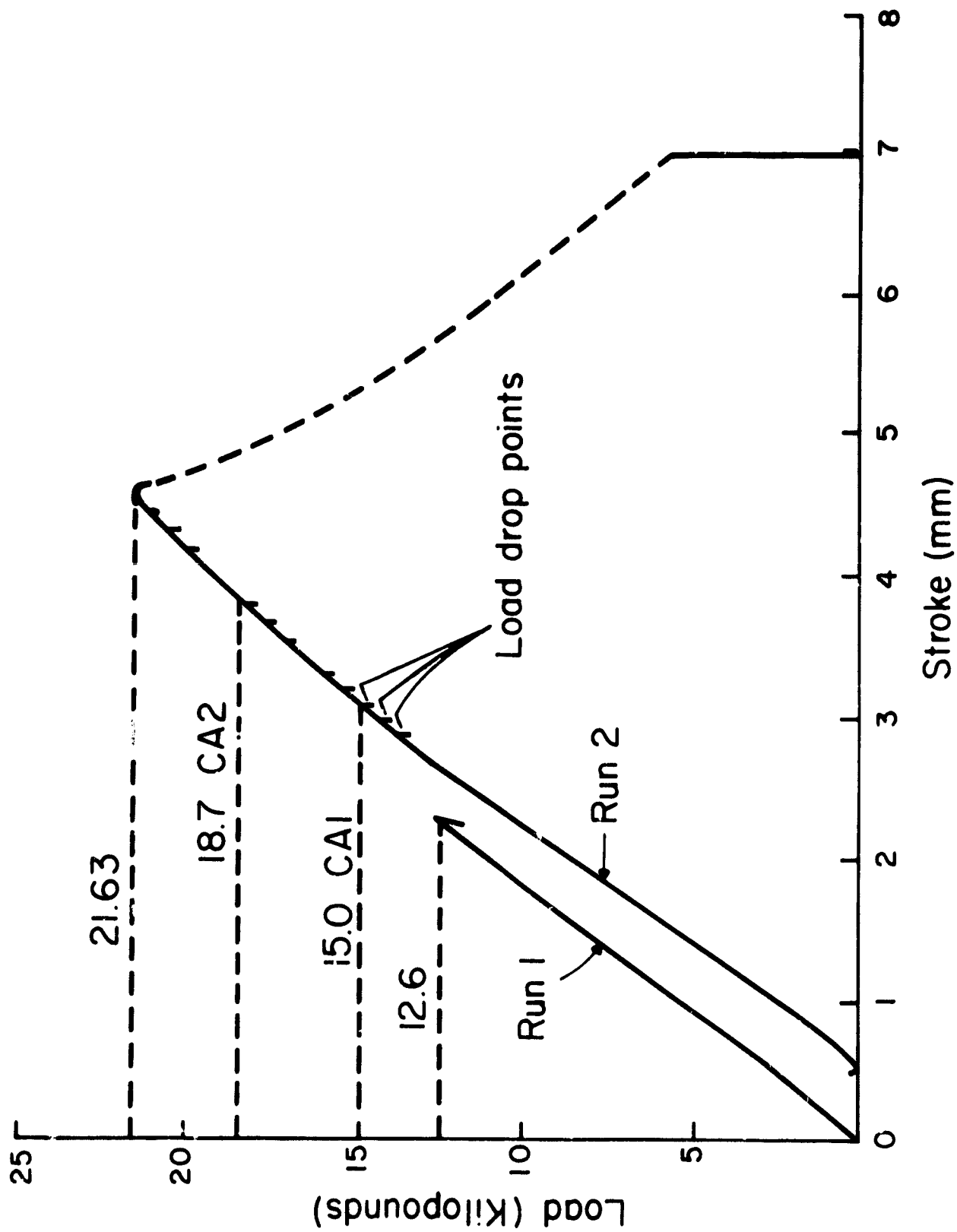


Figure IV-A-2-i. Specimen Load Versus Stroke Curve

ORIGINAL PAGE IS  
OF POOR QUALITY

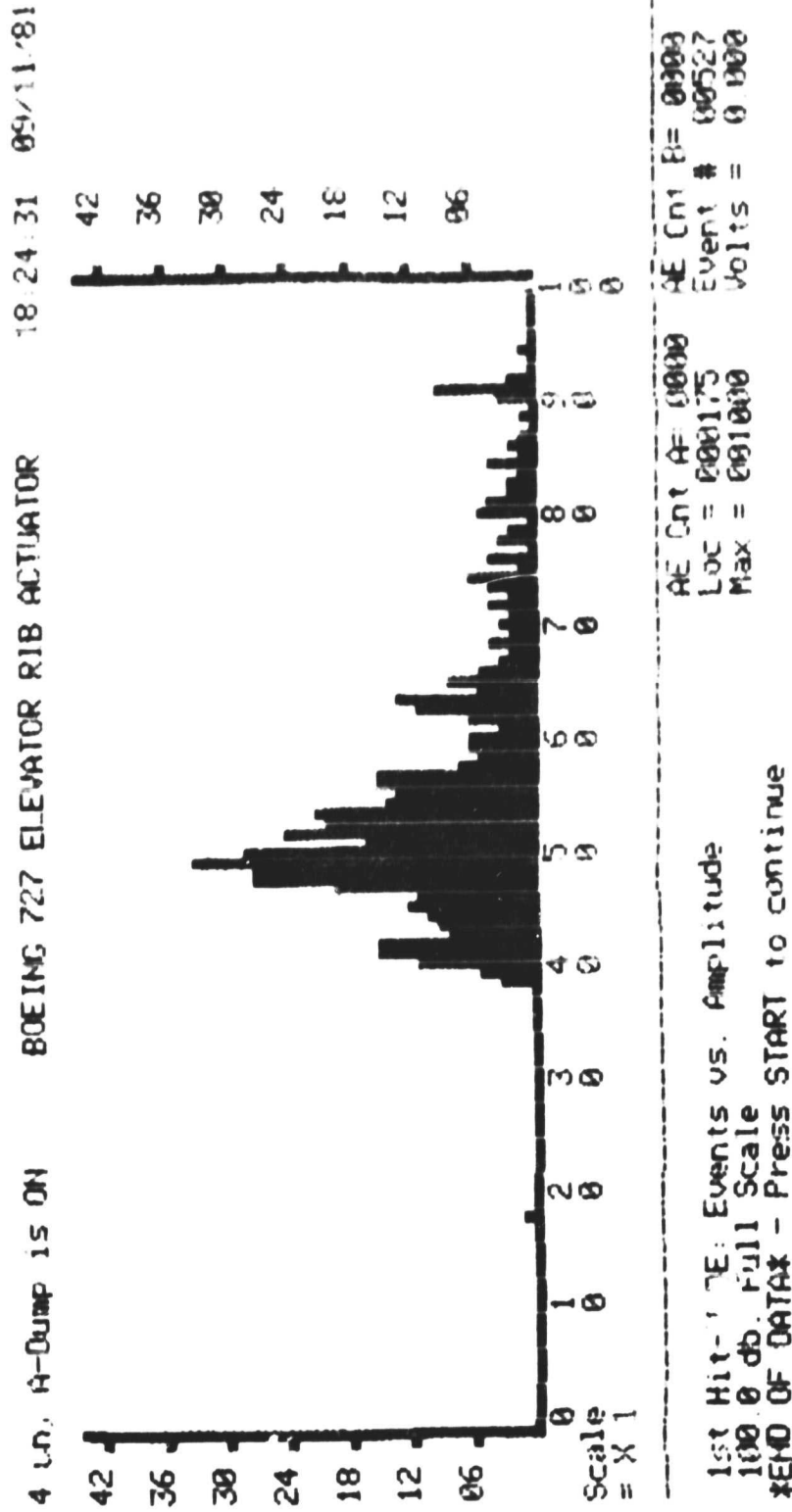


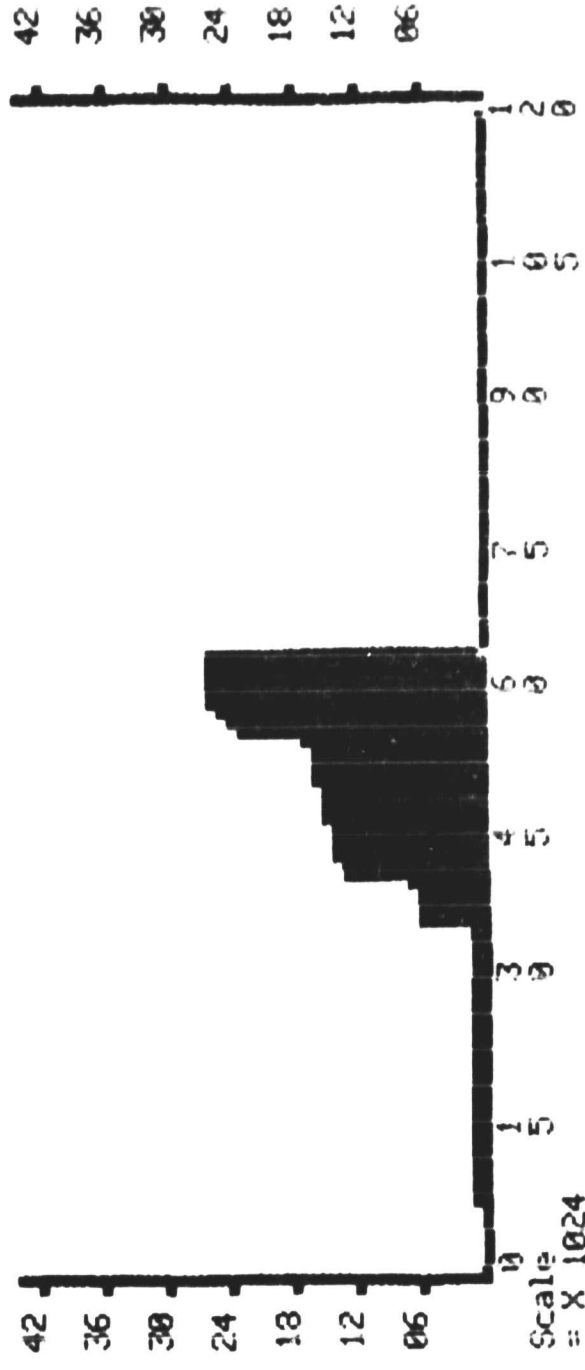
Figure IV-A-2-j. Amplitude Distribution at 43 kN (9700 pounds) During Run 1

ORIGINAL PAGE IS  
OF POOR QUALITY

16:59:24 09/11/81

BOEING 727 : RUN 2

4 Ch. A-Dump is ON



Scale = X 1024  
Time per TICK [ X 100 ms. ] : 125  
MODE: Counts vs Time  
Cumulative Display  
Max = 000120  
Event # 02571  
Volts = 0.015

Figure IV-A-2-k. Cumulative Counts Versus Time Run Number 2

examination of the amplitude distributions from the second data run with a slower loading rate shows a broader distribution of events with far less fiber breakage (i.e., fewer large amplitude events). The final amplitude distribution at failure (shown in Figure IV-A-2-l) indicates a curious build-up of counts at the 65 dB level. The 65 dB amplitude events (totaling 144) were observed throughout the test and may well be directly related to the specific failure mechanism. Also, there appears to be a reasonable correlation between the eleven sudden increases in AE counts (Figure IV-A-2-k) with the eleven load-drop points that are seen (Figure IV-A-2-i) in the discontinuous slope region of the load-stroke curve.

Examination of the strain gauge data shows a lack of symmetry in the readings between the two sides. At four of five comparison stations, side two had readings about 50% higher than those on side one. The fifth station showed side one readings 300% higher than side two. Examination of the two sides of the test rib shows significant differences in the characteristics of this fifth position, from side one to side two. These differences apparently came about from the combination of individually small inaccuracies in strain gauge placement and small variations in laminate stacking boundary positions between the two sides, in a region of rapid cross-section variations. The accumulation of these effects are believed to be the most likely explanation for

ORIGINAL PAGE IS  
OF POOR QUALITY

17:07:29 09/11/81

BDEING 727 : RUN 2

4 Ch. : Dump is ON



AE Cnt A= 6308 AE Cnt B= 0903  
LOC = 000106 Event # 02570  
Max = 001000 Volts = 0.016

1st Hit-MOIE: Events vs. Amplitude  
100 db FULL Scale  
\*END OF DATA\* - Press START to continue

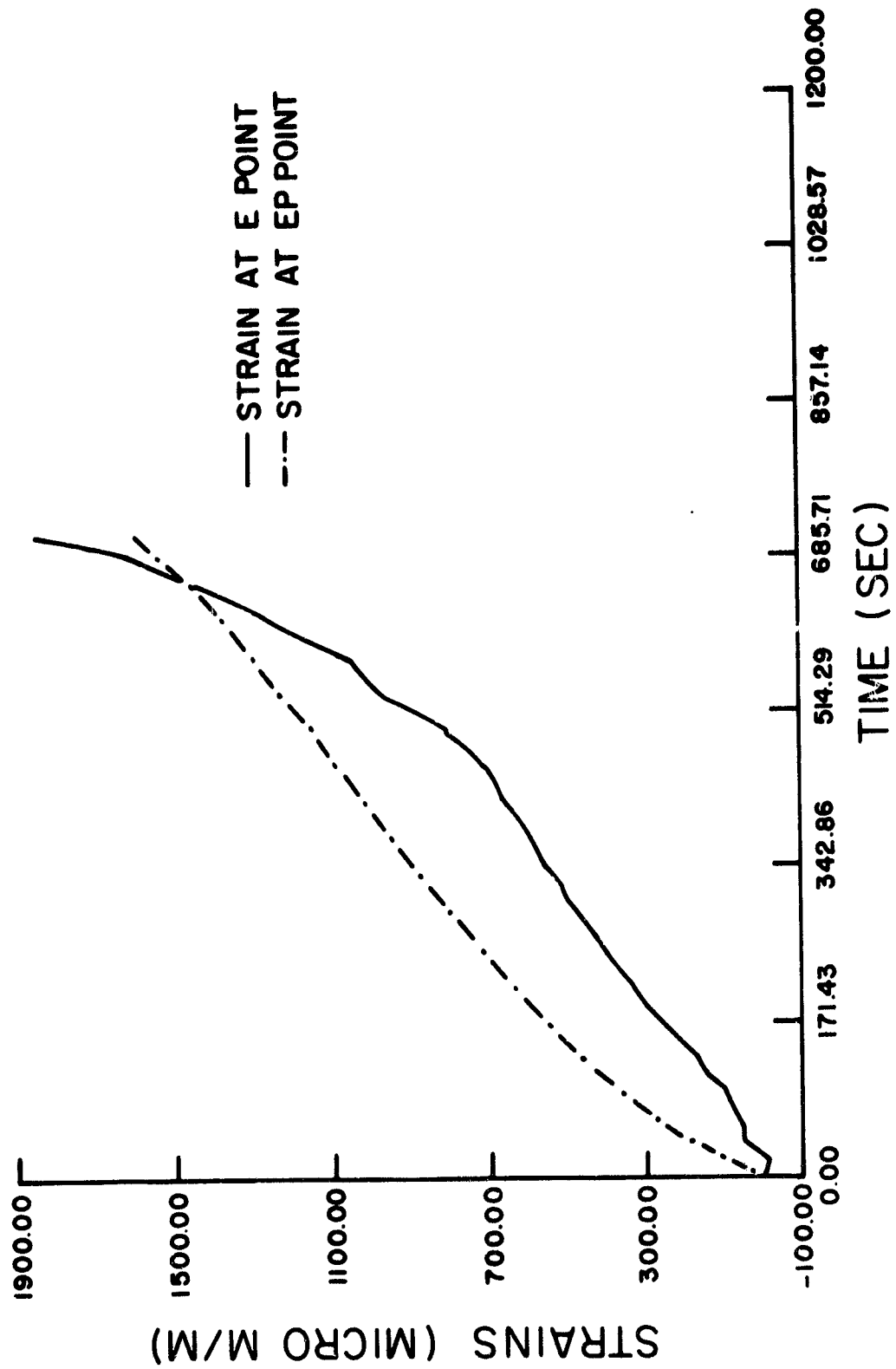
Figure IV-A-2-0. Final Amplitude Distribution at Failure

this 300% disagreement. The imbalance at the other four gauges is probably due either to additional asymmetries in the part itself or an imbalance in the application of the loading. There is little consensus on which is the correct explanation. Contact with Boeing acquired the information that in aircraft practice, care is taken to position loading pins centrally between lugs. Spherical bearings are used to prevent moments from inadvertently entering. In spite of this, safety margins of 20% or more are added to account for asymmetries. The failure actually occurred in our test on side one, which had the generally smaller measured strains (Figure IV-A-2-m). For example, Figure IV-A-2-m shows the unidirectional strain values for vertical strain at points E and EP (Figure IV-A-2-h). Figure IV-A-2-n shows the principal strain values and other selected strains at 707 seconds into the test. The load at this time was 94.3 kN (21,210 pounds). Using the material properties  $E = 40 \text{ GPa}$  (5.83 Mpsi) and  $\nu = 0.28$ , the principal stress values were computed from the principal strains. (Note that this condition is very near the ultimate failure that occurred only 13 seconds later.) Marked asymmetries were observed to exist, yet the observed stress levels are below that normally considered critical for this cross-section. The maximum bearing stress was 0.55 GPa (80 ksi), maximum shear stress was 0.15 GPa (22 ksi) and the maximum tensile stress was 0.19 GPa (27 ksi).

ORIGINAL PAGE IS  
OF POOR QUALITY

Figure IV-3-2-m.

### STRAIN VALUES IN Y DIRECTION AT E & EP



$E = 5.83 \times 10^6 \text{ psi (40 mpa)}$   
 $\nu = 0.28$

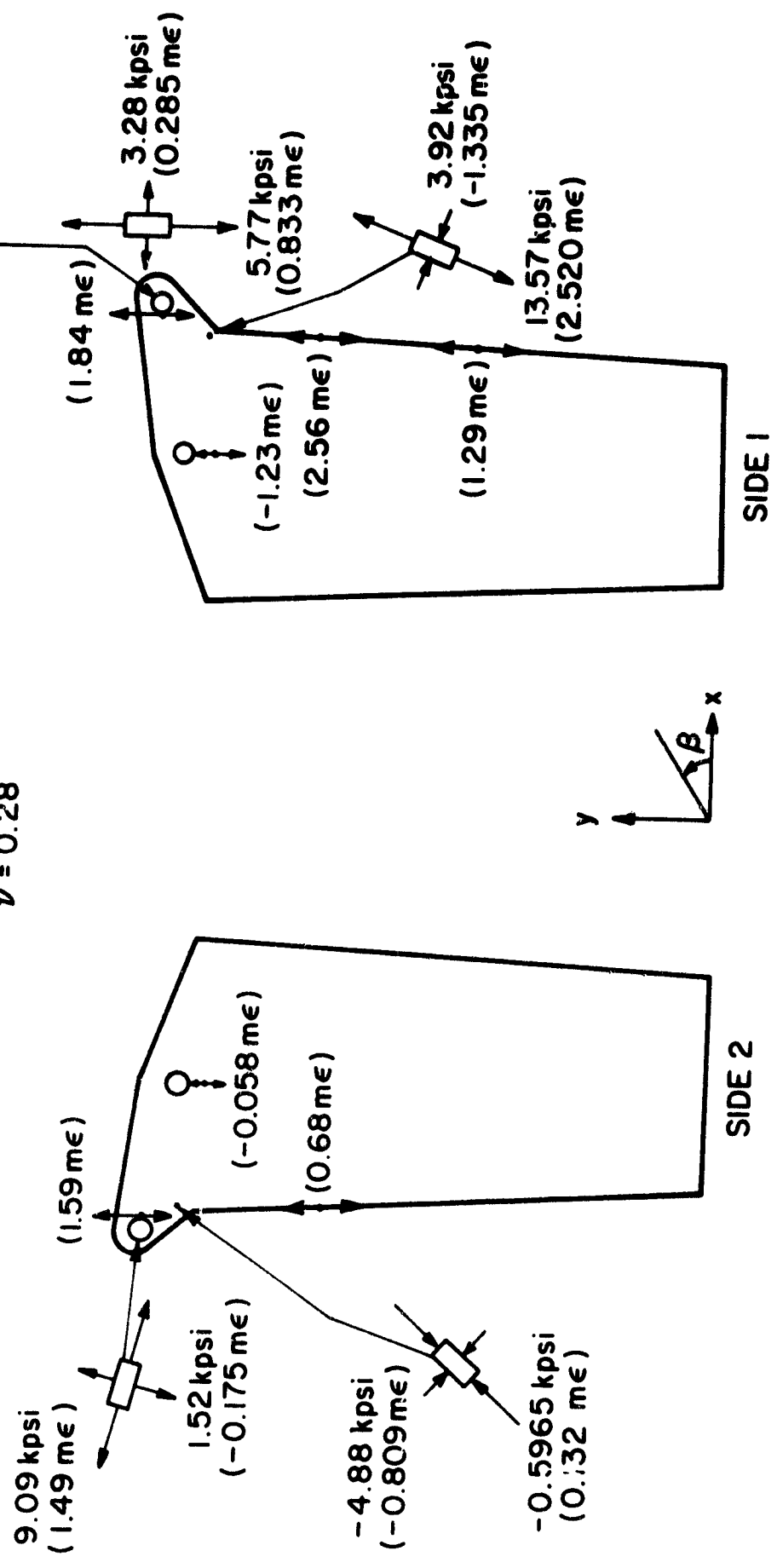


Figure IV-A-2-n.  
 Strains, Principal Strains and Principal Stresses at the Instant of Failure

Close analysis of Figures IV-A-2-o(1-6) suggests bearing failure at the pin. Failure occurred at a bearing stress of 65 ksi, which is well below the value of 80 ksi that was used in design. This is another instance in which the ability to predict lug strength is wanting, and indicates that improved lug design is an area which should receive additional study. This being the second 727 actuator attachment rib specimen to successfully sustain design load with adequate margin, we now consider this project concluded.

ACKNOWLEDGEMENT:

RPI gratefully acknowledges the help of Mr. John Crowell of the Physical Acoustics Corporation in conducting the Acoustic Emission portion of the tests reported above. We are most appreciative of the gracious expenditure of his time, effort, expense and equipment required to set up and run this test.

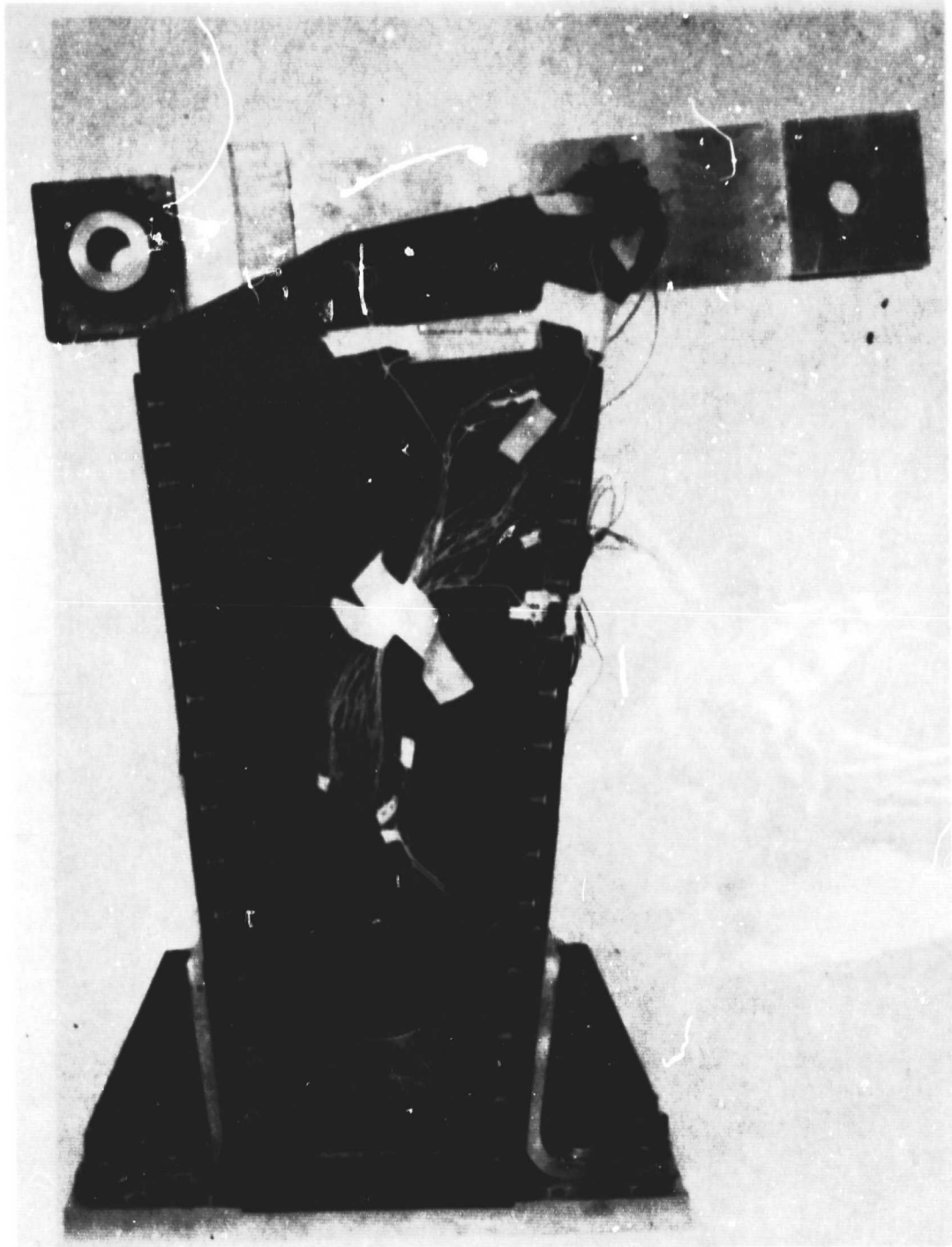


Figure IV-A-2-o(1).  
Failed Actuator: (a) Overall View, Side 1

ORIGINAL PAGE  
BLACK AND WHITE PHOTOGRAPH



Figure IV-A-2-o(2).  
Failed Actuator (b), Failure Site at Point E, View 1

ORIGINAL PAGE  
BLACK AND WHITE PHOTOGRAPH

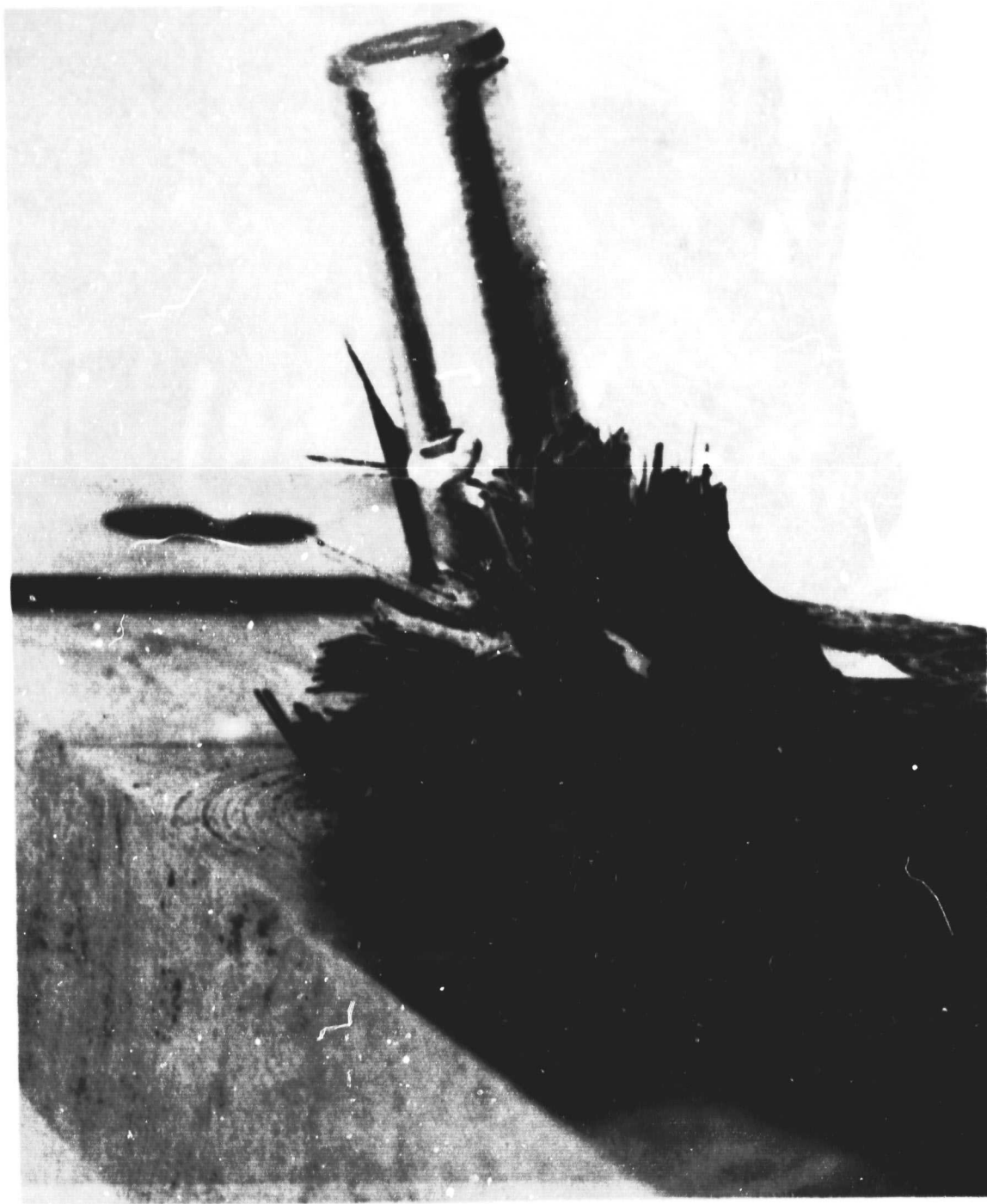


Figure IV-A-2-o(3).  
Failed Actuator (c), Failure Site at Point E, View 2

ORIGINAL PAGE  
BLACK AND WHITE PHOTOGRAPH



Figure IV-A-2-o(4).  
Failed Actuator (d), Failed Site at Point E, View 3

ORIGINAL PAGE  
BLACK AND WHITE PHOTOGRAPH

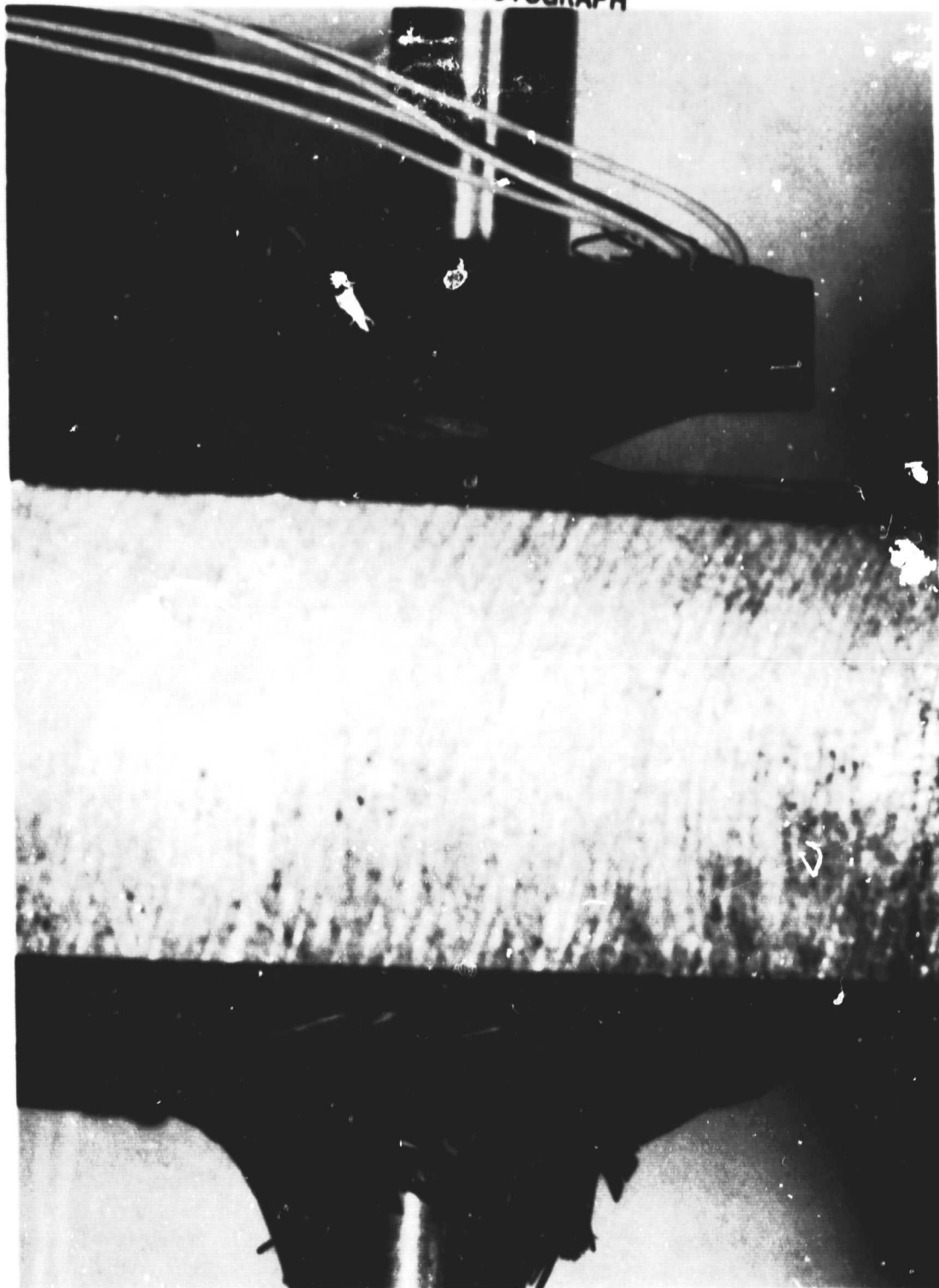


Figure IV-A-2-o(5).  
Failed Actuator (e), Top View

ORIGINAL PAGE  
BLACK AND WHITE PHOTOGRAPH



Figure IV-A-2-o(6).

Failed Actuator (f), Pin Rotation at Point E, Side 2

IV-B LOCKHEED L-1011 ENGINE DRAG STRUT (CAPCOMP II)

Senior Investigator: D. Goetschel

1. Introduction

Following a visit by Dr. R. Loewy to the Lockheed California Company on November 12, 1980 and subsequent meetings and discussions in the NASA Headquarters office of the Project Officer, we jointly selected the drag strut of the wing-mounted, jet engine nacelles of the Lockheed L-1011 commercial transport aircraft for redesign in composites as the second CAPCOMP project. A drawing of the strut, currently a steel forging is shown in Figure IV-B-1. The manner of its installation is shown in Figure IV-B-2. Both of these drawings, along with the first of the considerable information needed to perform this design, were graciously provided by the Lockheed Company.

2. Status

Preliminary studies were conducted to assess the magnitude of the total task. Some of these considerations were reported in the progress report dated July, 1981. Other aspects are summarized here.

Figure IV-B-3 is an extract of the design loads established by Lockheed for the part. Notice that compressive loads to 466.6 kips must be withstood. Accordingly, three basic compression failure criteria must be considered: material failure, Euler buckling and local buckling or

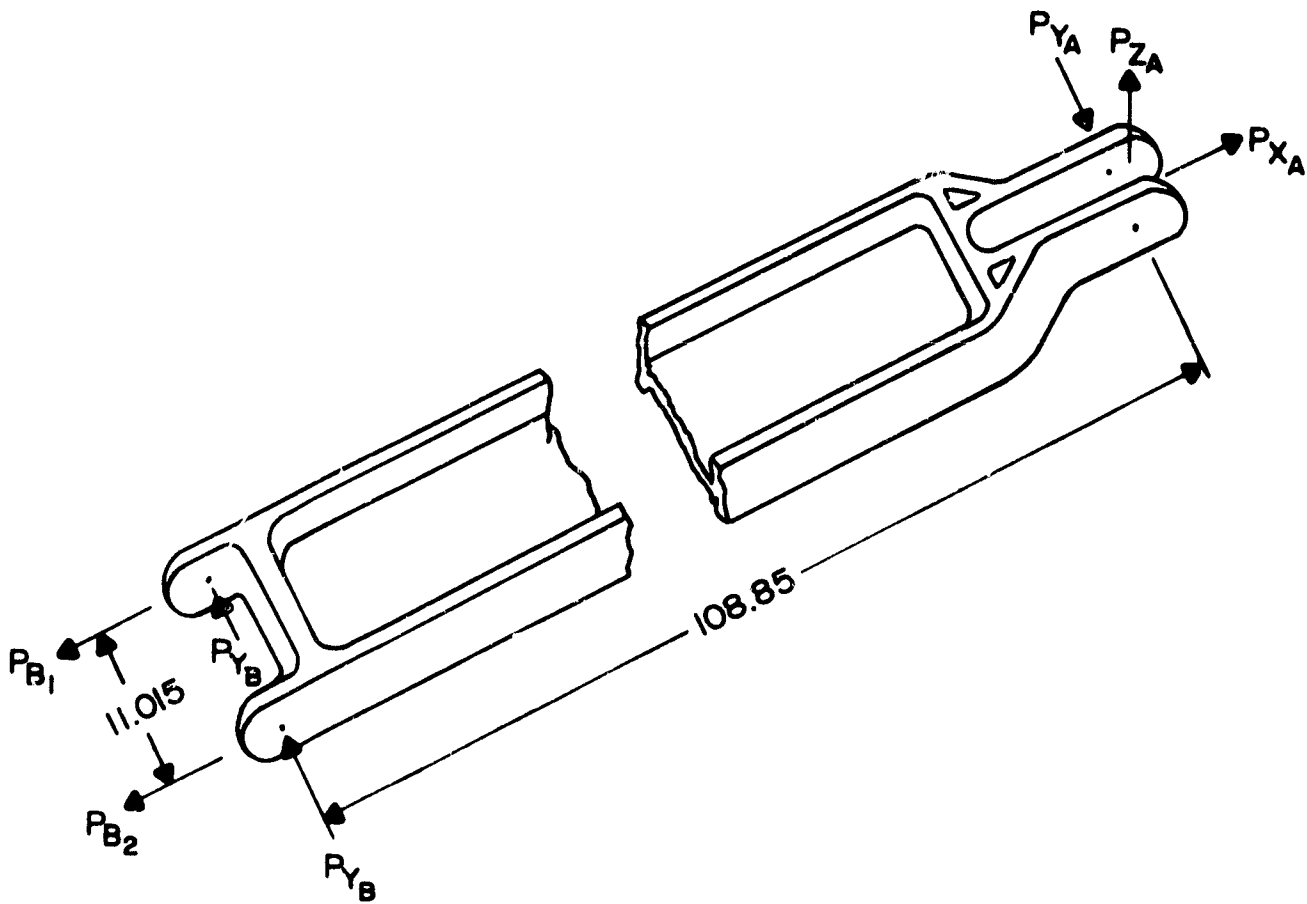


Figure IV-B-1.  
Lockheed L-1011 Engine Drag Strut (Schematic)

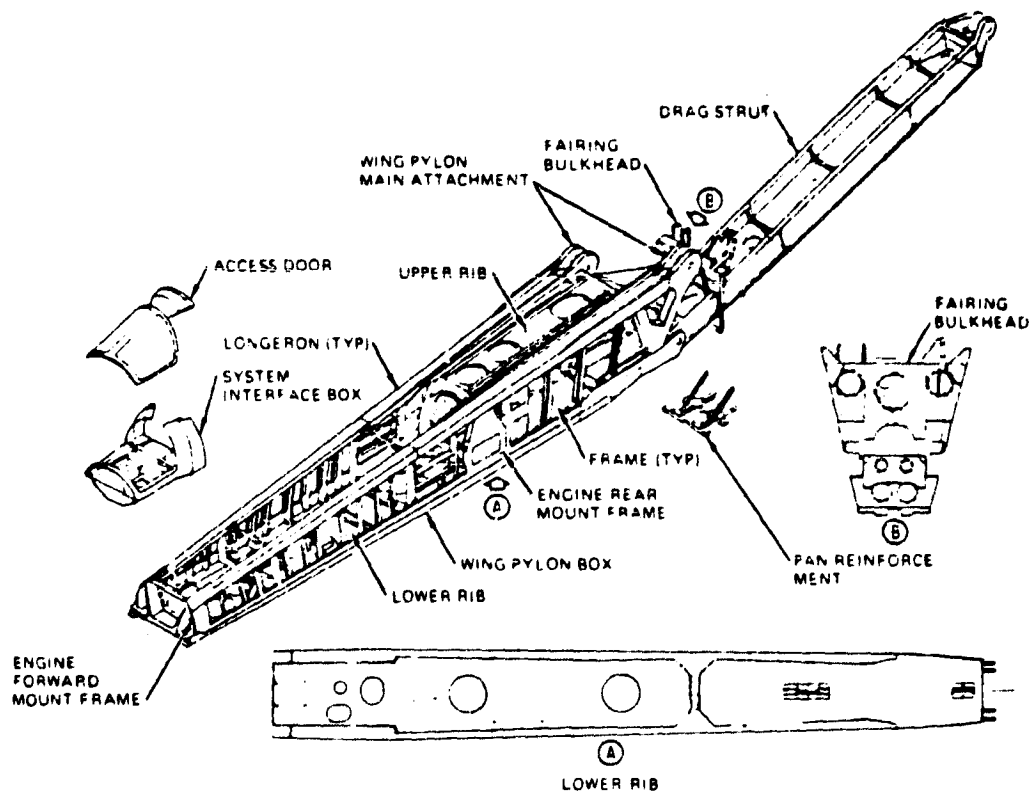
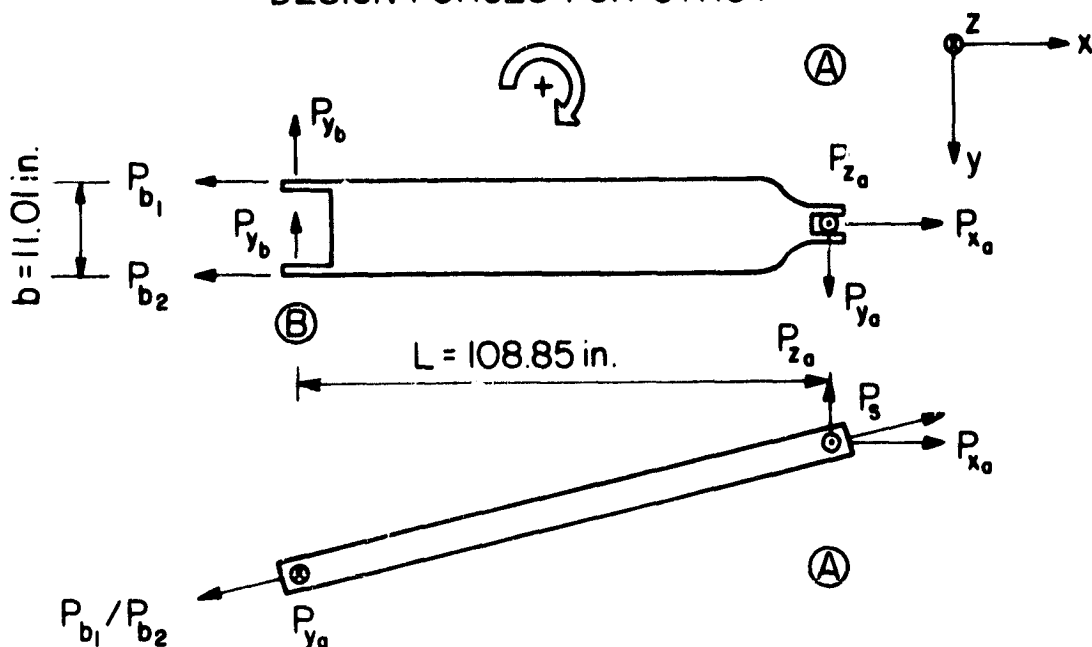


Figure IV-B-2.  
Lockheed L-1011 Wing Pylon Structure Assembly

Figure IV-B-3.

## DESIGN FORCES FOR STRUT

DESIGN ULTIMATE LOADS [ $10^3$  lbs.]

Load Condition Number	Components						
	$P_{x_a}$	$P_{y_a}$	$P_{z_a}$	$P_s$	$P_{b_m}$	$P_{b_1}$	$P_{b_2}$
3	-77.6	-12.0	-16.3	79.3	-118.68	-19.69	98.99
21	-456.6	-0.7	-96.2	-466.6	-6.92	-236.76	-229.84
33	341.2	1.6	71.9	348.7	15.82	182.26	166.44
25	-425.0	3.8	-89.5	-434.32	37.58	-198.4	-236.0
34	318.5	-9.1	67.1	325.5	90.0	117.7	207.7

DESIGN LIMIT LOADS [ $10^3$  lbs.]

3	-51.73	-8.0	-10.87	52.87	-79.12	-13.13	65.99
21	-304.40	-0.47	-64.13	-311.07	-4.61	-157.84	-153.23
33	227.47	1.07	47.93	232.47	10.55	121.51	110.96
25	-283.3	2.5	59.7	-289.5	25.1	-132.3	-157.3
34	212.3	-6.1	44.7	217.0	60.0	78.5	138.5

wrinkling. The formulas for handling the first two criteria are readily available in standard texts; however, formulas in a form suitable for design purposes for the local instability of an anisotropic plate or shell are not as readily available. One of the first tasks for this project is to obtain or develop such equations for various boundary conditions. A search of the literature and design guides is now being conducted to see what formulas are available. If suitable formulas are lacking, they will have to be developed for the pertinent and/or additional special cases of interest. Once these formulas are available, preliminary design concepts can be sized to determine their structural efficiency. Undergraduate student Frank DeTaranto, graduate student Shu-Ping Chen and postdoctoral fellow Christoph Muser have been pursuing this problem. So far both axisymmetric and nonsymmetric buckling formulas have been found for round tubes.

### 3. Progress During Report Period

Additional preliminary studies since the last reporting period have revealed the following facts. The size and load capacity of this part require special budgetary considerations. A full-sized strut will involve graphite/epoxy materials costs of about \$10,000; this severely limits the number of design iterations that can be performed on full-sized parts. The Instron testing machine available at RPI has a maximum grip spacing of four feet and a load capacity of 56,600 pounds. To test a full-sized part on-campus would,

therefore, require that a large and expensive mechanical lever mechanism be constructed. Testing off-campus would limit the number of Rensselaer personnel that could participate in the testing process. For these reasons we plan to perform most of the development on scale-model parts. Hopefully then it would only be necessary to fabricate and test a single full-scale drag strut as a final demonstration of the design. A scale factor of one-quarter has been selected. This would make the scaled drag strut 2.5 feet long, which should fit in the Instron testing machine, even allowing for test fixtures. Material volume and costs will scale as the cube of the scale factor  $[(\frac{1}{4})^3 = \frac{1}{64}]$ , reducing the material cost per strut to approximately \$150.

The remaining issue is whether the potential failure modes will all scale properly. Composite material failure stress is a composite material property; it should, therefore, not change with scaling except for cure chemistry thermodynamics. For Euler buckling, only two geometric factors - length and radius of gyration - are important, and they occur as a ratio of each other. Since they both scale with length, the Euler buckling stress should remain completely unaffected by scaling. For local buckling of isotropic materials, the geometric factors also occur as ratios of length parameters, so this failure stress should also remain unchanged by scaling for the anisotropic strut. With all the failure modes scaling in the same fashion, a full-sized strut

should fail in the same fashion as the quarter-scale model, unless the ratio of fiber size to minimum part dimension should somehow become important.

If the failure stresses do not change with scaling, the failure load should scale with the cross-sectional area or the square of the scale factor. With a maximum axial load of 466.6 kips being scaled by  $(\frac{1}{4})^2$ , the maximum axial load for the scaled part should be 29.2 kips. This is well within the capacity of RPI's Instron machine. The only remaining objection to scale models would be difficulty in achieving minimum gauge thicknesses. It appears that the scaled minimum wall thicknesses will still allow for at least several plies of composite material, so this is not now expected to be a major problem. For the above reasons, quarter-scale model testing should provide realistic results, while allowing multiple interactions of the design-fabrication-testing cycle.

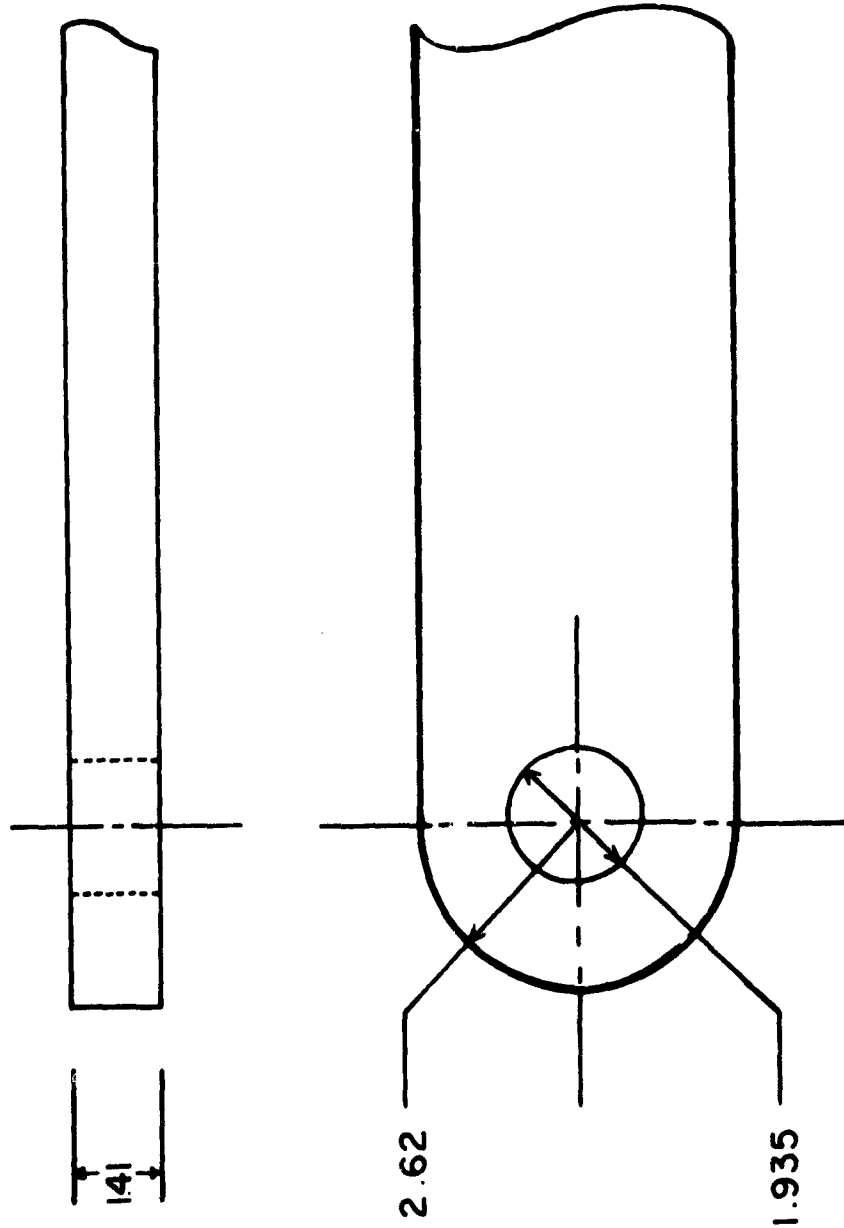
#### 4. Plans for Upcoming Period

A critical aspect of the drag strut design is the way load transfer is effected at the connecting lugs at the ends of the strut. They are highly loaded, and in tension they have a very complex stress state. The lugs should be designed to fall within the same dimensional envelope as those on the production strut. Since these lugs are made from 200 ksi steel, meeting the geometric constraints could prove to be a difficult task even with a design making maximum use of

unidirectional graphite epoxy. We plan to attempt this first, but should it not be feasible, there are two other options. First, the lugs could be made from high strength steel and attached to a composite strut. Second, the attitude could be taken that this redesign is part of a redesign of wider scope that would allow composite lugs to be dimensioned as needed.

The design of the lugs (see Figure IV-B-4) is important to the design of the rest of the strut, so this problem will be concentrated on first. Fixtures will be designed and constructed for testing one side of a quarter-scale model lug. Wrapping the graphite fibers around the mating pin would provide the greatest tensile strength around the pin, but this approach has two drawbacks; there are problems with the outer fibers bunching up during curing and potentially very low transverse compressive strength next to the pins. Such problems can be successfully dealt with, but they do compromise the effectiveness of this approach. Initially the suitability of a flat, symmetric angle-ply laminate will be investigated. Computer programs are being written to optimize the orientations and volume fractions of the plies. Scaled models of candidate lay-ups will then be tested to determine if this approach can be successful.

It is noteworthy that three research areas of generic interest to composite structural elements have emerged from our Lockheed 1011 drag strut redesign efforts to date. They



MAXIMUM TENSILE LOAD - 207.7 KIPS  
 MAXIMUM COMPRESSIVE LOAD - 236.8 KIPS  
 MAXIMUM LATERAL LOAD - 12.0 KIPS

**DIMENSIONS IN INCHES**

Figure IV-D-4. Lug Experiment: Full-Scale L-1011 Drag Strut

are (a) the need for quantified information regarding St. Verant's principle for typical cross-sections of compression-tension-bending members using composite materials (semi-annual progress report, July, 1981); (b) the degree to which design development of major structural elements can be conducted with confidence at reduced scale; and (c) whether all composite, heavily loaded lugs, which will meet stringent over-all geometric envelope constraints, can be successfully designed and fabricated. We anticipate dealing with all of these important problems to some extent in the months ahead.

#### IV-C MECHANICAL JOINTS IN COMPOSITES

Senior Investigators: D. Goetschel  
R. Loewy

The immediately preceding two sections of this report illustrate forcefully the importance of being able to deal with mechanical joints in composite plates. In this section progress is reported on two continuing research projects in this area. The first involves optimizing the laminates around a hole - first open and later to be pin-loaded - using special variations of the material properties with distance from the hole. This is the work of post-doctoral fellow C. Muser. The second involves attempts to predict accurately stresses in the region of a pin-loaded hole in composite plates of typical, spatially uniform lay-ups. The second research is that of graduate student W. Kim.

##### 1. Analysis of Heavily Loaded Mechanical Joints

###### a. Introduction

Today's composite materials provide flexibility in choosing material properties for special design applications. In principle it is possible to have the fibers running in any direction, straight or curved, and with spatial variations in their fiber directions. Structural elements made from these materials can, therefore, be designed to specific properties at specific locations in order to increase load-carrying capacity-to-weight ratios. This aspect of fiber

reinforced plastics is not understood well enough to allow designing mechanical joints and openings in composite plates in a way which exploits the "tailored material" opportunities available with composites. A detailed investigation seems to be justified.

#### b. Review of Previous Work

A closed form solution was found by N. J. Hoff for the stress distribution in a circular plate with a central hole of radius  $r = 1$  and an outer radius,  $r = R$ , under uniform uniaxial traction,  $\sigma$ , when the material is cylindrically orthotropic and homogeneous. Figure IV-C-1-a shows the geometry of such a plate. The maximum circumferential stress,  $\sigma_{\theta\theta}$ , at the boundary of the hole can be expressed as a function of the outer radius,  $R$ , of the plate and the two material property parameters,  $\bar{S}_{rr}$  and  $\bar{S}$ . Here the first parameter is defined as  $\bar{S}_{rr} = S_{rr}/S_{\theta\theta}$ , and the second parameter is  $\bar{S} = 2\bar{S}_{r\theta} + \bar{S}_{\theta\theta} = 2(S_{r\theta}/S_{\theta\theta}) + S_{\theta\theta}/S_{\theta\theta}$ . For any fixed geometry of the plate (radius  $R$  fixed), it is possible to draw lines of equal stress concentration-factors as a function of the two parameters  $\bar{S}$  and  $\bar{S}_{rr}$ . (Stress concentration-factor is defined as the highest circumferential stress,  $\sigma_{\theta\theta}$ , at the edge of the hole divided by the average stress,  $\sigma$ .) In other words, for a given geometry one can read the stress concentration-factor from a simple graph for any cylindrically orthotropic material (See Figure I-27, Semi-Annual Progress Report, July, 1981, pp. 66).

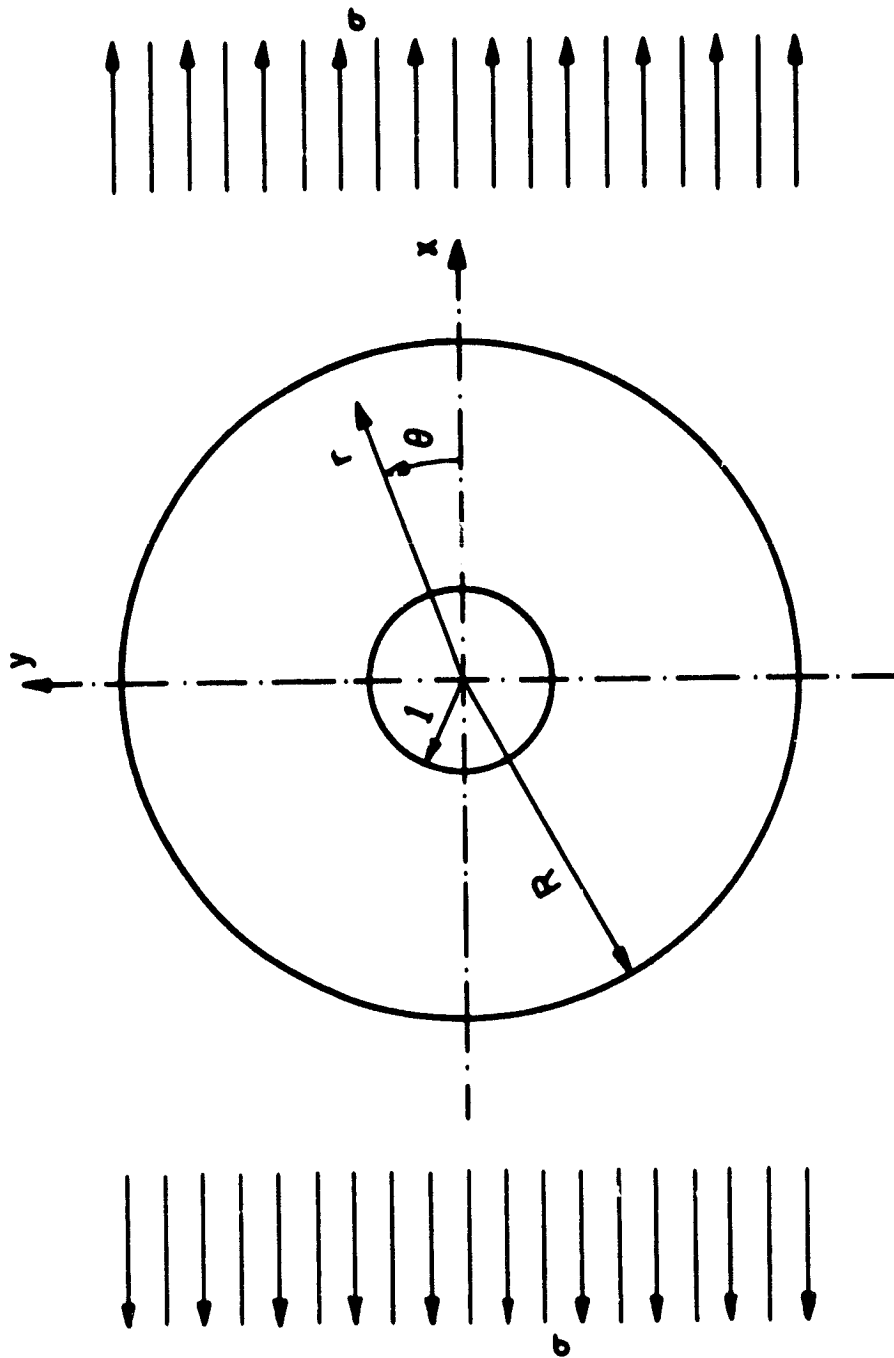


Figure IV-C-1-a.  
Geometry of the Cylindrically Orthotropic Plate with Unloaded Hole

Part of the work in this area was to find the expressions for the stress distributions in the same kind of circular plate when the material properties are not constant but rather a function of the distance from the central hole. The constitutive equation used in this case is:

$$\begin{pmatrix} \epsilon_r \\ \epsilon_\theta \\ \gamma_{r\theta} \end{pmatrix} = \begin{bmatrix} S_{rr}^* (1 + \delta_{rr} r^h) & S_{r\theta}^* (1 + \delta_{r\theta} r^h) & 0 \\ S_{r\theta}^* (1 + \delta_{r\theta} r^h) & S^* (1 + \delta_{\theta\theta} r^h) & 0 \\ 0 & 0 & S_{66}^* (1 + \delta_{66} r^h) \end{bmatrix} \begin{pmatrix} \sigma_r \\ \sigma_\theta \\ \tau_{r\theta} \end{pmatrix}$$

The two parameters  $S_{ij}^*$  and  $\delta_{kl}$  characterize the material properties at the edge of the hole and at the outer boundary of the disk. The parameter  $h$  is used to describe the change of material properties along the radius. The solution found is in the form of a power series of the radius  $r$ , and uses the exact closed-form solution for homogeneous materials as a starting point. The conditions for equilibrium and the boundary conditions are satisfied exactly. The condition for compatibility is satisfied in the limit. It was found that the stated solution does not converge for every combination. Convergence limits were established. Several numerical results were obtained.

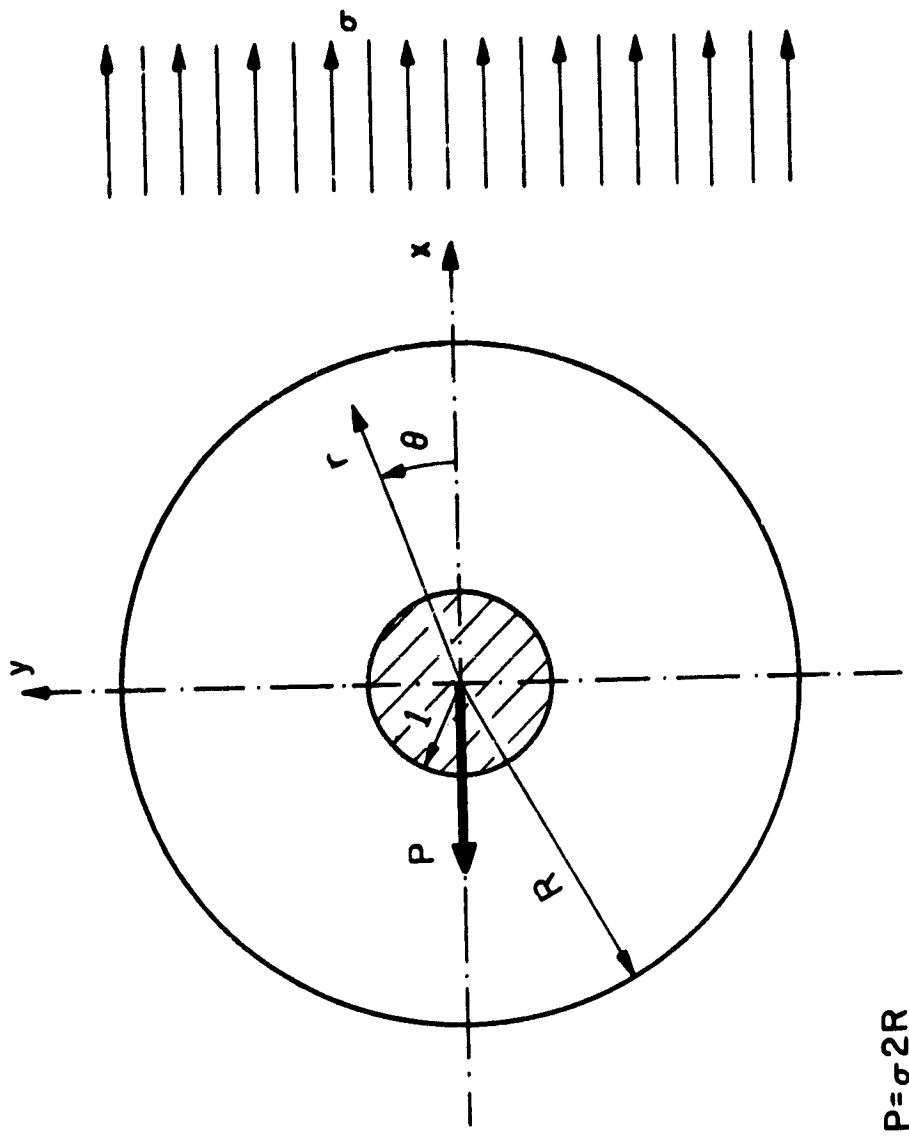
### c. Progress During Report Period

The first part of the current period was devoted to documenting and reporting the results obtained earlier.

Progress was also made in applying the solutions found for the unloaded hole to the case of a circular plate pulled

at its outer edge  $r = R$  in one direction and pulled in the opposite direction by a bolt inserted in a central hole. The material properties are still allowed to vary along the radius,  $r$ . The geometry used is shown in Figure IV-C-1-b.

It is believed that cylindrical orthotropy - as in the case of the open hole - will result in low stress concentrations around the loaded hole as well. The aim of the work is not to find the exact boundary conditions at the edge of the hole nor is it to find the proper failure criterion. The aim is rather to show the possible potential of cylindrical orthotropy as a means to design lugs more efficiently. Therefore, the calculations are kept strictly two-dimensional and the boundary conditions at the edge of the hole express only the presence of normal stress,  $\sigma_r$ , over one-half of the circumference. The common assumptions that the bolt fits snugly and that friction between the bolt and the plate does not exist were also made here. The boundary conditions can be expanded into a trigonometric series. It is possible to adjust the stress function found for the empty-hole case so that it can be used to solve the present problem. Moreover, it seems possible to solve for any boundary conditions which can be expressed in trigonometric series, so long as convergence is provided. As of this writing, no numerical results have been obtained.



$$P = \sigma 2R$$

Figure IV-C-1-b.  
 Geometry of the Cylindrically Orthotropic Plate with Loaded Hole

#### d. Plans for Upcoming Period

In the months ahead we plan to continue the investigation of stress distributions in circular, bolt-loaded plates, the material properties of which are cylindrically orthotropic and vary along the radius. In addition, we expect to make presentations of and to publish the results found for the open-hole case with radially varying material properties.

#### e. Current Publications or Presentations on this Subject

by Professor Hoff:

"Stress Concentrations in Cylindrically Orthotropic Composite Plates with a Circular Hole"

Published in the Journal of Applied Mechanics, September, 1981, Vol. 48, pp. 563-569.

Presented at the Joint ASME/ASCE Mechanics Conference, Boulder, Colorado, June 23, 1981.

by Dr. Muser:

"Cylindrically Orthotropic Circular Plates with a Concentric Hole and with Properties Varying Radially"

Thesis for the degree, Doctor of Engineering, Rensselaer Polytechnic Institute, August, 1981.

## 2. Pin-Loaded Holes in Uniform Composite Plates

### a. Introduction

To optimize a mechanical joint in composites, it is necessary to be able to predict the stress distributions around the hole. In this approach to solving this problem, analysis has been restricted to a single hole, plane problem, as a necessary first step.

Even this simplified problem falls in the category of mixed boundary value problems with unknown boundary conditions

on a part of a boundary. The amount of contact between the loading pin (assumed rigid) and the hole as it deforms under load is thus unknown. By introducing a semi-empirical analysis method, which we called the "mixed method", as explained in previous reports, the boundary conditions can be determined.

One of the most important results of this reporting period is that the possibility has emerged that resolution of the contact problem may be obtained - without the "mixed method" - by using interactive graphic computer terminals. This approach, as will be explained in the subsequent section, is based on the idea that an originally smooth curve, in or on the boundary of the material, must remain smooth after deformation, provided that the surface applying the load is also smooth.

#### b. Status

As noted in earlier reports, once the extent of the region of contact between the loading pin and the loaded hole is known (originally undetermined for clearance fit cases), the stresses in the domain can be obtained by various means. For example, a finite element analysis can be performed with displacement boundary conditions for points located in the contact region. These boundary conditions are determined by the rigid surface applying the load. During the previous period, a system of linear constraint equations was applied to the nodal points in the presumed contact region for this

purpose. The correct extent of the contact region (defined by the contact angle  $\theta_c$ ) was inferred by comparing the maximum strain contours from several such finite element analyses with different values of  $\theta_c$  with the isochromatic fringes from corresponding photoelastic experiments. Where the maximum shear strain distributions were well-matched, the assumed value for  $\theta_c$ , as well as the corresponding stress solutions, were taken as also correct.

The feasibility of this method for this particular problem has been discussed in previous reports. We note here, however, that this "mixed method" can be expanded for more complicated problem situations; for example, multiple pin connections; and second, that the results are not subject to uncertainties as to the adequacy of the finite element model or other assumptions, since the method is self-checking precisely because of its semi-empiricism.

#### c. Progress During Report Period

The linear constraint equation used to prescribe the motion of a node point on the boundary within  $\theta_c$  has been changed during this report period. It was derived as follows.

Let the undeflected position of a node point,  $p$ , be  $x$  and  $y$  in the cartesian coordinate system centered on the hole (Figure IV-C-2-a). If  $p$  is within  $\theta_c$ , for a particular level of applied load, then the final location of  $p$  after deformation is somewhere on the surface of the rigid, fixed pin;

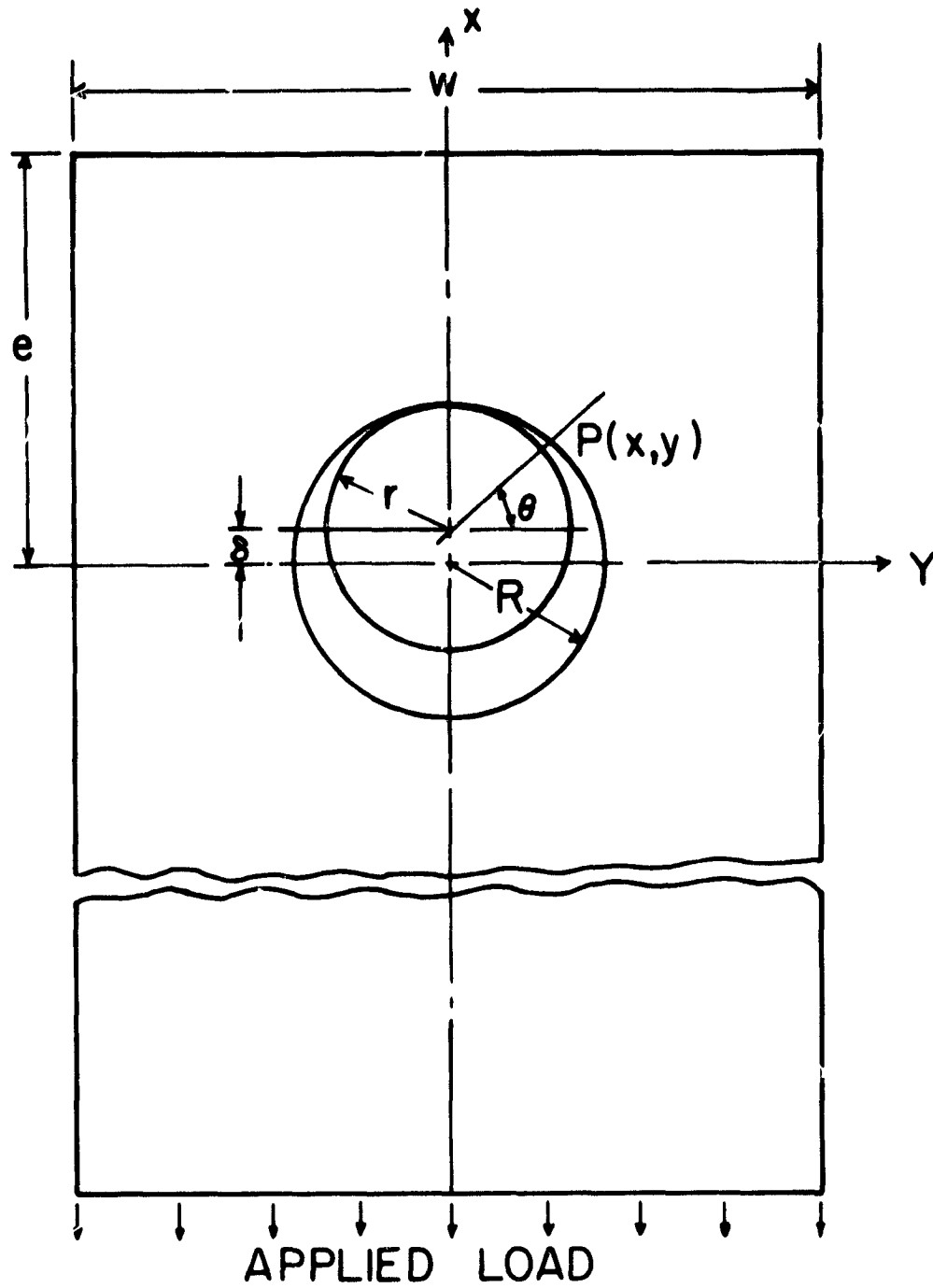


Figure IV-C-2-a. Problem Idealization

i.e., at a point described by

$$(x + u)^2 + [(y - \delta) + v]^2 = r^2 \quad (1)$$

where,  $u$  and  $v$  are displacements of  $p$ , in the  $x$  and  $y$  directions, respectively,  $\delta$  is the clearance and  $r$  is the radius of the pin. Equation (1) can be rewritten by expanding and neglecting  $u^2$  and  $v^2$ , since they are small, first order.

$$x^2 + 2ux + (y - \delta)^2 + 2v(y - \delta) \cong r^2 \quad (1')$$

Dividing both sides of Equation (1') by  $\sqrt{x^2 + (y - \delta)^2}$ , noticing that

$$\frac{x}{\sqrt{x^2 + (y - \delta)^2}} = \cos \theta$$

and

$$\frac{(y - \delta)}{\sqrt{x^2 + (y - \delta)^2}} = \sin \theta$$

and rearranging, one obtains

$$u \cos \theta + v \sin \theta = \frac{r^2 - [x^2 + (y - \delta)^2]}{2\sqrt{x^2 + (y - \delta)^2}} \quad (2)$$

This equation is the form in which the constraint equation was used.

If  $\delta = 0$  in Equation (2) (i.e., no clearance), then Figure IV-C-2-a makes it clear that the right-hand side of (2) is zero, so that

$$u \cos \theta + v \sin \theta = 0 \quad (3)$$

This is the constraint equation for the case of no clearance and is consistent with constraints used in previous reports.

Also during the reporting period, two photoelastic specimens were manufactured and tested. The overall dimensions of the new specimens are almost identical to those of previous specimens, except for the thickness. As shown in Table IV-C-2-a, the total number of layers was increased from 18, as used in the old specimens, to 23 for B-type lay-ups (i.e.,  $[\pm 45^\circ/0^\circ]_{ns}$ ). For this particular laminate,  $n$  was intended to be 8, since the design called for 24 layers, but one  $0^\circ$  layer was inadvertently left out during the lay-up process. However, symmetry was maintained, since it was a center  $0^\circ$  layer that was missing. The resulting thicknesses of plates after curing were 0.132 inch for  $[\pm 30^\circ/0^\circ]_{8s}$  and 0.127 inch for B-type plates. This matched well with what would be expected from manufacturer's standards for graphite/epoxy prepreg tapes.

Plate thickness increases were made the subject of investigation since earlier results suggested that outer layer delamination and subsequent buckling of separate fibers were mechanisms in bearing failures. This effect may be made a smaller fraction of total strength as the total number of layers increases.

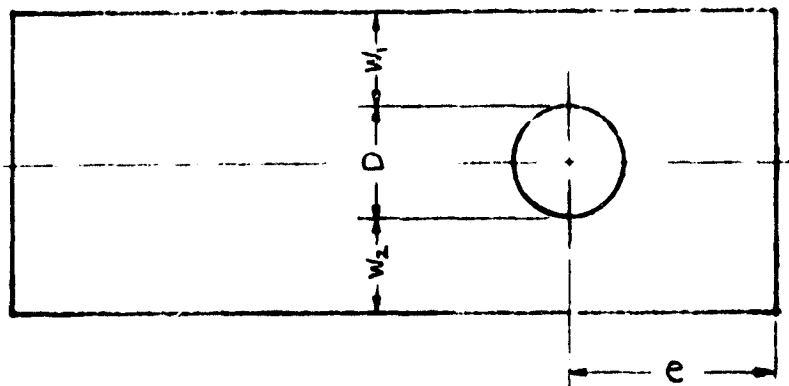
One may see from Table IV-C-2-a that the bearing strength of a composite plate is strongly dependent on the total thickness but not so much on the ratio of the hole diameter to the thickness ( $D/t$ ). More precisely, the  $D/t$  of Experiment II

TABLE IV-C-2-a  
STRENGTH AS INFLUENCED BY D/t FACTOR, [ $\pm 45^\circ/0^\circ$ ]<sub>ns</sub>

Experiment	Diameter D (inch)	Number of Layers	Thickness t (inch)	D/t	Average Bearing Stress (Psi)
I	0.25	18	0.103	2.43	71,706
II	0.5	18	0.103	4.85	70,526
III	0.4995	23	0.127	3.93	94,488

TABLE IV-C-2-b  
DIMENSIONS MEASURED (PHOTOELASTIC SPECIMEN, EXPERIMENT III)

Laminate	e (inch)	w <sub>1</sub> (inch)	w <sub>2</sub> (inch)	D (inch)	Number of Layers	Thickness t (inch)
B [ $\pm 45^\circ/0^\circ$ ] <sub>ns</sub>	2.001	1.0007	1.001	0.4995	23	0.127
[ $\pm 30^\circ/0^\circ$ ] <sub>ns</sub>	1.990	0.997	0.9965	0.5	24	0.132



(4.85) is twice as big as that of Experiment I (2.43), but the average bearing stresses at failure are roughly the same for both specimens and their thicknesses are exactly the same. On the other hand, the roughly 30% thickness increase of Experiment III resulted in more than a 50% increase of failure load compared to Experiments I and II, although the Experiment III plate's  $D/t$  fell between those of the earlier plates.

While this result indicates that the bearing strength of a composite joint depends highly on the overall thickness of a plate instead of on  $D/t$  ratio, we believe that there will be a limit to the total number of layers above which increasing the number of layers will affect bearing strength only negligibly. This follows since the loss of strength of the more easily delaminated outer layers becomes a smaller percentage of the total strength of the full number of layers as the laminate thickness grows, as noted earlier.

This has important meaning from a model scaling point of view. Apparently, one must take this effect into account whenever scaling up (or down) pin-loaded joints in composites.

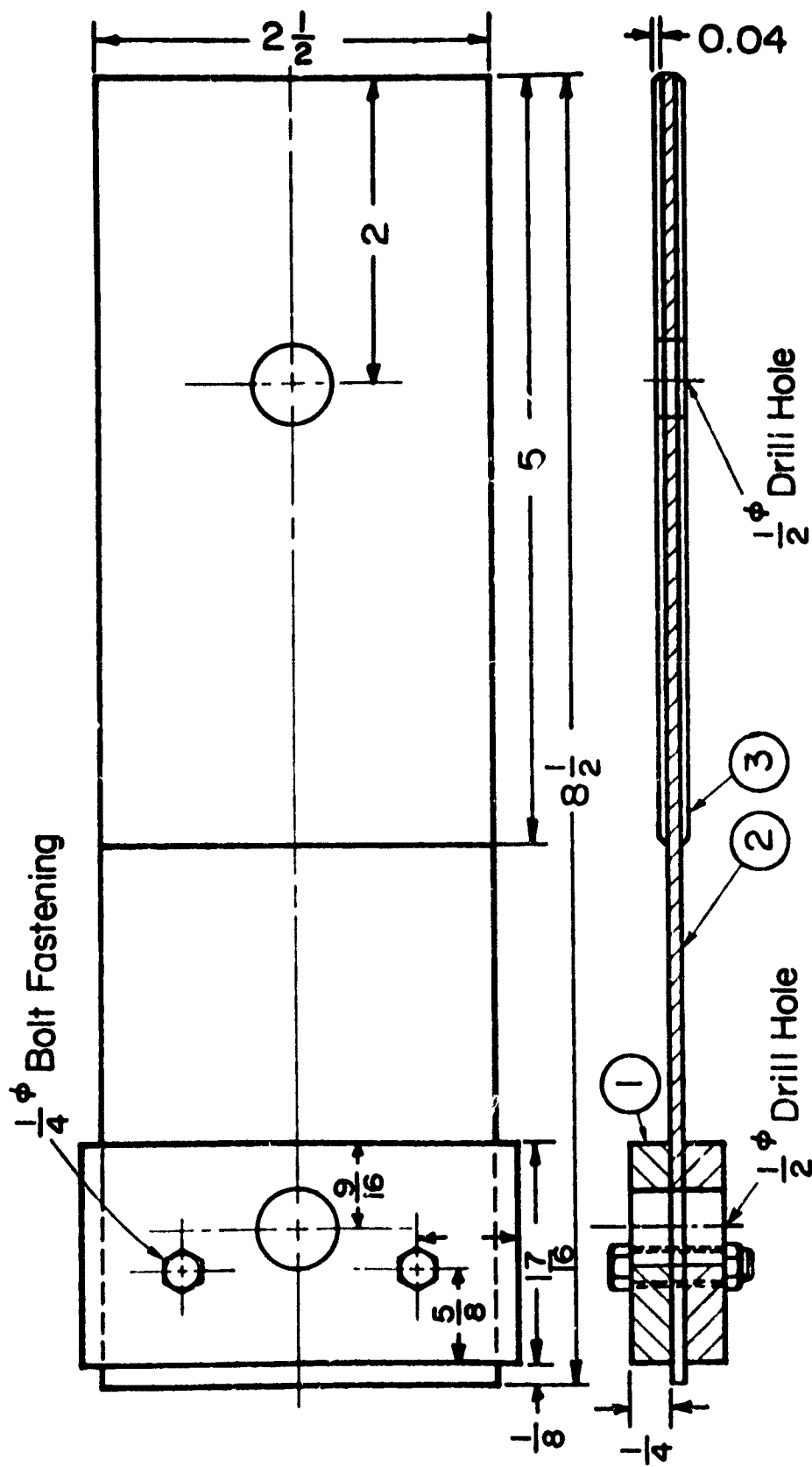
Other progress during the subject period includes improvement in the manufacturing processes of photoelastic specimens. Grid nets were engraved on the back side of the photo-elastic coatings, prior to bonding on the test specimens, for easy fringe position determination. Special attention was given to specimen dimensions to insure symmetry.

Final measurements showed that the eccentricity of the location of the hole was less than 0.001 inch for both specimens. Hole diameter was checked in several directions using a flexible radius gauge, which, when used skillfully to check roundness, can detect 0.0005 inch differences. The differences between maximum and minimum diameters in the holes in our specimens were too small to be detected using this instrument.

The loading pin used in these tests was manufactured so that the diametral clearance would be 0.0015 inch after all the necessary corrections and measurements had been made. Due to the increase of laminate thickness, several metal parts of the test fixture had to be heat treated to give higher strength (see Figure IV-C-2-b).

Photoelastic experiments were performed on an Instron testing machine. At every additional 500 pounds of load, isochromatic pictures were taken until the specimen failed. The failure loads were 6,000 pounds for B-type specimens and 5,860 pounds for F-type ( $[\pm 30/0^\circ]_{8S}$ ) laminates. It is interesting that the total number of layers of Specimen B was one layer less than that of F-type, but still showed higher strength. Table IV-C-2-b shows the detailed dimensions measured for both specimens.

Additional finite element analyses have been performed in this period, following the same process that has been described in several previous reports. Figure IV-C-2-c shows the isochromatic fringes of Specimen B at 4,000 pounds, and



1. Aluminum Reinforcement
2. Graphite / Epoxy Plate
3. Photoelastic Sheet

Figure IV-C-2-b. Photoelastic Specimen

ORIGINAL PAGE  
BLACK AND WHITE PHOTOGRAPH



Isochromatic Fringes \*

$[\pm 45^\circ/0^\circ]_{8s}$

4000 lbs.  $D = 0.4995$  in.  
2 = 0.0015 in.

---

\* One fringe is equal to 0.001892 in/in maximum shear strain.

Figure IV-C-2-c. Isochromatic Fringes

Figure IV-C-2-d shows the maximum shear strains resulting from the finite element analysis. The value of the maximum shear strains for corresponding contours are given at the upper right-hand side of Figure IV-C-2-d. These values correspond to those of Figure IV-C-2-c and will be seen to check very well. Figure IV-C-2-e is a scaled-up picture of Figure IV-C-2-d. The maximum shear strain distributed in both are almost identical to those in Figure IV-C-2-f, except for minor details. This leads to the conclusion that the contact angle of this specimen with 0.0015 inch no-load clearance between the loading pin and hole is about 75 degrees at a load level of 8,000 pounds.

The same procedures have also been completed for load levels of 1,000, 2,000, 3,000 and 5,000 pounds. The results allow plotting the relationship between applied load and contact angle as shown in the Figure IV-C-2-f. By extrapolating and interpolating this curve, one can obtain the contact angle at any load level including the failure point. This enables us to examine the stress situations at the maximum load with considerable confidence.

The ranges of contact angles shown in Figure IV-C-2-f are those within which the contour plots of maximum shear strain are too similar to allow selecting one as being a better match than the others. However, once those ranges of contact angle are put on one plot, as in Figure IV-C-2-f, and assuming the correct value is closer to the middle of



ORIGINAL PAGE IS  
OF POOR QUALITY

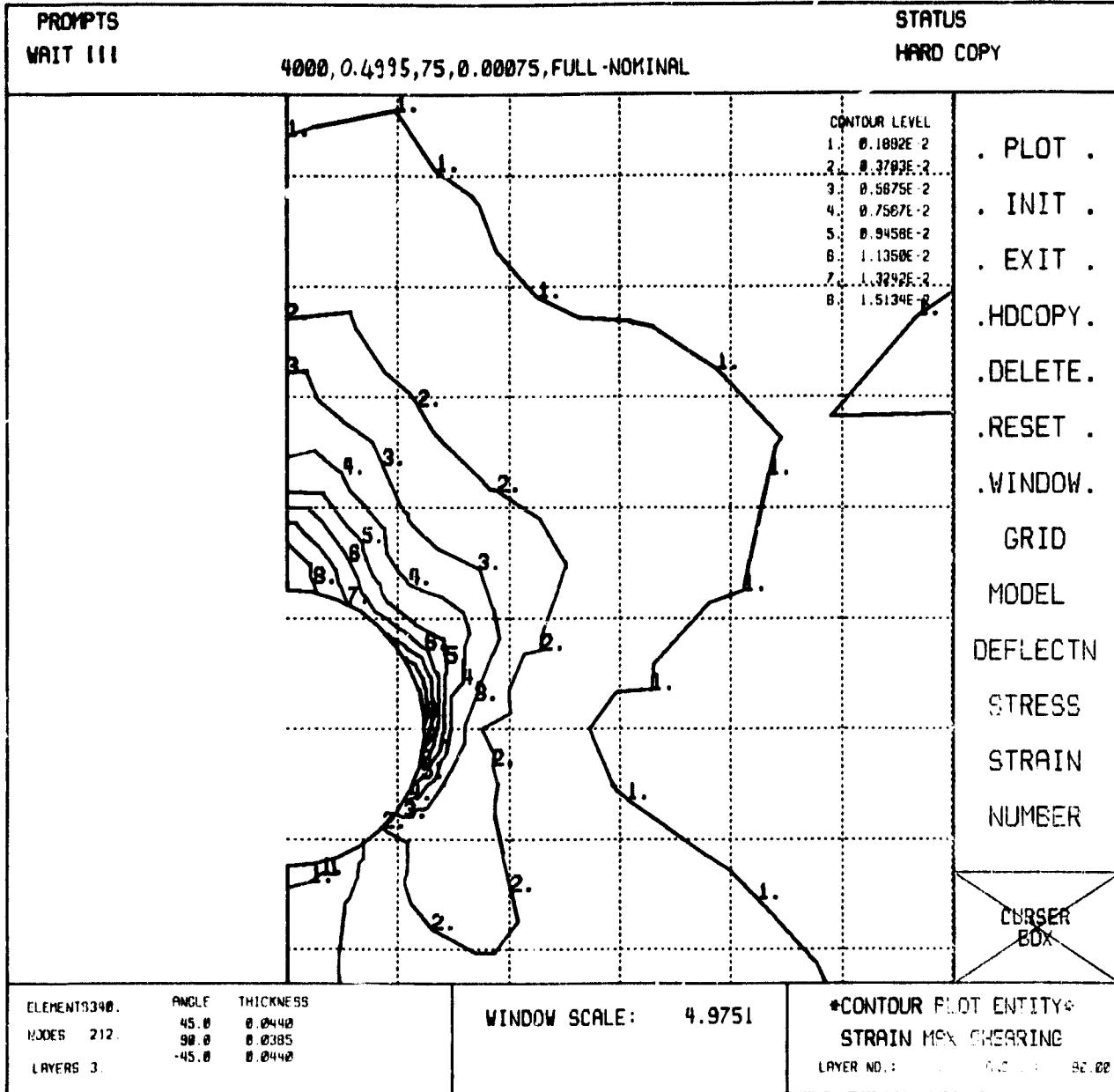


Figure IV-C-2-e. Enlarged Picture of Figure IV-C-2-d

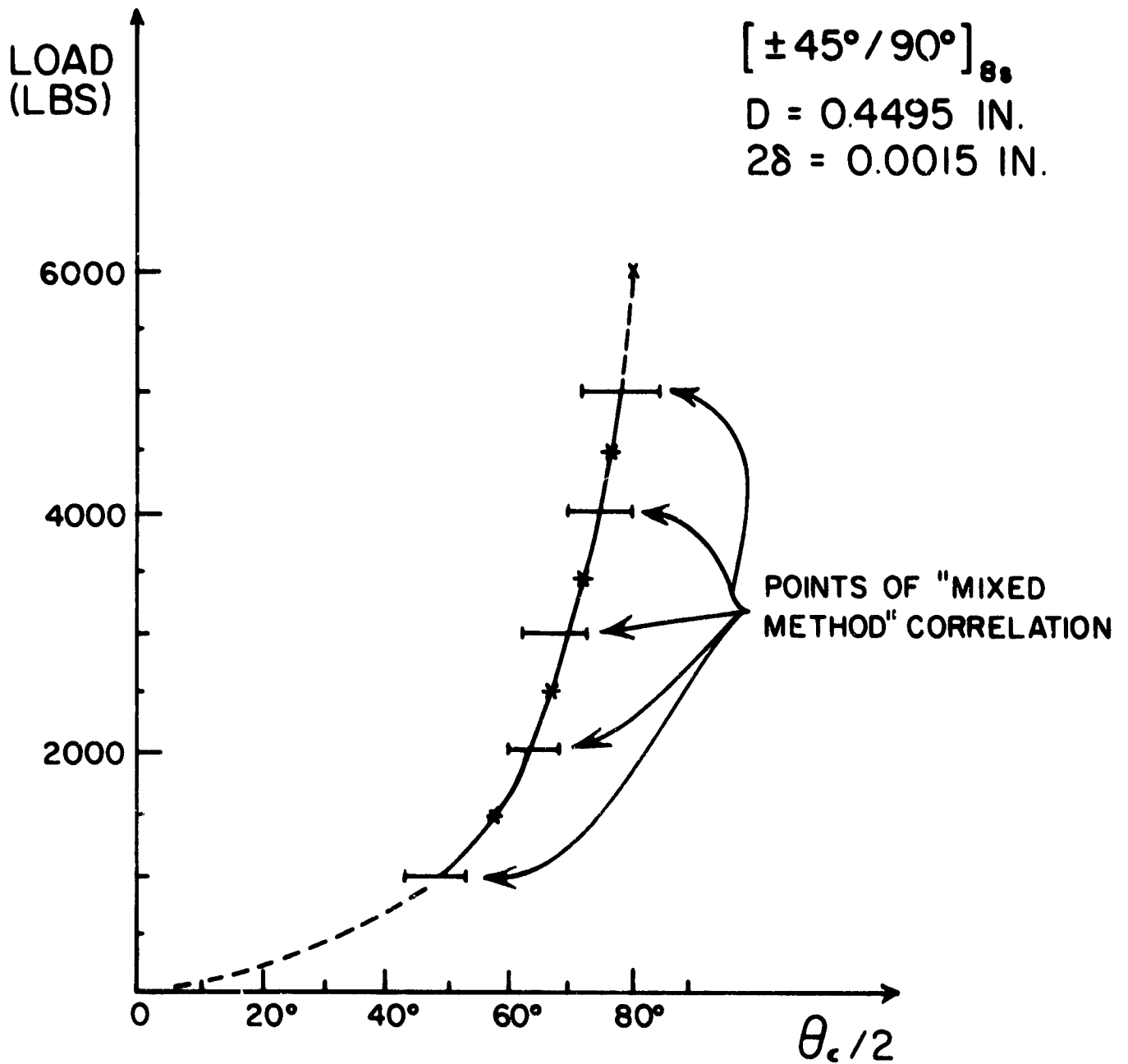


Figure IV-C-2-f. Applied Load Versus Contact Angle

of the range than the extremes, one can easily choose the best contact angle for analysis.

In the process of performing these experiments and calculations, it has become clear that, even beyond satisfying boundary constraint conditions on displacements, curves originally smooth in the material domain must remain smooth after elastic deformation. Thus, it may be possible to find a correct contact region by plotting deformed shapes and examining the smoothness of their contours.

One aspect is encouraging even at this point; the lowest maximum shear strain values were observed when the deformed shape was best matched to such a smoothness condition.

#### d. Plans for Upcoming Period

The "mixed method" has proven to this point to be a practical and reasonably good research approach to a complicated and uncertain boundary value problem. The alternative smoothness condition mentioned must be examined further. If it shows itself to be reliable, then it will be possible to produce stress data for various combinations of fiber arrangements without the time and labor of photoelastic experiments. We will investigate this and, if successful, try to apply a failure criterion for pin-loaded composite joints in bearing.

#### IV-D COMPUTER SOFTWARE DEVELOPMENTS

Senior Investigator: M. S. Shephard

##### 1. Introduction and Status

The objective of this portion of the project is to provide advanced and specialized computer "tools" for the analysis and design of composite structural elements. The major thrust to date has been and continues to be in the finite element area, with effort directed at implementing finite element analysis capabilities and developing interactive graphics preprocessing and postprocessing capabilities. Recent efforts have been directed at completing the two-dimensional interactive graphics programs in the POFES\* system and initial development of a three-dimensional program.

##### 2. Progress During Report Period

Effort during the current reporting period on POFES software has concentrated on the following:

- (a) Development of an edge load editor for the two-dimensional attribute editor.
- (b) Initial development of a surface load editor for the two-dimensional attribute editor.
- (c) Initial development of a preprocessor for general three-dimensional shell surfaces\*\*.

---

\* POFES (People Oriented Finite Element Software) is RPI's finite element software system.

\*\* Funding for this work is external to the composites program and through the Graphics Center's Industrial Associates Group.

The function of the edge load editor is to allow the user an efficient means to define edge tractions. This segment of the attribute editor has features that allow the user means to define his edge loads in terms of components normal to an edge, tangent to an edge or at any given angle to an edge. The load can be uniform along an edge or have a linear, quadratic or cubic variation. All such loads, however, are understood to lie in the plane of the object. Figure IV-D-1 has three edge loads applied. The upper left edge load is a quadratically varying normal edge load while the second is a constant load acting at an angle to the edge. The length of the arrows used to display the load indicates the relative magnitude of the load, and the load direction is indicated by the orientation of the arrows. The third load is a linearly varying tangential load on the horizontal line at the top of region 2. The relative magnitude of tangential loads is indicated by the size of the arrow heads used to display it. Figure IV-D-2 shows the use of the ECHO<sup>\*</sup> function to check the edge load.

The function of the surface load editor is to allow the user an efficient means to define loads acting over and normal to the surface of the object. Figure IV-D-3 shows the surface load menu page with a constant normal surface load applied to the right-hand region. In Figure IV-D-4 a linearly varying load has been applied to the next region, which matches the constant load on the neighboring region. Figure

---

\* ECHO is a function by which the operator can call back for review any part of data or program.

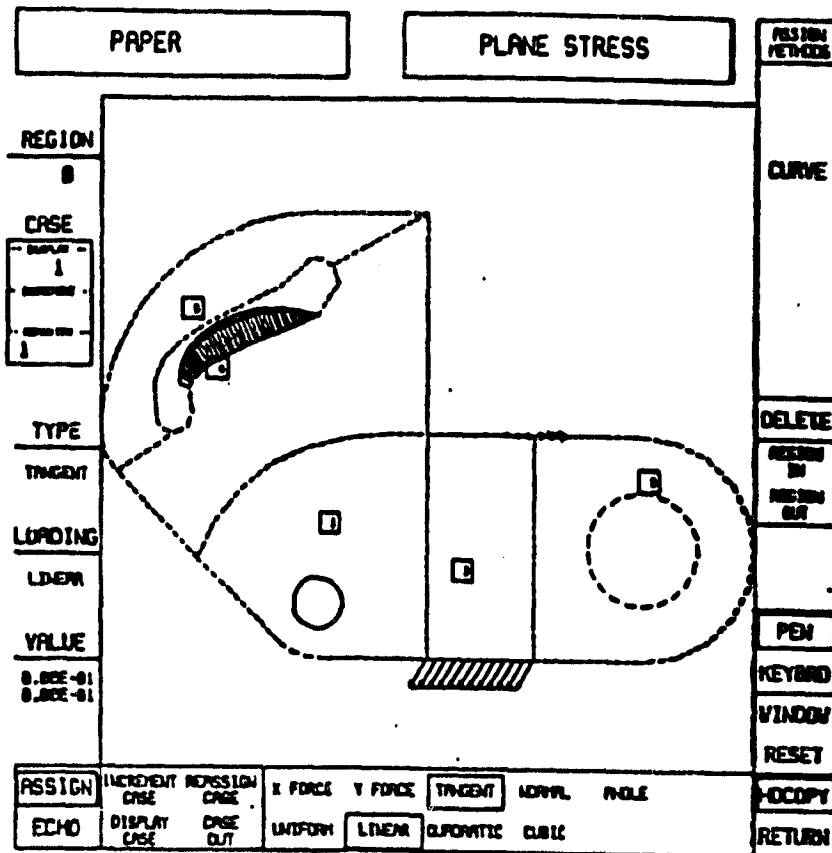


Figure IV-D-1.  
Control Page for Edge Load Segment of Attribute Editor

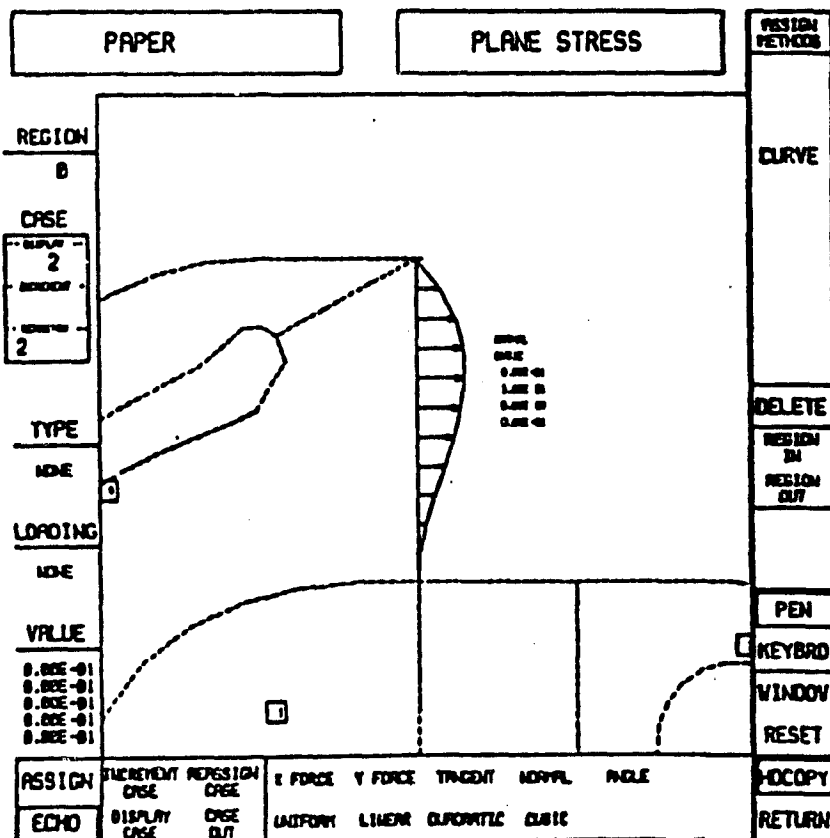


Figure IV-D-2. Use of ECHO Function to Check Edge Load

ORIGINAL PAGE IS  
OF POOR QUALITY

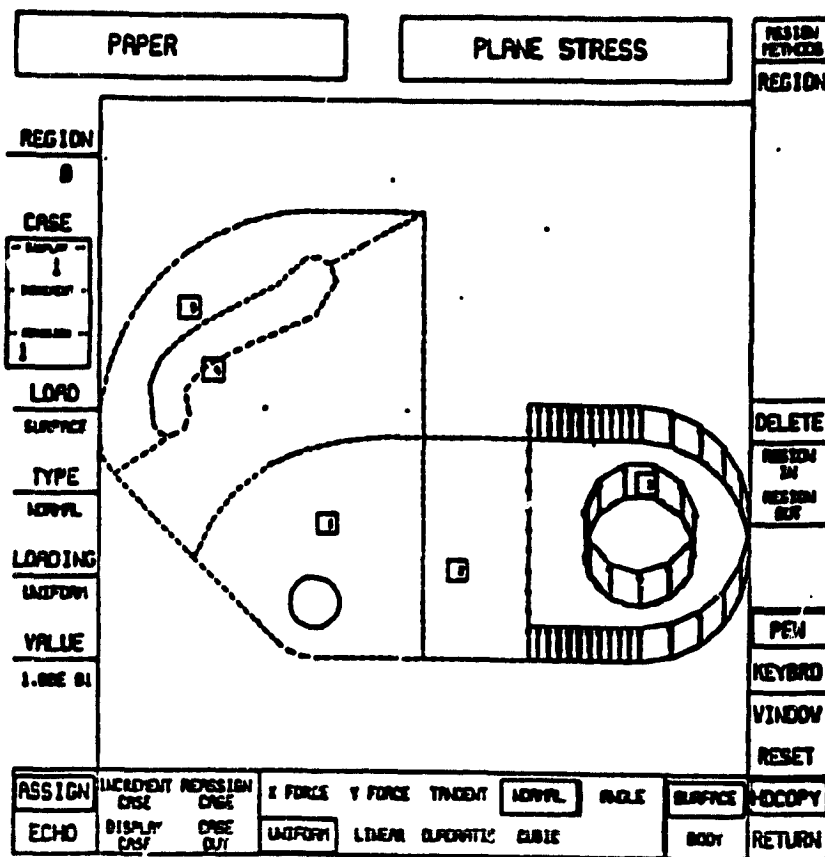


Figure IV-D-3.  
Control Page for Surface Load Segment of the Attribute Editor

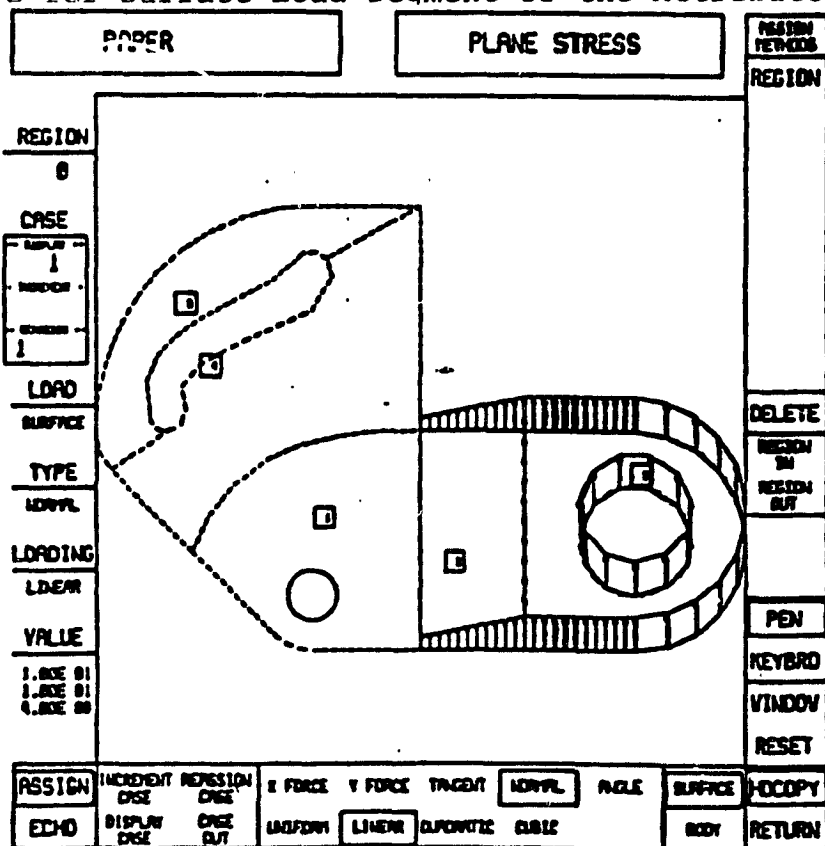


Figure IV-D-4.  
Application of Linearly Varying Surface Load  
Matching Neighboring Constant Surface Load

IV-D-5 shows a complete set of surface loads on the same structure. The user can also check the values of the surface loads applied using the ECHO function as shown in Figure IV-D-6.

A surface mesh preprocessor for the generation of finite element meshes for three-dimensional shell structures is being developed. As with the other graphics programs in the POFES system, the objective of the surface mesh preprocessors is to offer the user an interactive graphic tool that is easy to use.

The process of defining a finite element surface mesh begins with defining the space the user wishes to work in and defining the three-dimensional boundary curves. Several features have been built into the program to aid the user in the input of the three-dimensional boundary curves. The most important of these gives the user a means to obtain the exact values of specific three-dimensional locations by "Hit-testing"\* against the two-dimensional projection of various points displayed on the screen. The points against which the "hit-test" may be conducted include the ends of previously defined curves, the key points used to define the curves and the currently active grid plane which is user-selected from the user-defined three-dimensional grid. The user is also given three different methods for rotating and translating the

---

\* "Hit-testing" is a process in which the coordinate values given by the interactive input device are set to those of an existing location, if the "distance" between the two locations is less than some prescribed value.

ORIGINAL PAGE IS  
OF POOR QUALITY

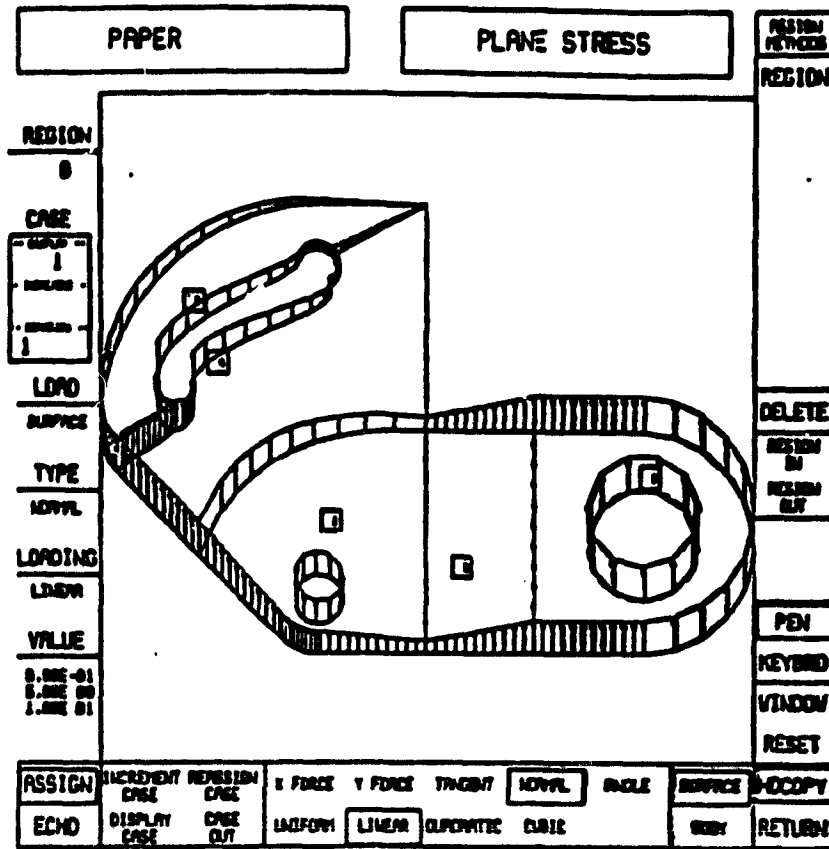


Figure IV-D-5. Completed Set of Surface Loads

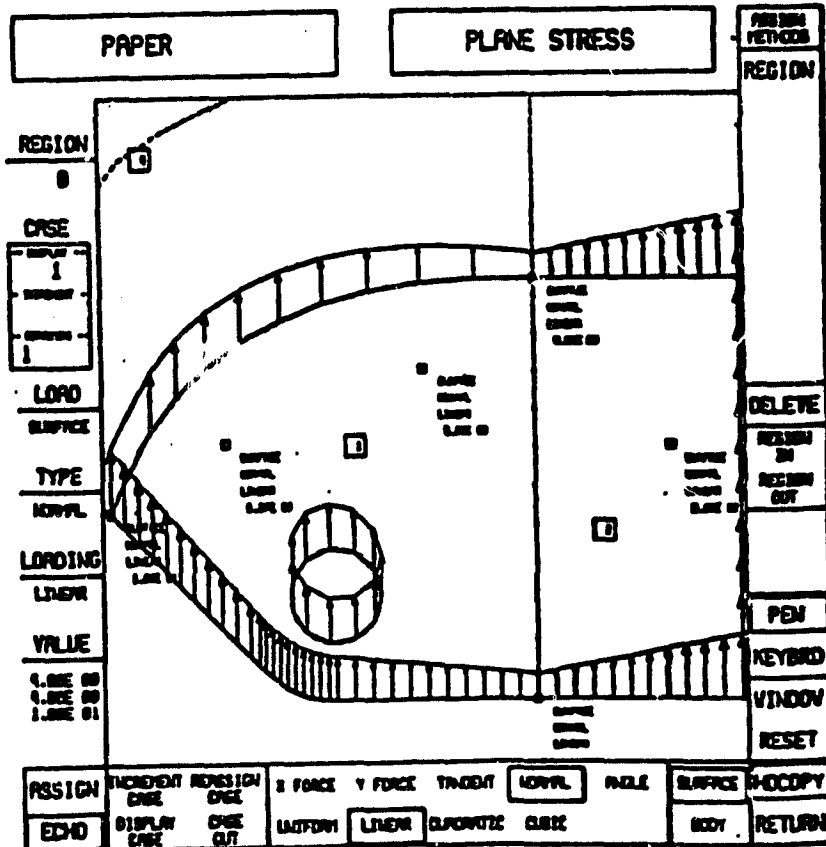


Figure IV-D-6. Use of ECHO Function to Check Surface Loads

object, along with the ability to zoom in or out, to translate and change the scale of the display. Figure IV-D-7 shows a set of curves interactively input using the feature just defined. The user can choose to use either cubic splines or straight lines to define the boundary curves.

The curves are then set to the mesh-generating portion of the program. Here the user interactively breaks up the curves into the desired number of element edges, specifies the desired element type and selects the curves that make up the surface mesh. Figure IV-D-8 shows the surface mesh generated using the boundary curve shown in Figure IV-D-7. Figures IV-D-9 and 10 show two views of another surface mesh example.

### 3. Plans for Upcoming Period

During the next reporting period the final programming on the attribute editor will be finished and complete user documentation prepared. Other work on POFES software will include further development of the surface meshing program, along with improvements to the inhouse general purpose finite element analysis program to be carried out by a small group of students working on course projects.

### 4. Current Publications or Presentations by Professor Shephard on this Subject

- 1) "The University's Role in Meeting Industry's CAD/CAM Needs"  
Published in "Education and Industry - A Joint Endeavor", Vol. 1, Proc. ASEE Nat. Meeting, June, 1981, pp. 232-235.



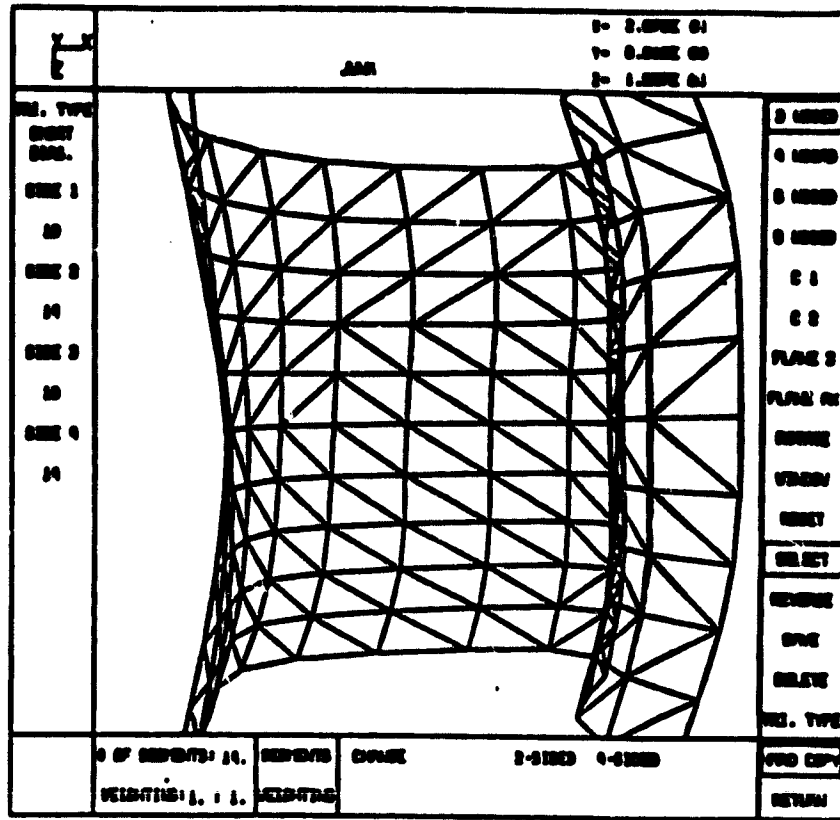


Figure IV-D-9. Surface Mesh Example

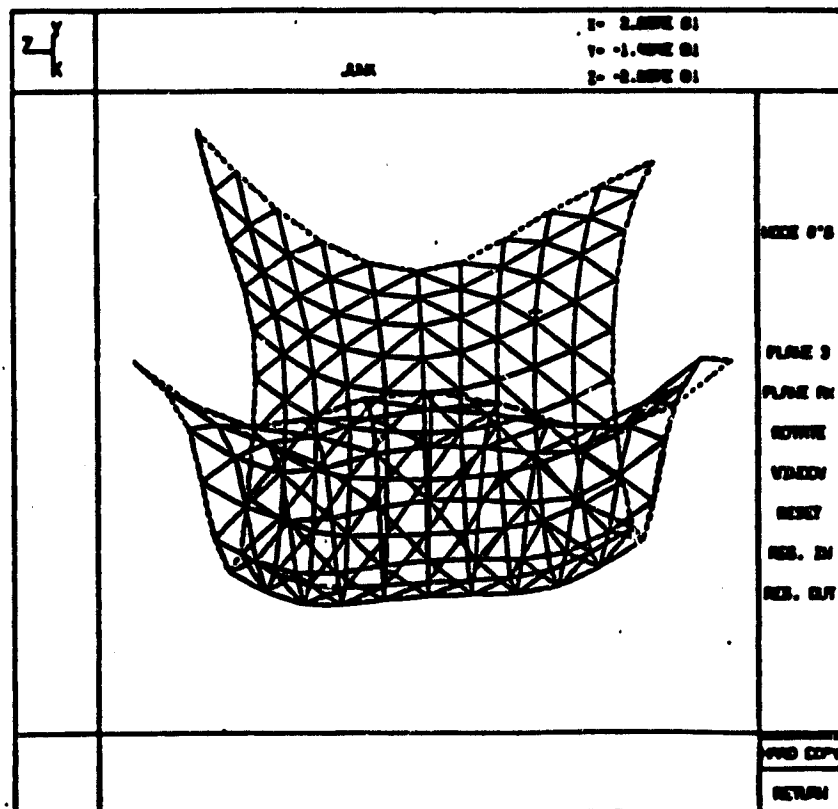


Figure IV-D-10. Rotated View of Surface Mesh Example

- 2) "A Generalized Two-Dimensional, Graphical Finite Element Preprocessor Utilizing Discrete Transfinite Mappings", (with R. B. Haber, J. F. Abel, R. H. Gallagher and D. P. Greenberg).  
Published in Int. J. Num. Meth. Engng., Vol. 17, July 1981, pp. 1015-1044.
- 3) "Finite Element Model Generation"  
Presented at Battelle Columbus Laboratories, Ohio, September, 1981.
- 4) "Finite Element Solutions to Point-Load Problems", (with R. H. Gallagher and J. F. Abel).  
To be published in J. Eng. Mech. Div., ASCE, Vol. 107, No. EM5, October, 1981, pp. 839-850.
- 5) "The Finite Element Modeling Process - Will It be Automated"  
To be published in "New and Future Developments in Commercial Finite Element Methods", J. Robinson, Editor, October, 1981, pp. 451-468.
- 6) "Adaptive Finite Element Analysis Accounting for Material Interfaces", (with S. M. Yunus).  
To be presented at the ASCE Conference, St. Louis, Missouri, October, 1981.

PART V  
PROCESSING SCIENCE AND TECHNOLOGY

- V-A INITIAL SAILPLANE PROJECT: THE RP-1
- V-B SECOND SAILPANE PROJECT: THE RP-2

V-A INITIAL SAILPLANE PROJECT: THE RP-1

Senior Investigators: F. Bundy  
R. J. Diefendorf  
H. Hagerup

Flight tests of the first ultra-light all-composite glider resumed in the Summer of 1981, with the number of flights of the RP-1 reaching a total of thirty-six at the end of the season. A camera was installed to record flight instrument readings, and several flights were conducted in the still air of the early morning hours, so that a glide-polar could be determined. The preliminary results are shown in Figure V-A-1, from which the 1981 configuration of the RP-1 can be seen to have a best glide ratio of 11.3 : 1 and a minimum rate of sink of 4.2 fps.

It is necessary to bear in mind that during these flights the aircraft was equipped both with an unfaired landing wheel and with a camera mounted in an exposed position. It is estimated that the cleaner, 1980 configuration had a parasite drag coefficient about fifteen per cent lower. The aircraft has also become seventy pounds heavier since then. Consequently, an effort will be made during this winter to reverse some of these adverse aerodynamic developments by installing the necessary fairings under and behind the pilot. Not the least of these aerodynamic improvements will be a closure for the open fuselage bottom. This opening was originally to allow foot-launching, but the degree of success obtained to date with winch-launching has made that mode of

148

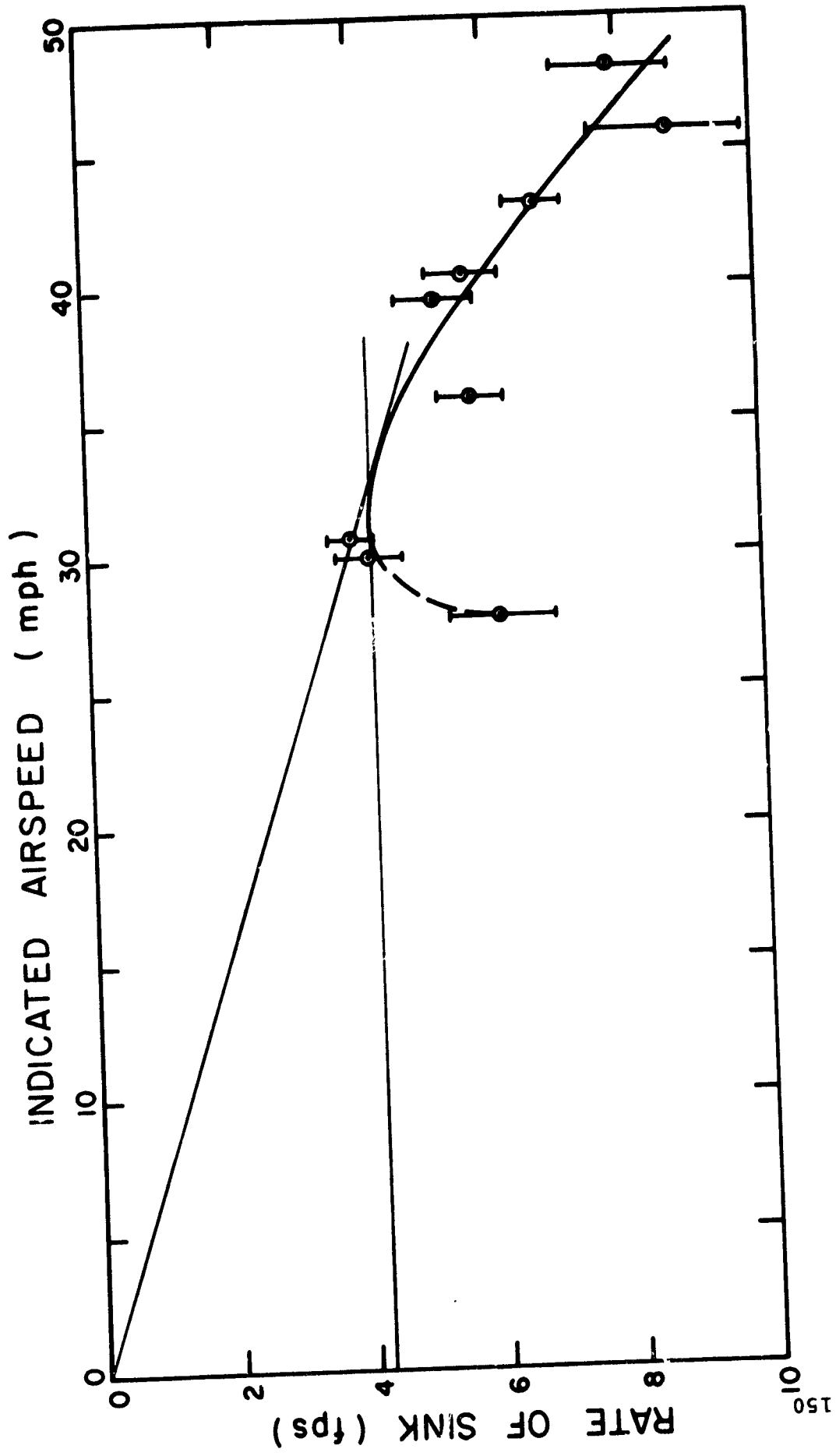


Figure V-A-1. FV-1 Glide Polar - Preliminary Data

launching unnecessary. Accordingly, the fuselage closure is possible, and this should result in much lower induced drag and less lift-loss associated with "leakage" inboard of the wing roots. We expect to be able to report a best glide ratio close to fifteen for the RP-1 by the end of the Summer of 1982 and fairings which add very little to the aircraft's gross weight.

V-B SECOND SAILPLANE PROJECT: THE RP-2

Senior Investigators: F. Bundy  
R. J. Diefendorf  
H. Hagerup

This project encompasses the design, fabrication and testing of an ultra-light, high performance, all composite sailplane. A number of sophisticated design aspects have been selected to challenge innovation in fabrication processes for low cost aerospace structures beyond the level encountered in the first project, which led to the RP-1. The RP-2 design is now complete and includes such features as a partial span split-flap, horizontal tail with field splices at roughly 2/3 span, double-taper wing planform and tail length to mean aerodynamic chord ratio of 5.3.

Fabrication has progressed to the point where empennage and wings are now ready for static proof testing to design loads. Since the last report, the partially completed framework of the wings was inspected by the FAA, and the quality of the work was approved.

The final design for the L-section stringers, which stiffen wing skins against buckling, incorporates a hybrid lay-up with the following stacking sequence: 0° graphite, ±45° Kevlar cloth and 0° graphite. These stringers are sufficiently stiff to eliminate the use of additional shear webs between the spar and the leading edge, looking forward, or between the spar and the flap/aileron hinge line, looking aft. The low linear density of 23 g/m achieved for these stringers results in a significant weight saving.

The wing skins were installed after FAA inspection, without the use of external molds of any kind during wing construction. Tolerances of the finished wings were determined to be completely satisfactory, confirming our expectations of the labor-saving wing construction technique used for the first time on the RP-2. The all-graphite split flaps have been designed with skins laid-up as 4-ply, ( $\pm 45^\circ$ )<sub>g</sub>, and assembled on triangular ribs with foam spacers to maintain cross-sectional shape. Bell cranks, pushrods and torsion-rods for aileron and flap controls have been installed, with removable, covered inspection ports for ease of access at the appropriate locations.

The most interesting structural feature of the fuselage design for the RP-2 is the use of two large, curved hybrid graphite/Kevlar foam sandwich beams which carry the loads from towline, pilot weight and landing wheel reactions into the center box which connects wings and tailboom. One such full-scale prototype curved beam, referred to as a "tusk" and designed to carry 500 pounds with a safety factor of three, was tested to destruction with very satisfactory results; failing in shear at 1,650 pounds. The production beams, consequently, were laid-up precisely as the prototype and have now been installed, thus completing the structural framework of the aircraft. Control linkages within the fuselage have also been essentially completed, and the only major fabricating task remaining on the RP-2 is the construction

of the fuselage fairing enclosing the pilot and framework. This task is expected to be completed during the Fall and Winter of the next reporting period, in anticipation of initial flight of the RP-2 in the Summer of 1982.

PART VI  
PERSONNEL  
AUTHOR INDEX

## PERSONNEL

Co-Principal Investigators

Ansell, George S., Ph.D.	Dean, School of Engineering
Loewy, Robert G., Ph.D.	Institute Professor
Wiberley, Stephen E., Ph.D.	Professor of Chemistry

Senior Investigators

Brunelle, E. J., Jr., SC.D. (Aeroelastic and structural design and analysis, applied mechanics of composite structures, research)*	Associate Professor of Aeronautical Engineering
Bundy, F., Ph.D. (Physical chemistry and CAPGLIDE)*	Research Professor of Materials Engineering
Diefendorf <sup>i</sup> , R. J., Ph.D. (Fabrication, CAPGLIDE, fiber behavior, research)*	Professor of Materials Engineering
Feeser <sup>i</sup> , L. J., Ph.D. (Computer applications and graphics, computer aided design, optimization)*	Professor of Civil Engineering
Goetschel, D. B., Ph.D. (Structural analysis and design, CAPCOMP)*	Assistant Professor of Mechanical Engineering
Hagerup, H. J., Ph.D. (Aerodynamics, configuration, pilot accommodation, CAPGLIDE)*	Associate Professor of Aeronautical Engineering
Hoff, N. J., Ph.D. (Structural design and analysis, CAPGLIDE)*	John A. Clark and Edward T Crossan Professor of Engineering
Krempl, E., Dr.Ing. (Fatigue studies, research)*	Professor of Mechanics and Director of Cyclic Strain Laboratory
Scarton, H., Ph.D. (Acoustic emission NDE)*	Associate Professor of Mechanical Engineering and Mechanics

\* Fields of Speciality.

<sup>i</sup> Member of Budget Committee together with co-principal investigators.

FILE 154

Senior Investigators

Shephard, M., Ph.D.  
(Computer graphics, finite  
element methods)\*

Sternstein<sup>i</sup>, S. S., Ph.D.  
(Failure analysis, matrix  
behavior, research)\*

Assistant Professor of Civil  
Engineering

William Weightman Walker  
Professor of Polymer Engineer-  
ing

Research StaffManager & Master Technician, Composites Laboratory

Paedelt, Volker

Graduate Assistants

Bobal, Gail, M.E.

Chang, Chi-Min, M.S.

Chen, Chikuang, B.S.

Chen, Shu-ping, B.S.

Cummings, Delwyn, B.S.

Das, Nripendra, B.Tech.

Helmer, James, B.S.

Kim, Wonsub, M.S.

Lumban Tobing, Frida, M.S.

Muser, Christoph, Dipl.Mech.Ing.

Niu, Tyan-Min, M.S.

Oyibo, Gabriel, M.S.

Uzoh, Cyprian, B.S.

Valicenti, Raymond, B.S.

Winckler, Steven, M.E.

Yang, Phillip, M.S.

Undergraduate Assistants - Seniors

Adel, Paul

Applewhite, Keith

Bertolazzi, Andrew

Blake, William

Bristol, Brian

Cox, Mary

DeTaranto, Francis

Dhimitri, William

Fairchild, Kendall

Fisher, Steven

Niederer, Melvin

Northrop, Steven

Putnam, David

Staniorski, Anthony

Vaney, Philippe

\* Fields of Speciality.

<sup>i</sup> Member of Budget Committee together with co-principal investi-  
gators.

Undergraduate Assistants - Juniors

Baucom, Allan

Kuntsmann, Debra

Carbone, James

Lagreniere, Suzanne

DeMint, Thomas

Lundquist, Cheryl

Ehrgott, Darhl

Malusa, Stephen

Ficarra, Robert

Melendez, Hermenegildo

Kirshenbaum, Susan

Undergraduate Assistants - Sophomore

Schroeder, Hans

## AUTHOR INDEX

	<u>Page (s)</u>
Brunelle, E. J., Jr. ....	111
Bundy, F. ....	149, 152
Diefendorf, R. J. ....	21, 149, 152
Goetschel, D. B. ....	73, 105, 115
Hagerup, H. J. ....	149, 152
Krempl, E. ....	47
Loewy, R. G. ....	73, 115
Scarton, H. A. ....	73
Shephard, M. S. ....	58, 64, 137
Sternstein, S. S. ....	49

FILE 160